Ministry of Higher Education
and Scientific Research
University of Babylon
College of Science
Department of Physics

Synthesis and Characterization of PAAm-PEG Blend and the Effect of Ag, Sb_2O_3 Nanoparticles on Structural, Optical Properties and Dispersion Parameters

A Thesis

Submitted to the Council of Physics Department, College of Science, University of Babylon in Partial Fulfilment of the Requirements for the Degree of Master of Science in Physics

By

Ahed Ali Kadhim Zbala

B.Sc. of Physics /2018

Supervised by

Prof. Dr.

Abdulazeez O. Mousa Al-Ogaili

Prof. Dr.

Khalid Haneen Abass Hassan

2022A.D. **1444A.H.**

وزارة التعليم العالي و البحث العلمي
جامعة بابل
كلية العلوم
قسم الفيزياء

تصنيع وتوصيف خليط PAAm-PEG وتأثير جسيمات Sb_2O_3, Ag النانوية على الخصائص التركيبة, البصرية ومعاملات التفريق

رسالة

مقدمة الى مجلس قسم الفيزياء - كلية العلوم - جامعة بابل وهي جزء من متطلبات نيل درجة الماجستير في العلوم / الفيزياء

من قبل

عهد علي كاظم زبالة
بكالوريوس علوم فيزياء / 2018

بإشراف

الاستاذ الدكتور
عبد العزيز عبيد موسى العگيلي

الاستاذ الدكتور
خالد حنين عباس حسن

١٤٤٤ هـ

٢٠٢٢ م

Supervisors Certification

We certify that this thesis is titled **(Synthesis and Characterization of PAAm-PEG Blend and the Effect of Ag, Sb_2O_3 Nanoparticles: Structural and Dispersion Parameters)** wastft prepared by **(Ahed Ali Kadhim Zbala)** under our supervisions at Department of Physics, College of Science, University of Babylon, as a partial fulfillment of the requirements for practical work of Physics Master thesis.

Signature:

Supervisor: Dr. Abdulazeez O. Mousa
Title: Professor
Address: Department of physics - College of Science University of Babylon
Date: / / 2022

Signature:

Supervisor: Dr.Khalid Haneen Abass
Title: Professor
Address: Department of physics College of Education for Pure Sciences- University of Babylon
Date: / / 2022

Certification of the Head of the Department

In view of the available recommendation, I forward latter thesis for debate by the examination committee.

Signature:

Name: Dr. Samira Adnan Mahdei
Title: Professor
Address: Head of Physics Department, College of Science, University of Babylon
Date: / / 2022

الخلاصة

تضمنت هذه الدراسة تحضير أغشية خليط البوليمر عن طريق خلط (PAAm-PEG) وإضافة كميات مختلفة من المادة النانوية (Sb_2O_3، Ag) بطريقة الصب. يذاب 0.75 غم من PAAm في مل لتر 60 من الماء المقطر، ويحرك عند 70 درجة مئوية ، ويضاف غم 0.25 من PEG إلى المحلول مع الخلط عند 40 درجة مئوية. بعد ذلك، تمت إضافة (Sb_2O_3، Ag) إلى المحلول بمحتوى مختلف غم (0.02 ، 0.04 ، 0.06) بنفس حجم الجسيمات لتكوين العينات. تم الخلط لمدة ساعتين للحصول على خليط متجانس ثم ترك لمدة 24 ساعة قبل الصب. يوضع المحلول في طبق بتري دش قطر (9) سم ويُترك ليجف في درجة حرارة الغرفة (25±5) درجه مئويه ولمدة 10 أيام ، وقد درس التجانس وتوزيع جزيئات (Sb_2O_3, Ag) النانوية في اغشية (PAAm-PEG-Sb_2O_3, Ag) باستخدام مجهر ضوئي والمجهر الالكتروني الماسح.

درست الخواص البصرية بواسطة مقياس الطيف الضوئي بالأشعة فوق البنفسجية والضوء المرئي في نطاق (200-1100) نانومتر .زادت معظم الخواص الضوئية بزيادة الطول الموجي باستثناء فجوة الطاقة والنفاذيه. تم تحضير العينات الناتجة بمدى سمك (120±3) ميكرومتر. تم قياس السمك بميكرومتر رقمي.

بينما أظهرت الخصائص الهيكلية للتحليل الطيفي تحويل فوريه للأشعة تحت الحمراء (FT-IR) تغيرًا في موضع الذروة بالإضافة إلى تغير في الشكل والكثافة مقارنةً بمزيج (PAAm-PEG).

أظهرت صور المجهر الالكتروني الماسح (SEM) أن إضافة الجسيمات النانوية في المركبات النانوية (PAAm-PEG-Ag, Sb_2O_3) تظهر تغيرات في التشكل السطحي لهذا النظام. يتضح من الصور أن الحبوب تتراكم مع زيادة نسبة الجسيمات النانوية. يُظهر التشكل السطحي لأغشية المركبات النانوية (PAAm-PEG-Ag, Sb_2O_3) العديد من التكتلات أو القطع الموزعة عشوائيًا على السطح العلوي. أظهرت النتائج زيادة في عدد التكتلات على السطح مع زيادة تركيز الجسيمات النانوية (Ag، Sb_2O_3). نلاحظ من خلال (FT-IR) ، إذا كانت الجسيمات النانوية موجودة في الأفلام (PAAm-PEG- Sb_2O_3, Ag) ، فإنها تؤدي إلى تقييد الحركة الاهتزازية الجزيئية ، والحركة الاهتزازية الخاصة في ثلاثة أبعاد لمركب (PAAm-PEG) و على الأرجح ستتأثر طاقة الأشعة تحت الحمراء. تؤدي إضافة (Sb_2O_3، Ag) بوزن مختلف إلى مادة الأساس (PAAm-PEG) إلى زيادة عدد الروابط لكل وحدة مساحة وبالتالي زيادة الكثافة.

من خلال حساب معاملات التشتت نلاحظ انخفاض الزخم البصري M_{-1} و M_{-3} مع زيادة الجسيمات النانوية. باستخدام عملية Wemple-DiDomenico تم تحديد معاملات التشتت. ويلاحظ أنه مع زيادة الجسيمات النانوية تقل طاقة التشتت (E_d) والطاقة الانتقالية الإلكترونية لمذبذب واحد (E_o) كما تشير القيم الصغيرة جدًا لفجوة الطاقة إلى أن الأفلام شبه موصلة ، مما يجعلها مناسبة للأجهزة البصرية.

Summary

This study includes the preparation of polymer blend by mixing of 0.75g Poly (acrylamide) (PAAm) and 0.25g Poly (ethylene glycol) (PEG) with(2, 4 and 6)wt.% of (Sb_2O_3, Ag) nanomaterials by casting method. 0.75 g PAAm was dissolved in 60 mL from distilled water stirred at 70 °C, then 0.25 g of PEG was included in the solution with agitation at 40 °C. Sb_2O_3 and Ag was added to the solution with different contents (0.02, 0.04 and 0.06) g with the same particle size to form the nanocomosites. The mixture was mixed for two hour to obtain a homogeneous mixture and then left for 24 hours before pouring. The solution was placed in a petri dish (9 cm) and allowed to dry at room temperature (25±5) °C for 10 days. Homogeneity, and distribution of Sb_2O_3 and Ag nanoparticles in (PAAm-PEG-Sb_2O_3, Ag) films were studied using an optical microscope and electron scanning microscope (SEM).

The UV-Vis was used to investigate optical properties light spectrophotometer in the range (200-1100) nm. Most of the optical properties increased with the increasing wavelength except for the transmittance and energy gaps. The resulting samples were made with a range of thicknesses (120±3) μm. The thickness was determined by micrometer digital.

The structural properties of the spectral analysis Fourier transforms infrared (FT-IR) showed a weak change in the peak position as well as a change in the shape and density compared to the blend (PAAm-PEG).

The (SEM) images showed that the addition of nanoparticles in the nanocomposites (PAAm-PEG-Ag, Sb_2O_3) changes in the surface morphology of this system. Furthermore the grains accumulate as the percentage of nanoparticles increases. The surface morphology of the nanocomposites films (PAAm-PEG-Ag,

Sb_2O_3) shows many randomly distributed aggregates or pieces on the upper surface. The outcomes showed a rise in the number of white dots on the surface with increasing concentration of nanoparticles (Ag, Sb_2O_3). We notice through (FT-IR), if a nanoparticle presents in films (PAAm-PEG-Ag, Sb_2O_3) nanocomposites lead to restriction of molecular vibrational motion, and special vibrational motion at three dimensions for (PAAm-PEG) blend and will be most probably affected by IR energy. Adding (Sb_2O_3, Ag) with different weight to basis material (PAAm-PEG) led to increase in the number of bonds per unit area and hence density increases, the optical micrographs showed a good diffusion of nanoparticles with some agglomerations.

The M_{-1} and M_{-3} visual perception moments decrease with increasing nanoparticle thickness. Using the Wemple-DiDomenico technique, the parameters of dispersion were established. It is observed that as time goes on nanoparticles, the scattering energy (E_d) and energy of electronic transition of one oscillator (E_o) are lowered. Very low values of the energy gap tending to film is semiconductors, which makes them suitable for optical devices.

Contents

List of Figures

List of Tables

List of Symbols and Abbreviations

Symbol	Description	Unit
PEG	Polyethylenclycol	-
PAAm	Polyacrylamide	-
Sb_2O_3	Antimony (III) Oxide	-
Ag	Silver	-
FDA	Food Drug Administration	-
T	Transmittance	-
A	Absorption	-
hυ	Photon Energy	J
h	Planks Constant	J.s
α	Absorption Coefficient	cm^{-1}
k_o	Extinction Coefficient	-
I_o	Photon Beam Intensity	-
I_t	Intensity of Light Transmitted	-
t	Thickness	µm
n	Refractive Index	-
d	Density	g/cm^3
c	Light Speed in Vacuum	m/s
v	Light Speed in Matter	m/s
R	Reflectance	-
λ	Wavelength	nm
σ_{op}	Optical Conductivity	s^{-1}

Symbol	Description	Unit
WDD	Wemple–DiDomenico	-
E_o	The Energy of the Effective Single Oscillator	eV
E_d	The Dispersion Energy	eV
E_g	Energy Gap	eV
(M_{-1}, M_{-3})	Moments of Optical Spectra	Kg/m.s
m	Mass	g
D	Distance	M
P	Evaporated Density of Materials	g/cm^3
L.R.O.	Long Range Order	-
S.R.O.	Short Range Order	-
V	Volume	m^3
η_s	Shear Viscosity	g/cm.s
ρ_1	Grain Resistivity	-
ρ_2	The Grain Boundaries Resistivity	-
η_o	Viscosity of Water	g/cm.s
t_s	Solution Flow	**s**
t_o	Solvent Flow	**s**
OM	Optical Microscopy	-
SEM	Scanning Electron Microscope	-
FT-IR	Fourier Transforms Infrared	-

Symbol	Description	Unit
BDH	British Drug Houses	-
ε_1	Real Part	-
ε_2	Imaginary Part	-
M.P	Melting Point	K
T_g	Glass Transition Temperature	K
T_m	Melting Point Temperature	K
T_b	Boiling Point Temperature	K
α_{op}	absorption coefficient	-

1.1 Introduction

Several factors are affecting the preparation and fabrication of the polymer-based nanocomposites, such as strong interfacial interaction, good homogeneity, and fine dispersion in the matrix [1, 2]. That is significant to achieve high performance and enhancements in the properties of the nanocomposites. The functional group of both polymer and nanofillers are very important to achieve this goal.

The functional group is one of the important factors and keys that matrix and a direct effect on fabricated nanocomposites that the nanofillers in the matrix and the polymer have a strong interfacial interaction. In addition to it is important for a stable and scattering of the nanofiller in the polymer matrix. This could be greatly improved the properties of polymer nanocomposites [3, 4].

Whereas, lack in the functional groups could lead to loss of bonding and aggregation that could be associated with weak interaction and drawbacks in the improvement of properties of the new nanocomposites. Therefore, several experiments have been carried out to advance the homogeneity of the diffusion of the filler and interactions to enhance the compatibility of nanofillers in the polymer matrix applying to functionalize the nanofillers, such as graphene [5,6], and silica nanoparticles [7].

Therefore, getting a homogeneous sample with good interfacial interaction is important to achieve properties improvement that could achieve applying the functional group either in the matrix or nanofillers. This important factor does not fully understand and limited study focused and reports this issue.

Polymers were first discovered in the 1920s, and their acceptance is closely linked to the name of H. Staudinger, who won the Nobel Prize in 1953. Many synthetic polymers can be listed; some are well-known, such as polyesters, while others are less well-known, such as those used in medical applications for organs and degradable sutures [8].

Polymer is derived from the Greek words poly (many) and mere (parts) or units of high molecular mass molecules that are made up of a large number of single structural components. In other words, polymers are huge molecules with a high molecular weight, known as macromolecules that are made up of a large number of small molecules, known as monomers, linked together. Polymerization is the process of monomers reacting together to form a polymer.

Polymerization is a chemical reaction in which two or more chemicals join with or without the addition of anything else, such as water, heat, or other solvents, to form a high-molecular-weight molecule [9].

1.2 Nanomaterials

Nanomaterials are the particles (crystalline or amorphous) of organic or inorganic materials having sizes in the range of (1-100) nm. Nanomaterials are classified into nanostructured materials and nanophase materials. The former refer to condensed bulk materials that are made of grains with grain sizes in the nanometer size range while the latter are usually the dispersive nanoparticles [10].

Nanomaterials can be nanoscale in one dimension (surface films), two dimensions (strands or fibers), or three dimensions (particles). They can exist in single, fused, aggregated or agglomerated forms with spherical, tubular, and irregular shapes. Common types of nano materials include nanotubes, quantum dots and fullerenes.

The classification of nanomaterials is based on the number of dimensions, which are in nano range ($\leq$ 100 nm) [10, 11] as shown in figure (1.1):

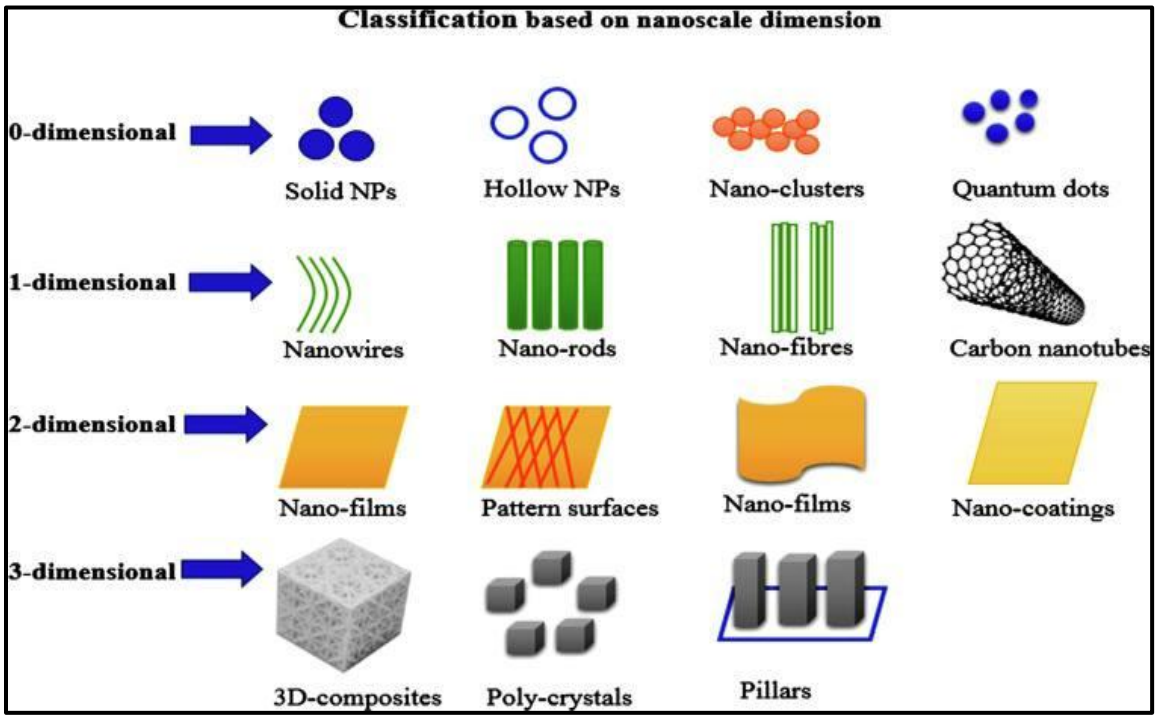

Fig.(1.1): Classification of Nanomaterials (a) 0D nanomaterials; (b) 1D nanomaterials; (c) 2D nanomaterials; (d) 3D nanomaterials[12].

a- 0-D nanomaterials have the entire dimension within nanoscale, i.e. no dimension is larger than 100 nm. The most common example of 0D- dimensional nanomaterials is the nanoparticle. These nanoparticles can be crystalline or amorphous, metallic, ceramic, or polymeric.

b- 1D nanomaterials have two dimensions in nano range. This leads to needle like shaped materials having one dimension at nanoscale. 1D nanomaterials include nanoplatelets, nanorods, nanoclays and nanosheets.

c- 2D nanomaterials at least one dimension in nano range. 2D nanomaterials include nanofibers, nanotubes, nanorods and whiskers. Carbon nanotubes are good example of 2D nanomaterials.

d- 3D nanomaterials have all three dimensions in nano range. 3D nanomaterials include nanogranules, nanoclays and equiaxed nanoparticles.

The nanomaterials can be crystalline or amorphous or polycrystalline. They can compose of single or multi-phase chemical elements. They could be in various forms and shapes, metallic, ceramic or polymeric. There are many different ways of creating nanostructures, macromolecules or nanoparticles or buck balls or nanotubes and so on can be synthesized artificially for certain specific materials [10].

1.3 Polymer Structure

The physical characteristics of polymer materials depend not only on molecular weight and shape but also on molecular structure. The different types of polymer chains, as shown in Figure (1.2) [13]:

1. Linear polymers: Van der Waals bonding between chains. Examples: polyethylene and nylon, as in part (a) of the figure (1.2).

2. Branched polymers: chain packing efficiency is reduced compared to linear polymers - lower density, as in part (b) of the figure (1.2).

3. Cross-linked polymers: chain is connected by covalent bonds. Often, it is achieved by adding atoms or molecules that form covalent links between chains. Many rubbers have this structure, as in part (c) of the figure (1.2).

4. Network polymers: 3D networks made from trifunctional mers. Examples: epoxies and phenol-formaldehyde, as in part (d) of the figure (1.2).

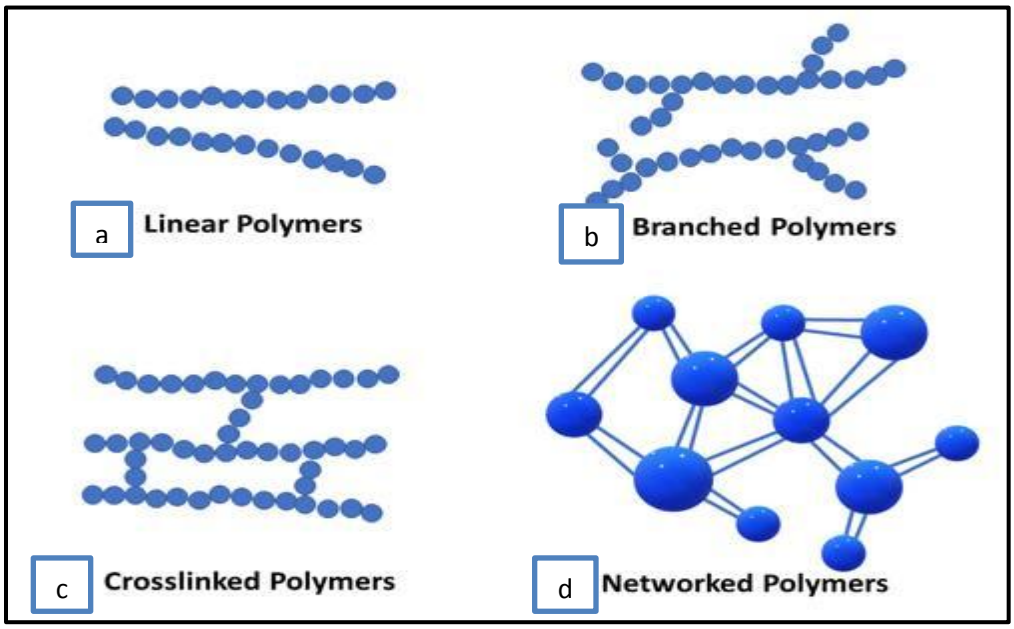

Fig. (1.2): Polymer types a) Linear polymers b) Branched polymers c) Cross-linked d) Network polymers [13].

1.4 Polymer Used in the Study

There are two types of polymers used in this work:

1.4.1 Poly (acrylamide) (PAAm)

Polyacrylamide (PAAm) is another water soluble polymer, with a wide range of industrial applications as flocculants, rheology-control agents, drag-reducing polymers PAAm use in industrial areas, used also in water treatment, mining and extraction of oil in the polymers sclerotic industry thermally, it is also used medically in the field of soft tissue industry, and in cosmetic surgery, the industry artificial corneas of the eye, and manufacturing of contact lenses and in the special cover burns the tissue industry, as well as many other medical uses and enters in the paper industry, and made into the plastic, toys, water tanks, and is often used for agricultural land benefactor of the soil and erosion control, as well as it is used as an antioxidants [14]. Fig. (1.3-1.4) various formats for

Polyacrylamide. Also, PAAm is used as a thickening agent for materials and as a flocculent[15].

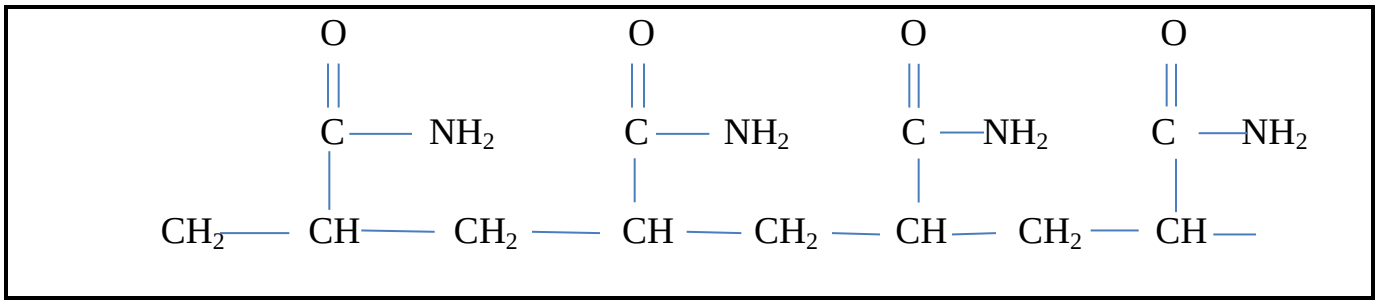

Fig. (1.3): The Chemical Formula of Poly Acryl Amide [14].

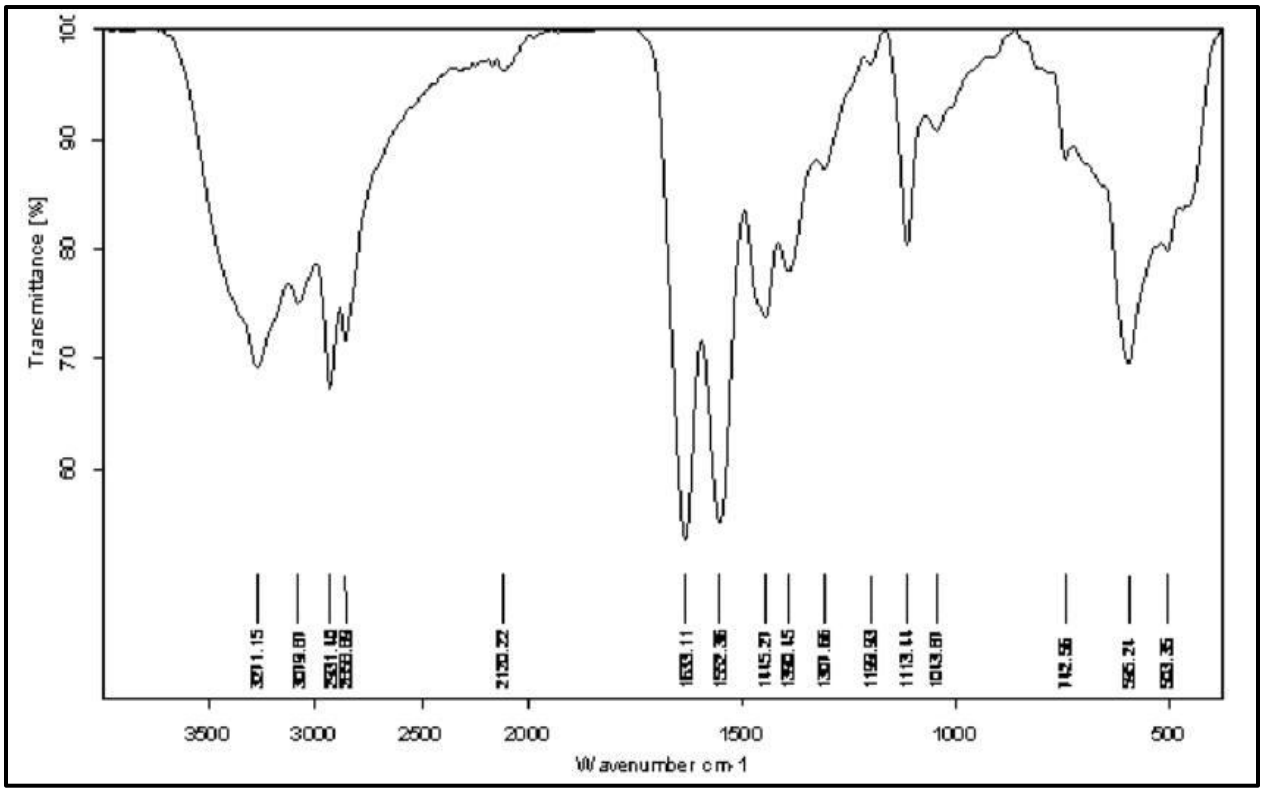

Fig. (1.4): FT-IR Spectrum for Polyacrylamide [16].

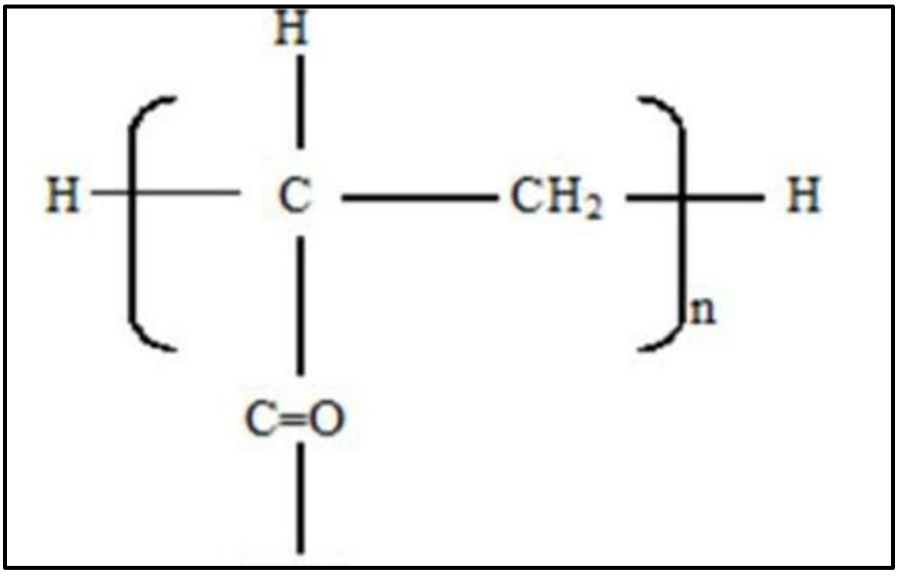

Fig. (1.5) : Chemical Formula of Pure PAAm [17].

Table (1.1): Physical and chemical properties of Polyacrylamide (PAAm) [18].

Property	PAAm
Appearance	white crystalline solid at room temperature
Molecular formula	C_3H_5NO
Solution Ph	5
Refractive index	1.8
Glass transition temperature (T_g) ^oC	84.5
Melting temperature (T_m) ^oC	192.6

Polymers include the familiar plastic and rubber materials. Many of them are organic compounds that are chemically based on carbon, hydrogen, and other nonmetallic elements (viz. O, N, and Si). Furthermore, they have very large molecular structures, often chain-like in nature that has a backbone of carbon atoms. Some of the common and familiar polymers are polyethylene (PE), nylon, poly (vinyl chloride) (PVC), polycarbonate (PC), polystyrene (PS), and silicone rubber.

1.4.2 Poly (ethylene glycol) (PEG)

The production of polyethylene glycol was first reported in 1859. Both A. V. Lourenço and Charles Adolphe Wurtz independently isolated products that were polyethylene glycols [18]. PEG is a polyether compound with many applications, from industrial manufacturing to medicine. PEG is also known as polyethylene oxide (PEO) or polyoxyethylene (POE), depending on its molecular weight. The structure of PEG is commonly expressed as $H-(O-CH_2-CH_2)n-OH$ as shown in figure (1.6) [20]. PEG is considered biologically inert and safe by the FDA. However, a growing body of evidence shows the existence of anti-PEG antibodies in approximately 72% of the population based on plasma samples from 1990–1999. The FDA has been asked to investigate the possible effects of PEG in laxatives for children [21], Numerical designation of PEGs generally indicates the number average molecular weight (e.g., PEG-4000), although typically they are not menders polymers. Liquid PEG is miscible with water in all proportions, and solid PEG is highly soluble in water, for example, PEG-4000 has a solubility of about 60% in water at 20 ^{o}C[21].

Lower molecular weight liquid PEGs can be used as solvents in their own right with or without addition of water. These we define loosely here as low molecular weight PEG has a number of benign characteristics that underlie, physical basis of this behavior is dependent upon the amphipathic nature of the polymer chain with its hydrophobic methylene groups interspersed with ether groups which can similar phase incompatibility may be found in a number of different polymers such as PEG–PPG co-polymers, polyvinylpyrolidon poly-N-isopropyl acrylamide [22]. There are many physical and chemical properties of PEG as shown in the table (1.2).

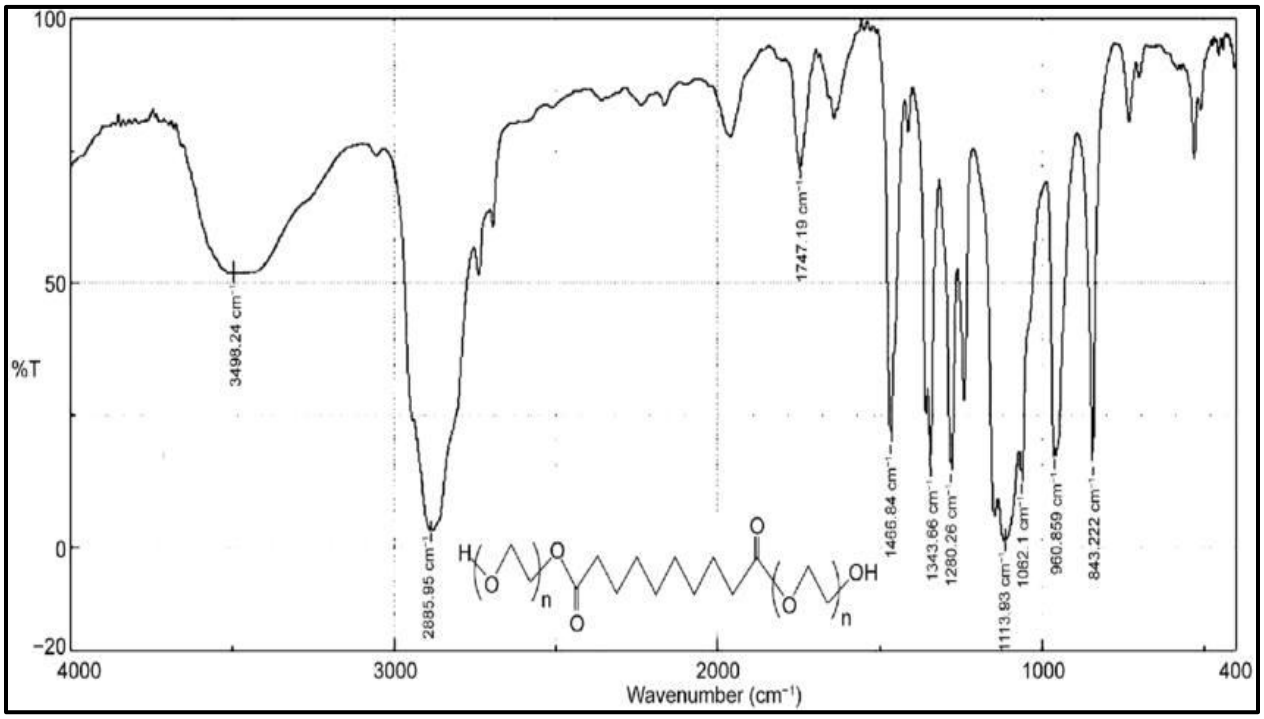

Fig. (1.6): FT-IR for Polyethylene glycol [23].

Table (1.2): Physical and chemical properties of Polyethylene glycol (PEG)[24].

Properties	**PEG4000**
Appearance	white crystalline solid at room temperature
Molecular Weight(g/mol)	4000
Density(g/cm^3)	1.2
Solubility Parameter$(MPa)^{1/2}$	20.2
Glass Temperature Transition (T_g) ^oC	-53-45
Melting Point(T_m) ^oC	53-59

1.5 The Additives Materials Used

In this work, two types of nanoparticles were added:

1.5.1 Sb_2O_3 Nanoparticle

Antimony (III) oxide is the inorganic compound with the formula Sb_2O_3. It is the most important commercial compound of antimony. There are also other formulas with different properties depending on the chemical composition as in table (1.3). It is found in nature as the minerals valentinite and senarmontite as shown in figure (1.7) [25]. Like most polymeric oxides, Sb_2O_3 dissolves in aquous solutions with hydrolysis. A mixed arsenic-antimony oxide occurs in the nature as the very rare mineral stibioclaudemtite [25].

Antimony (III) oxide is an amphoteric oxide, it dissolves in aqueous sodium hydride solution to give the meta-antimonite $NaSbO_2$, which can be isolated as the rehydrate. Antimony (III) oxide also dissolves in concentrated mineral acids to give the corresponding salts, which hydrolyzes upon dilution with water. With nitric acid, the trioxide is oxidized to antimony (V) oxide [25].

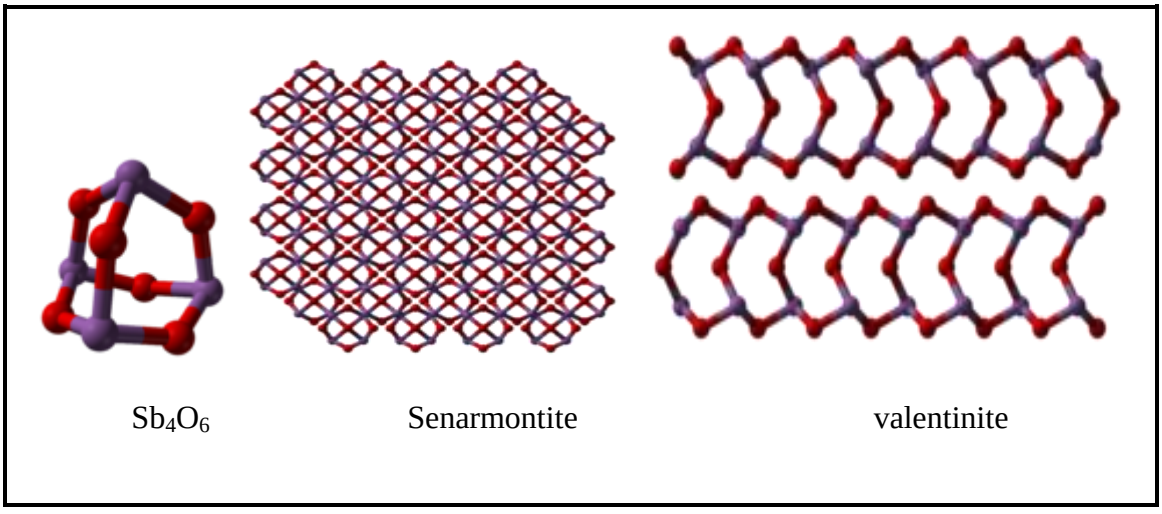

Fig. (1.7): Structure of Sb_2O_3 [26].

Table (1.3): The physical and chemical properties of Sb_2O_3 nanoparticles[27].

Properties	**Sb_2O_3**
Appearance	White solid
Molecular weight(g/mol)	291.52
Density(g/cm^3)	5.2
Melting point ^oC	656
Boiling point ^oC	1425
Crystal structure	Cubic or Orthorhombic
Solubility in water	Insoluble

1.5.2 Ag Nanoparticle

A versatile substance with pharmacological, anti-microbial, conductive, and chemical applications, silver nano powder/nanoparticles appear as colored powders available in various granule sizes and coatings. Susanna can provide silver nano powders ranging from particles of (15) nm to particles measured in millimeters, with various treatments and coatings for all your needs.

Nanoparticles of noble metals have recently become the focus of research because of their unique properties, which are different from those of bulk materials as in table (1.4). These properties depend on the size, shape and differences in the environments of nanoparticles [28]. Silver nanoparticles are generally unstable and tend to grow larger, even in the presence of polymeric stabilizers, especially at high solid [29].

Nano powders dissolve into a variety of solvents, including water, ethanol, and propanol, to produce convenient suspensions. Research continuously reveals new applications of silver nanoparticles in fields including biotech, medicine, electronics, and

manifesting, where it often achieves the same end results as more costly solutions [30, 31].

Table (1.4): The physical and chemical properties of silver nanoparticles [32].

Properties	Silver (Ag)
Atomic number	47
Mass number	107.86
Structure	FCC
Lattice constant (nm)	0.409
Metallic radius (nm)	0.16
Density ($g.cm^{-3}$)	10.5
Melting temperature (°C)	961.8
Boiling temperature (°C)	962
First ionization energy (k J/mol)	731
Electrical conductivity $(Ohm.cm)^{-1}$	62.1×10^{6}

1.6 The Methods of Preparation Polymer Films

There are many methods can be used in preparation thick and thin films as [33]:

a- Casting Method

To prepare a film in the casting method, a certain amount of polymer material dissolved in a suitable solvent as water. The polymer solution applied to a horizontal rotating disc set at a suitable temperature, to obtain a homogeneous solution, the speed of solvent evaporation must reduce and the preparation time must be long and this method has been used in this study where all polymeric materials were casted in (9 cm) diameter petri dishes. Casting is a process in which molten flows by gravity or other force into a mold where it solidifies in the shape of the mold cavity.

There are other techniques can used to prepare the films and thin films as [33]:

b- Spin Coating Method.

c- Dip Coating Method.

d- Sol-Gel Method.

e- Langmuir- Blodgett (LB) Method.

f- Electrochemical Method. .

1.7 Literature Survey

This section includes previous studies by researchers and the results of their works:

In (1984) Lee J. Y., ***et al.***, [34] studied a novel method is proposed of preparing thin Ag–Hg alloy on PAAm film surface at room temperature: The film of interest is formed by holding PAAm aqueous solution with $AgNO_3$ in Hg-saturated atmosphere. Two kinds of films, one of which is a conductor and the other an insulator, can be selectively formed with pH-controlled PAAm solution by ammonia. The conducting surface is assigned to the α phase of Ag–Hg alloy by means of X-ray analysis. Potentio metric titration and IR spectral studies suggest the existence of PAAm–Ag^+ complexes. On the basis of their structure and the oxidation and reduction potential of Ag^+ and Hg^{2+}, the mechanism of film formation is also discussed.

In (1991) Cakmak I., ***et al***.,[35] studied polymerization of acrylamide using Ce(IV) with poly(ethylene glycol) having azo and hydroxyl functions, was carried out to yield acrylamide-(ethylene glycol) block copolymers with labile azo linkages in the main chains. These prepolymers were used to induce the radical polymerization of acrylonitrile and acrylamide through the thermal decomposition of the azo group, resulting in the formation of multiblock copolymers.

In (2001) Park Y. S., ***et al.***,[36] studied solid poly (acrylamide) (PAAm) composite membranes containing silver ions have been investigated for olefin/paraffin separation. The propylene presence increased significantly for a solid PAAm/$AgBF_4$ composite membrane with increasing loading amount of silver ions. Silver ions in solid PAAm

form reversible complexes with propylene, resulting in the facilitated transport of propylene. The propylene selectivity of 100 over propane was obtained when the mole ratio of silver ions to acrylamide unit was 1. This high separation performance would be obtained predominantly because of the high loading of the propylene carrier, silver ions. PAAm-graft/$AgBF_4$ composite membranes were prepared in order to improve the gas permeance. Introduction of PAAm grafts on a polysulfone microporous membrane surface was confirmed by FT-IR spectroscopy.

In (2004) Ma X., ***et al.***, [37] studied the small-scale Sb_2O_3 octahedron can be synthesized via a simple PEG-1000 polymer-assisted hydrothermal pathway (PAHR) in a temperature range of (160–180) °C for (10–14) h. The optical properties of the Sb_2O_3 micro-octahedron were studied by photoelectron spectroscopy. Moreover, the potential growth mechanism of the precisely measured Sb_2O_3 octahedra is discussed on the basis of a series of complementary experiments. It was found that PEG-1000, sodium tartrate, reaction temperature and reaction time have significant effects on the final form of Sb_2O_3, while the pH value has an effect on the formation of Sb_2O_3 crystals.

In (2007) Swamy T. M.,[38] immiscibility studies have been performed on blended solutions of polyacrylamide (PAAm) and polyethylene glycol (PEG) over a wide range of concentrations in water. Ultrasonic refractive index of mixtures were measured for different compositions such as, 0/100, 10/90, 20/80, 30/70, 40/60, 50/50, 60/40, 70/30 and 80 /30, 90/10 and 100/0 of the PAAm/PEG mixture at 30 °C. Reaction parameters such as α were evaluated using viscosity data to verify mixing.

In (2009) Guorong S. and Zhihai C., [39] the concept of two-stage hydro-polymerization is studied and a new polymerization method for the preparation of water-soluble polymers is presented. The phase diagram of the poly(acrylamide)

(PAAm)–poly(ethylene glycol) (PEG)–biphasic system was measured by gel permeability chromatography (GPC). Two aqueous phases of the PAAm-PEG water system can be easily formed. The critical concentration of the phase separation was affected by the molecular weight of PEG. The two-phase hydropolymerization of acrylamide (AAm) was successfully carried out in the presence of PEG using ammonium persulfate (APS) as the initiator.

In (2016) Banerjee S. L., ***et al.***, [40] studied this investigation reports a one pot synthesis of silver nanoparticles (Ag Nps) using aqueous solution of chitosan-graft-poly(acrylamide) (Cts-g-PAAm) as a reducing agent and polyethylene glycol (PEG) as a stabilizing agent. The as synthesized Ag Nps was characterized by ultra violet-visible (UV-Vis), Fourier transform infrared (FT-IR) and X-ray diffraction (XRD) analysis. Field emission scanning electron microscopy (FESEM). The prepared Ag Nps exhibited strong antimicrobial activity against different gram positive bacteria (*Alkaliphilus*, *Bascillus substillis*, *Lysinibascillus*) and gram negative bacteria (*Enterobacter aerogenus*, *Vivbrio vulnificus* and *Escherichia coli*).

In (2017) Hamood F. J., ***et al.***, [41] studied electrical properties for (PVA-PEG-Sb_2O_3) composite material at different frequencies which they ranged from 100 Hz-6 MHz. The PVA-PEG- Sb_2O_3 composite prepared using solution casting method. The experimental results have shown that the dielectric constant (ε) and dielectric loss (δ) decreases with increasing the frequency, it also appeared that ε and δ are increased with the increasing of antimony oxide (Sb_2O_3) content.

In (2017) Xu J., ***et al.***, [42] studied cetyltrimethylammonium bromide, polyethylene glycol (PEG-4000), and their compounds as surfactants, the surface of Sb_2O_3 nanoparticles was modified by mechanical and chemical method based on high-energy ball milling. The microstructures, scattering, and hydrophobicity of Sb_2O_3 nanoparticles were characterized by X-ray diffraction, transmission electron

microscopy, Fourier transform infrared spectroscopy, and surface contact angle measurement. The results showed no obvious change in the crystal structure of Sb_2O_3 nanoparticles after surface modification. The resulting Sb_2O_3 nanoparticles were successfully coated by experimental surfactants.

In (2018) Nadir F. H., ***et al***, [43] studied polyvinyl alcohol polymer was dissolved in water in order to prepare films with different concentration of Fe utilizing casting method. The optical properties were obtained by recording the transmittance spectrum in the wavelength range (300-900) nm. The dispersion parameters were calculated using the Wemple–DiDomenico method. Dispersion energy (E_d) and the single oscillator energy of electronic transition (E_o) were decreased with the increasing of Fe content in the PVA-Fe films. The energy gap decreased from 4.08 eV to 3.52 eV for PVA: 4% Fe film.

In (2021) Fan X., ***et al***, [44] studied the antimicrobial and antiviral behaviors of Ag and Cu nanoparticles (NPs) are well known, and possible mechanisms for their actions, such as released ions, reactive oxygen species (ROS), contact killing, the immunostimulatory effect, and others have been proposed. Ag and Cu NPs, and their derivative NPs, have different antimicrobial capacities and cytotoxicities. Factors, such as size, shape and surface treatment, influence their antimicrobial activities. The biomedical application of antimicrobial Ag and Cu NPs involves coating onto substrates, including textiles, polymers, ceramics, and metals. Because Ag and Cu are immiscible, synthetic AgCu nanoalloys have different microstructures, which impact their antimicrobial effects. When mixed, the combination of Ag and Cu NPs act synergistically, offering substantially enhanced antimicrobial behavior.

In (2021) Liu S., ***et al***, [45] studied a liquid-like but non-toxic polyethylene glycol (PEG) polymer has been attempted as a solvent component of hydrogels. In the mixed PEG-water hybrid solvent, polyacrylamide (PAAm) was polymerized in situ,

overcoming the inevitable water loss caused by the high osmotic pressure of the PEG solution and achieving customized water capacity. Interestingly, the mechanical strength ("soft to hard" transition) and antifreeze properties of aqueous organic gels can be tuned simultaneously over a very wide range by tuning the PEG content. This was because with the increase of PEG in the solvent, the PAAm chains shifted from the stretching to the twisted conformation, while the PEG is attached to water molecules via hydrogen bonds, impairing the crystallization of water at subzero temperature.

In (2021) Al-Shammari A. K. and Al-Bermany E., [46] studied Poly (acrylic acid) (PAA) and poly (acrylamide) (PAAm) were considered as the model polymer in this investigation. These polymers were mixed with poly (vinyl alcohol) (PVA) separately after being dissolved in distilled water (DW) then reinforced with GO applying the developed acoustic-sonication-casting method. The applying method was successfully fabricated the new nanocomposites from mixing these materials for the first time with a ratio of 4.5:4.5:1 wt. % of PAA: PVA: GO and PAAm: PVA: GO as blended polymers and their nanocomposites, respectively. Several characterizations were applied to characterize the new nanocomposites.

In (2021) Al-shammari A. K. and Al-Bermany E., [47] studied Poly (acrylic acid) (PAA) and Poly (acrylamide) (PAAm) were the model polymer. These polymers mixed with Poly (vinyl alcohol) (PVA) separately after dissolved in distilled water (DW) then reinforced with GO applying the developed acoustic-sonication-casting method. The applying method was successfully fabricated the new nanocomposites from these mixed materials for the first time with a ratio of 4.5:4.5:1 wt. % of PAA: PVA: GO and PAAm: PVA: GO as nanocomposites, respectively. The new nanocomposites exhibited homogeneous combinations with an acceptable dispersal of GO in the polymers matrix as presented in the visual microscopy (OM). Coupled with the strong interplay between

polymers in the matrix and the polymer with GO nanoparticles as nanocomposites, Fourier transform infrared (FT-IR) verified the successful preparation of GO.

In (2021) Kadim A. M., ***et al.***, [48] studied Polymer blend films were prepared using dextrin at different compositions of (PVA- PMMA-PAAm) by solvent casting method. The prepared blend films were flexible and transparent and characterized using was examined by scanning electron microscopy to examine the surface morphology of the samples that show the good distribution of starch in the blend, while FT-IR was used to identify the active groups, which refer to the interaction among the materials. Also, we have studied the optical properties and recording the absorption spectrum with a visible ultraviolet spectrophotometer. Absorption spectra were recorded in the wavelength range of 200–1100 nm. The absorbance and optical conductivity were increased by dextrin additive, while the transmittance and energy gap decreased. Based on the overall results, the prepared films can be used in drug delivery and optical devices.

In (2022) Samanta H. S. and Ray S. K. [49] stueied several composite hydrogels were synthesized by free radical crosslink copolymerization of acrylic acid (AA), acrylamide (AM), and N'N-methylene bis acrylamide (MBA, crosslinker) in water in the presence of varied amounts of polyethylene glycol (PEG) and nano sized sodium montmorillonite (NaMMT) clay. The structures of the hydrogels were characterized. The effect of the synthesis and process parameters on the swelling, diffusion, network parameters, and drug release properties of the polymer networks were studied. The hydrogel containing 3.2 wt% NaMMT clay and 24 wt% PEG showed the best equilibrium swelling ratio (33.2 g/g), drug entrapment efficiency (86%), and drug release properties (96.6% in 30 h at pH of 7.4) for a model drug riboflavin. The results indicate a significant improvement of swelling and drug release properties of the polymer in the presence of PEG and NaMMT clay in the gel network.

1.8 Aim of the Work

The goal of the work includes several points, the most important of which are:

1-Synthesis and characterization of the PAAm-PEG blend.

2-The effect addition of the nanoparticles (Ag, Sb_2O_3) on the mixture and study its potential in optical applications.

3-Used dispersion parameter to study the energies and to know the extent of benefit from these films in the applications of optical devices.

2.1 Introduction

This chapter discusses the theory and the mathematical relations used to determine some of the physical properties. These physical properties are classified in general the optical, structure and dispersion parameters.

2.2 Polymer Blends

Polymer blends can be defined as the physical mixtures of two or more photopolymer or copolymers, which interact with secondary forces such as hydrogen bonding with no covalent bonding. Polymer blends are prepared by many methods and among them solution blending is very simple and brisk, and the latter properties of the blends mainly consist on the properties of the constituent polymers and also on the phase morphology developed during blending [50]. The Polymer blends are includes both crystalline and amorphous polymers. The mixing of two chemically dissimilar polymers is miscible or not depends on the thermodynamics of mixing [51].

When any two polymer materials are blended together, or mixed, the properties of the resulting blend depend on the level at which intimate mixing takes place and on whether any chemical reactions between the components of the mixture take place.

The most intimate form of mixing is at the molecular level; two substances that have mixed at this level may each be said to have dissolved in the other. If the molecules have similar sizes, each type of molecule is then surrounded, on average, by molecules of the two types in proportion to the numbers of the two types in the mixture [52].

2.3 Structural and Morphological Characterizations

A wide variety of characterization techniques were used to evaluate the material quality of the thin films before using the films in applications.

2.3.1 Optical Microscopy (OM)

Microscopy studies the enlargement of the image of objects too small to be properly seen by the unaided eye. Microscopy accomplishes its task making use of the radiations emitted, absorbed, transmitted, or reflected by the specimen to be observed as shown in figure (2.1). The nature of the radiation specifies the type of microscopy: electron microscopy, X-ray microscopy, acoustic microscopy, etc. The visible part of electromagnetic spectrum is the type of radiation used by optical microscopy. Historically, optical microscopes were easy to develop and are popular because they use visible light, so samples may be directly observed by the eye [53].

Optical microscopes are designed to create magnified visual or photographic images of small objects as shown in figure (2.1). To accomplish this, the microscopy is designed to perform three tasks: create a magnified image of the sample, distinguish different details of the image, and make the final image visible to the human eye or camera. This class of characterization instruments includes everything from a simple magnifying glass to advanced multi-lens microscopes [54].

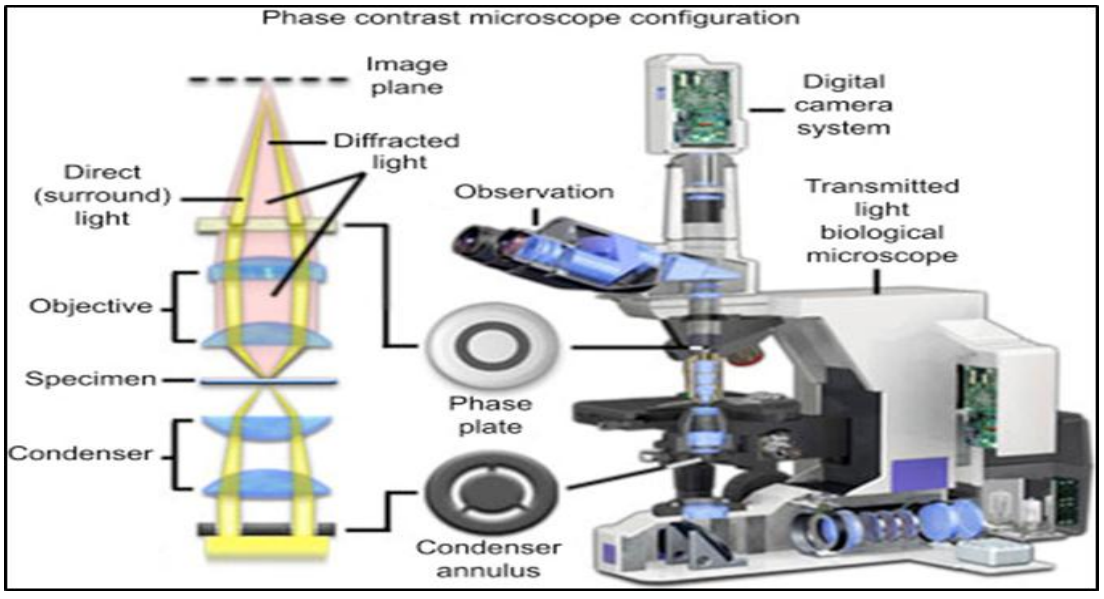

Fig. (2.1): Optical Microscopy [55].

2.3.2 Scanning electron microscope (SEM)

The scanning electron microscope (SEM) is a vital research and manufacturing instrument that is widely utilized in many industries throughout the world. The instrument's appeal stems from the necessity to inspect and gather information about samples whose structure is deteriorating.

The SEM provides a better level of resolution for examination and inspection than existing optical microscope techniques. In addition, unlike the optical microscope, the SEM has a range of analytical modes as in figure (2.2), each of which provides unique information on the physical, chemical, and electrical properties of a certain specimen, device, or circuit. Because of recent advances that eliminate or at least minimize sample degradation and contamination, allowing continuous nondestructive in-process inspection, the SEM is currently finding increased uses in research and production quality control [56].

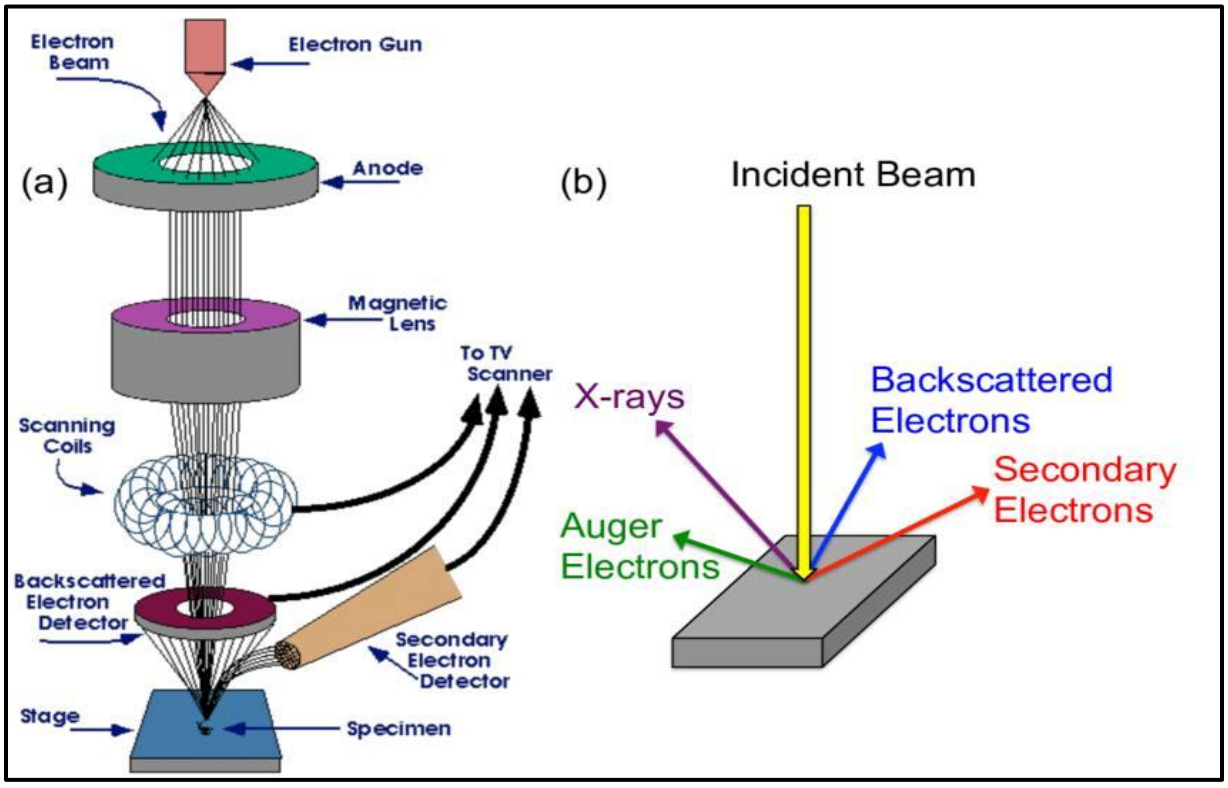

Fig. (2.2): Set-up Illustrates the SEM [57].

2.3.3 Fourier Transforms Infrared (FT-IR) Spectroscopy

Fourier Transforms Infrared (FT-IR) is chemical investigative spectroscopy. This measures the infrared intensity with light wavenumber. The wavenumbers consist of infrared light that is divided into three regions, far-infrared, mid-infrared and near-infrared, which are between (4 ~ 400) cm^{-1}, between (400 ~ 4.000) cm^{-1}, and finally, between (4.000 ~ 14.000) cm^{-1}, respectively [58].

The permissible of this technology depends on detects the chemical functional group's vibration in a sample. Where the chemical bonds will stretch when the interaction happened between the infrared light and the matter. Here, the infrared radiation is absorbed by the chemical functional group at a specific range of wavenumber irrespective of the rest of the molecule structure [58]. More complex molecules have more than one bond and different types of vibrations may occur. Vibrations fall into the two main categories of bending and stretching. Figure (2.3) shown structure devices.

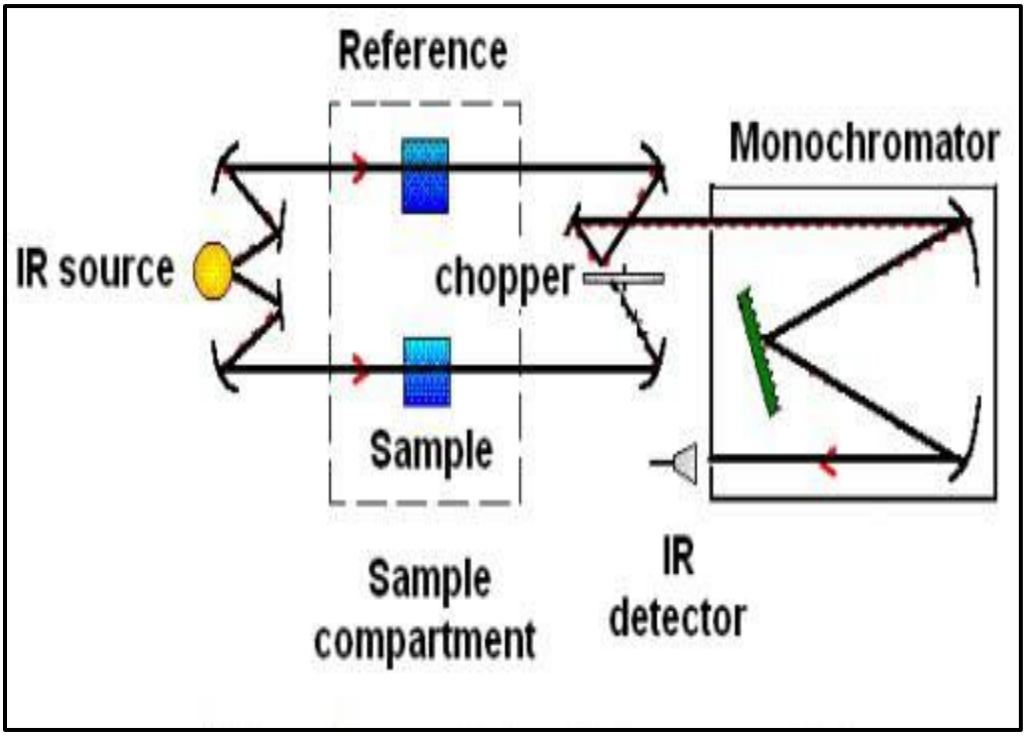

Fig. (2.3): Schematic Illustration of the FT-IR System [58].

2.4 The Optical Properties

Optical properties of polymers constitute an important aspect in study of electronic transition and the possibility of their application as optical filters, a cover in solar collection, selection surfaces and green house [59]. The optical properties of materials can be defined as any property that involves the interaction between electromagnetic radiation and light with the matter, including absorption, polarization, reflection, and scattering effects [60].

The optical constants fully describe the optical behavior of materials; they are important and fundamental properties of matter. Knowledge of optical constant of a film from a given material is basic importance in determining the characteristics of light transmission in the film. Such knowledge of the optical parameters of the material is importance when designing devices through which electromagnetic radiation absorbed or transmitted.

Study of the optical properties of polymers increases our knowledge of the type of polymer internal structure, nature of the bonds and expands the potential scope of polymer application. Knowing the spectrums of absorption and transmittance of a polymer assist in identifying many optical properties in different ranges of wavelengths. Conducting examination at the ultraviolet spectrum range enables us to know the type of the bonds, orbital and energy beams. The study at the visible spectrum range provides sufficient information about the behavior of a matter to solar applications. The study at the infrared range is very important in knowing the general structure of a polymer and the elements consisting its chemical structure [61].

2.4.1 Reflectivity

Reflectivity can be obtained from absorption and transmission spectrum in accordance to the law of conservation of energy by the relation [62]:

$$R+T+A=1 \qquad (2.1)$$

where:

R: is the reflectivity, T: is the transmittance and A: is the absorbance.

2.4.2 Absorbance (A)

The ratio of absorbed light intensity (I_A) by substance to incident light intensity (I_o) is known as absorption [63].

$$\mathbf{A} = \frac{\mathbf{I_A}}{\mathbf{I_o}} \qquad (2.2)$$

2.4.3 Transmittance (T)

Dividing the intensity of the rays transmitting from the film (I_T) over the intensity of the incident rays on it (I_o) is called transmittance (T) and given in equation (2.3) [64]:

$$\mathbf{T} = \frac{\mathbf{I_T}}{\mathbf{I_o}} \qquad (2.3)$$

2.4.4 Optical Constants

There are many ways to find the optical constants of absorption coefficient, refractive index, extinction coefficient and optical conductivity

2.4.4.1 The Absorption Coefficient

Is defined as a ratio decrement in incident ray energy flux relative to distance unit in the direction of incident wave diffusion. The absorption coefficient (α) is determined by incident photon energy (hυ), material characteristics where electronic transitions are type (n) or (p), and forbidden energy gap gives the following equation [65].

$$\mathbf{E = h\upsilon} \qquad (2.4)$$

When incident photon energy is less than the forbidden energy gap, then photon will be transmitted and transmittance gives the following equation [65]:

$$\mathbf{T_r = (1 - R)^2 \, . e^{-\alpha t}} \qquad \textbf{(2.5)}$$

If the intensity of incident ray (I_o) that incident on blend film material of thickness (t), the intensity of transmittance ray (I) gives by Beer Lambert law.

$$\mathbf{I = I_0 \, e^{(-\alpha t)}} \qquad \textbf{(2.6)}$$

The absorption coefficient is measured by cm^{-1}.

$$\mathbf{\alpha t = 2.303 \log \frac{I}{I_0}} \qquad \textbf{(2.7)}$$

where the amount of log (I/I_o) represents the absorbance (A).

The absorption coefficient can be calculated using the following equation: [66]

$$\mathbf{\alpha = 2.303 \left(\frac{A}{t}\right)} \qquad \textbf{(2.8)}$$

where (t) represent a thickness of sample.

2.4.4.2 Refractive Index (n)

It is the ratio of light speed in vacuum to its speed in a medium. This index shows how far a matter is affected by the electromagnetic waves. The refraction index consists of two parts: real and imaginary. It can be expressed by the following equation [64].

$$\mathbf{n = c/v} \qquad \textbf{(2.9)}$$

Where (n) is the refraction index, (c) is the light speed in vacuum and (v) is the light speed in matter. Reflectance (R) can also be defined as the ration of the reflected ray relation at the borderline between two mediums to the incident ray. The relation between reflectivity and refractive index is shown in the following equation [64].

$$\mathbf{R = (n - 1)^2 + k_o^2 / (n+1)^2 + k_o^2} \qquad \textbf{(2.10)}$$

where (k_o) is the extinction coefficient.

The rate of absorption of light is directly proportional to the intensity of the incident light at a specific wavelength, and this physical phenomenon is common and lead to the decay of the light intensity exponential as it passes.

Refractive index can be expressed by the following equation [64]:

$$n = [4R/(R-1)^2 - k_o^2]^{1/2} + (R+1)/(R-1) \qquad (2.11)$$

2.4.4.3 Extinction coefficient (k_o)

The coefficient of inertia represents the amount of photons absorbed by the membrane, that is, the energy absorbed by the electrons of the material, and expresses the following relation [67]:

$$k_o = \alpha\lambda/4\pi \qquad (2.12)$$

Where (λ) is the wavelength of the incident radiation and (α) absorption coefficient.

2.4.4.4 Optical Conductivity

The optical conductivity (σ_{op}) has been determined from the following equation[68]:

$$\sigma_{op} = \alpha_{op} \frac{nc}{4\pi} \qquad (2.13)$$

where α_{op} is the absorption coefficient.

2.4.5 Absorption Regions

Absorption regions can be classified to three regions as in figure (2.4):

A) High absorption region: the absorption coefficient value in this area is about ($\alpha \geq 10^4$ cm^{-1}) and obeys tauce equation [69].

B) Exponential region: the absorption coefficient value in this area is about Urbach equation $1<\alpha<10^4$ cm^{-1} [70].

C) Low absorption region: the absorption coefficient value in this area is about ($\alpha < 10^{-4}cm^{-1}$)) [71].

2.5 Electronic Transitions

There are two basic forms of electronic transition: direct and indirect transition.

2.5.1 Direct Transitions

This kind of transitions occurs in semi-conductors, where the bottom of the conduction is precisely above the top of the valance band, thus implying that they share similar wave vector values i.e. ($\Delta K= 0$). In such a case, the absorption would occur at ($h\upsilon = E_g^{opt}$.). Therefore, the phonons do not take part in direct transition since the phonon's wave vector (K) is much greater than that of the photons. This transition type requires the laws of conservation in momentum and energy. The direct photon transition to the energy of the minimum gap reaches no satisfaction of the demand for conserving the wave vector, as the photon wave vectors could be neglected in the given energy range [72]. There are two kinds of direct transitions [73].

2.5.1.1 Direct Allowed Transition

This transition occurs from the top points in the (V.B.) and the bottom point in the (C.B.), as shown in figure (2.4 a) [74].

2.5.1.2 Direct Forbidden Transitions

This transition occurs from near top points of (V.B.) and the bottom points of (C.B.), as shown in figure (2.4 b).

The absorption coefficient for this type of transition is equal to [74]:

$$\alpha h\upsilon = B(h\upsilon - E_g^{opt})^r \qquad (2.14)$$

Where E_g energy gap between direct transition .

B: the constant depended on the type of material

r: the exponential constant, its value depended on type of transition.

r =1/2 for the allowed direct transition.

r =3/2 for the forbidden direct transition.

2.5.2 Indirect Transitions

In these transitions type, the bottom of (C.B.) is not over the top of (V.B.), in curve (E-K). The electron transits from (V.B.) to (C.B.) is not perpendicularly when the value of the electron's wave vector before and after the transition is not equal ($\Delta K \neq 0$), this transition type occurs with the help of a particle named Phonon. For conservation of the energy and momentum law. Indirect transitions are classified into two types [75], they are:

2.5.2.1 Allowed Indirect Transitions

This type of transition occurs in a different region of K-space that is the electrons transmitted between the V.B. top and the C.B. bottom, as exposed in figure (2.4 c).

2.5.2.2 Forbidden Indirect Transitions

Forbidden indirect transitions are displayed between the nearest points in the top and the bottom of the valance and conductive bands respectively, as shown in figure (2.4 d).

The equation (2.15) gives the transition absorption coefficient and the phonon absorption [76]:

$$\boldsymbol{\alpha h\upsilon = B(h\upsilon - E_g{}^{opt} \pm E_{ph})^r} \qquad \textbf{(2.15)}$$

E_{ph}. is the phonon energy, where the sing (-) applied when phonon absorption, whereas the sing (+), used when phonon mission. The exponential constant is represented as r in the equation, in which its value is determined by the transition r=2 and r=3 for the allowed indirect, and forbidden indirect transitions, respectively.

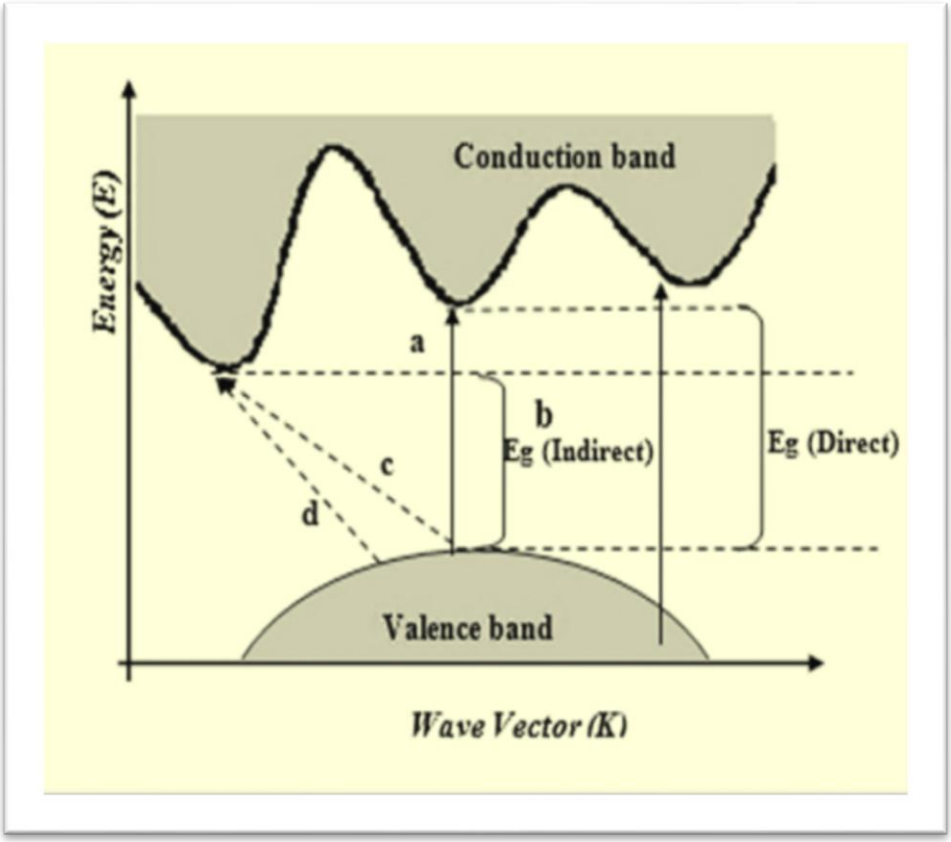

Fig. (2.4): The Electronic Transitions Types

(a) Allowed Direct Transition (b) Forbidden Direct Transition,

(c) Allowed Indirect Transition and (d) Forbidden Indirect Transition [76].

2.6 Dispersion Energy Parameters

Energy dispersion parameters have an important role in identifying the characteristics of the optical material. As through them one can calculate the necessary factors required designing the optical communication and the spectral dispersion devices.Wemple–DiDomenico (WDD) single effective oscillator Model successfully describes the dispersion of the refractive index [71-77]. This model has an advantage in fitting the experimental data because it provides an intuitive physical interpretation of the measured quantities [78]. The main outputs of this model are the energy of the effective single oscillator (E_o) and the dispersion energy (E_d).

The energy (E_o) or sometimes called average energy gap gives quantitative information on the overall band structure of the material. It must be taken into consideration that, the information obtained from E_o is completely different from those obtained from the optical energy gap (E_g). Optical energy gap is related to the optical properties near the fundamental absorption edge of the material. In spite of the difference between E_o and E_g, yet there is an approximate empirical equation. Showing that the oscillator energy, E_o is often twice the optical energy gap, E_g i.e. ($E_o \approx 2E_g$) [77].

On the other hand, the dispersion energy E_d, which represents oscillator strength, measures the average energy of interbank optical transitions and is associated with adjustment in the structural order of the sample i.e., it is related to the ionicity, anion valence and cordnation number of the material. It is worth to mention here that, the dispersion energy, (E_d) is very nearly independent on the effective single oscillator energy (E_o). This is because (E_d) is proportional to the dielectric loss, while (E_o) does not rely on the dielectric loss, either close or from afar. According to (WDD) model, the relationship between (E_o, E_d) and the incident photon energy (hυ) is given as follows [76, 79]:

$$(n^2 - 1) = \frac{E_d E_0}{{E_0}^2 - (h\nu)^2} \qquad \textbf{(2.16)}$$

where:

n: refractive index

E_o: the energy of the effective single oscillator

E_d: the dispersion energy

hυ :incident photon energy

The moments of optical spectra (M_{-1} and M_{-3}) can be calculate from the relations [68]:

$$E_o^2 = \frac{M_{-1}}{M_{-3}} \qquad \textbf{(2.17)}$$

$$E_d^2 = \frac{M^3 - 1}{M_{-3}} \qquad (2.18)$$

2.7 Thickness Measurement

Thickness is one of the most important parameters of thin films because it largely determines the properties of the film. The thickness of the membranes is usually measured by digital micrometer the resulting with a thickness range (120) μm.

2.8 The Materials Conductivity

Solid-state materials, according to their conductivities, can be classified into three classes: conductors, semiconductors, and insulators. At room temperature, the conductor has conductivities between (10^8-10^3) $\Omega^{-1}cm^{-1}$, semiconductor between (10^3-10^{-8}) Ω^{-1} cm^{-1}, and insulator between (10^{-8}-10^{-18}) Ω^{-1} cm^{-1} [80]. According to the atomic arrangement of solid, the materials can be divided into three types known as crystalline, polycrystalline and non-crystalline (or amorphous) solids [81].

In crystalline solid, the atoms or molecules have a regular geometric arrangement or periodicity. These solids have a high degree of ordering, and thus have long range order (L.R.O.) in three dimensions, as shown in figure (2.5.a).

The polycrystalline materials have a high degree of ordering over many small regions. These regions are called grains and they are separated from one and another by grain boundaries. These materials are characterized by short range order (S.R.O.) as shown in fig. (2.5.b). The amorphous materials have ordering only within a few atomic or molecular, as shown in fig. (2.5.c).

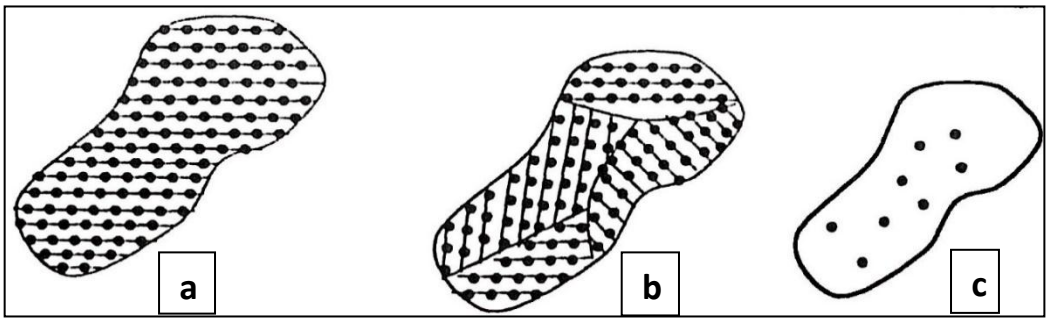

Fig. (2.5): Schematics of Three General Types of Solids [82]:

a) Single Crystalline, b) Polycrystalline and c) Non crystalline (amorphous).

2.9 Density

Density is the mass of a unit volume of a material substance. The formula for density is:

$$d = m/V \qquad (2.19)$$

where d is density, m is mass, and V is volume. Density is commonly expressed in units of grams per cubic centimeter [82].

3.1 Introduction

This chapter is devoted to the experimental part, which plays an important role in determining the results. Where films are prepared (PAAm –PEG- Sb_2O_3, Ag) by casting method as figure (3.1). Then the optical and structure measurements and dispersion parameters.

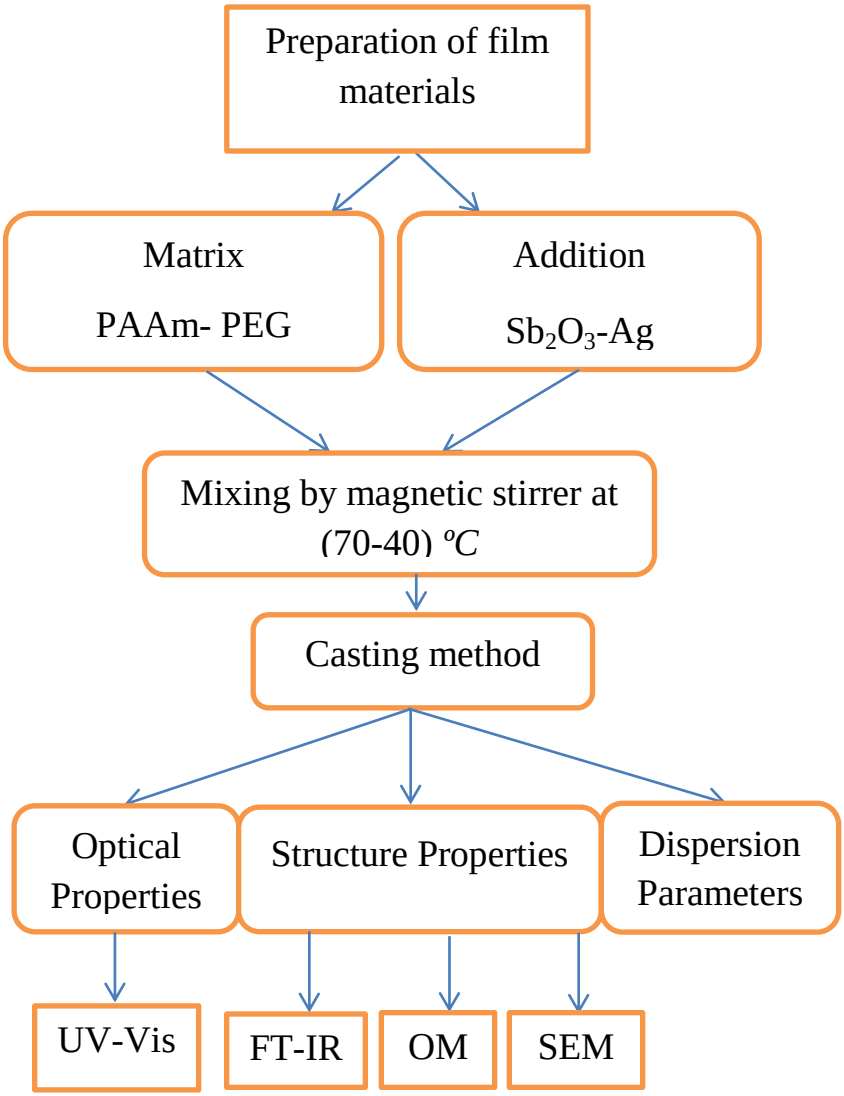

Fig. (3.1): Scheme of experimental part.

3.2 Utilized Materials

The utilized materials in this study are:

3.2.1 Matrix two types of polymers were used in this work:

3.2.1.1 Polyacrylamide (PAAm)

The polymer was used in a white granular form soluble in distilled water, and its molecular weight was (5×10^6 g/mol), with high purity (99.99%). It is manufactured by a company (Central Drug Houses (CDH)).

3.2.1.2 Polyethylene glycol (PEG)

The polymer was used in a white granular form soluble in water, was purchased from EMPROVE ESSENTAL Ph Eur with molecular weight was (4000) and purity (99%).

3.2.2 Additions

Two types of materials were used in this work:

3.2.2.1 Antimony (III) Oxide of (Sb_2O_3)

Molar mass (291.92) g/mol the appearance (the basis is frosted white) density (5.76) g/cm^3 melting point (656)°C boiling point (1425)°C, insoluble in water purchased from US Research Nanomaterials, Inc.

3.2.2.2 Silver (Ag)

Silver nanoparticles (Ag): was obtained in powder form and was obtained from (Sky Spring Nano materials, Lnc) with average grain size (20-30) nm and high purity (99.95 %).

3.3 Preparation Procedures (Preparation of (PAAm-PEG-Ag, Sb_2O_3))

The micro casing was prepared by casting method from polymer blend by adding the weight percentages of the additives that were (2, 4 and 6) by wt.% of (Ag, Sb_2O_3) to the (PAAm-PEG) mixture as shown in table (3.1) in (60) mL, of distilled water using a magnetic stirrer for a two hour mixing process at a temperature of (70-40) °C until a highly homogeneous polymer solution is formed. These homogenous solutions are poured into a petri dish of diameter (9 cm). The entire assembly is placed in a dust-free room and the solvent is allowed to work slowly it evaporates in air at room temperature for 10 days. Then it is peeled from the petri plate using a micrometer. The thickness of these films was measured and found to be within (120±3) micrometers.

Table (3.1): Weight percentages for (PAAm-PEG-Ag, Sb_2O_3) nanocomposites.

PAAm (g)	**PEG (g)**	**(Ag, Sb_2O_3)(g)**
0.75	0.25	0
0.73	0.24	0.02
0.72	0.24	0.04
0.70	0.23	0.06

3.4 Part of Principle Measurements

Types of instruments used in this study:

3.4.1 Optical Microscopy (OM)

The change of surface morphology samples of (PAAm-PEG-Ag), (PAAm-PEG-Sb_2O_3)composites are examined using the optical microscope, which was supplied from Olympus name (Top View) type (Nikon-73346), equipped with light intensity automatic

controlled camera under magnification (40x,100x), it is implemented in the university of Babylon /college of education for pure sciences/ department of physics.

3.4.2 Field Emission Scanning Electron Microscope (SEM)

FESEM (Zeiss Sigma 300- HV) GERMANY. Examination was carried out in Iran / Tehran / University of Tehran

3.4.3 Fourier Transform Infrared Spectroscopy (FT-IR)

FT-IR spectra were recorded by FTIR (Bruker Company, German origin, type vertex 70). FT-IR was implemented at University of Babylon /College of Education for Pure Sciences/Department of Physics. In this study, the considered wavenumber range (WNR) is (400-4000) cm^{-1}.

3.4.4 Ultraviolet-Visible Spectrophotometer (UV-Vis)

Computerized spectrophotometer, it is used to determine the absorption of light from a sample. The sample is placed in specific position of UV / Vis device. The double beam spectrophotometer (Shimadzu model UV-1800A^{o} (JAPAN) was used to record the absorption spectrum of (PAAm-PEG-Ag), (PAAm-PEG-Sb_2O_3) composites in the wave-length range (200-1100) nm. It is located at the University of Babylon /College of Education for Pure Sciences/Department of Physics.

4.1 Introduction

This chapter contains the results and discussion of the structural and optical properties of the (PAAm-PEG) blend before and after adding different weights of nanoparticles (Sb_2O_3, Ag) that prepared by casting method at room temperature. The structural properties, such as OM, SEM, FT-IR, optical properties and dispersion parameters.

4.2 Structural Properties

In this paragraph several measurements are included:

4.2.1 Optical Microscope

The current study conducted an experiment to dissolve 1 g of PAAm-PEG and cast it in a (9) cm diameter petri dish, using the same method of preparation, and get a very fragile film was formed with cohesion but we got the complete melt as shown in Figure (4.1).

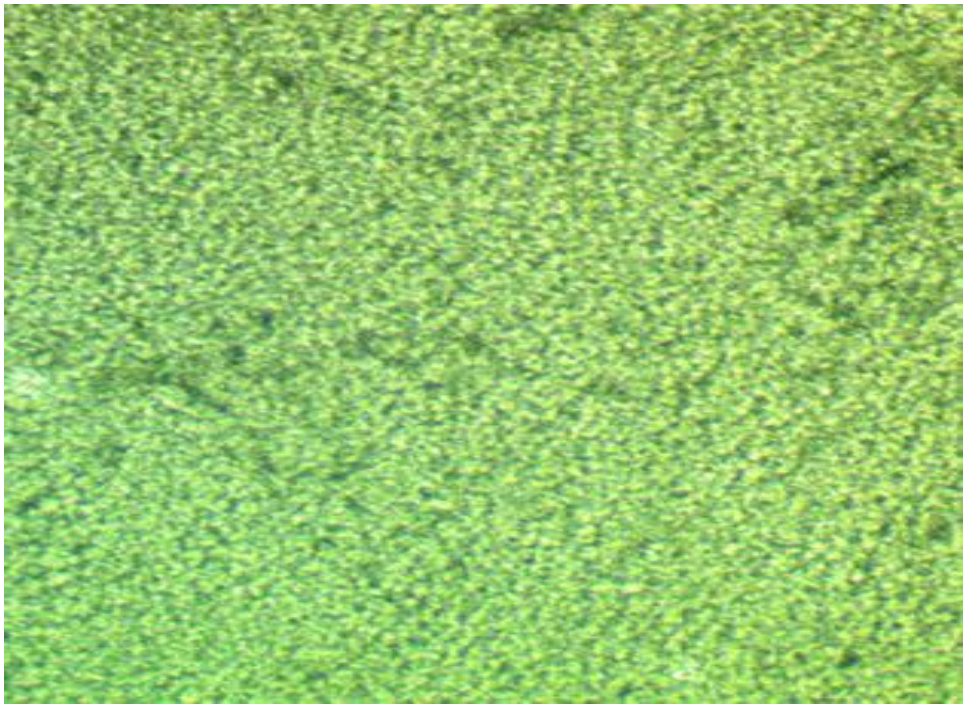

Fig. (4.1): Photomicrographs (100X) of (PAAm-PEG) blend.

Figure (4.2) shows the images of nanocomposite films (PAAm-PEG-Sb_2O_3) and Figure (4.3) shows the images of nanocomposite (PAAm-PEG-Ag), taken from samples with different concentrations at a magnification of 100X. (a, b and c), these images illustrated fine homogeneity of the matrix with a good distribution of (Sb_2O_3, Ag), Nps into the polymer composites. The OM images exhibited a successful preparation of the (PAAm-PEG-Sb_2O_3, Ag) nanocomposites as in the fig. (4.3). The fine distribution was considerably got better with increasing the ratio of the NPs in (PAAm-PEG) films; where the additions are in different ratios (0.02, 0.04 and 0.06) the nanoparticles form a continuous network inside the polymers. This network contains pathways in which charge carriers are allowed to pass through the pathways, causing material properties to change [83, 84]. This is consistent with the researchers' findings [85, 86].

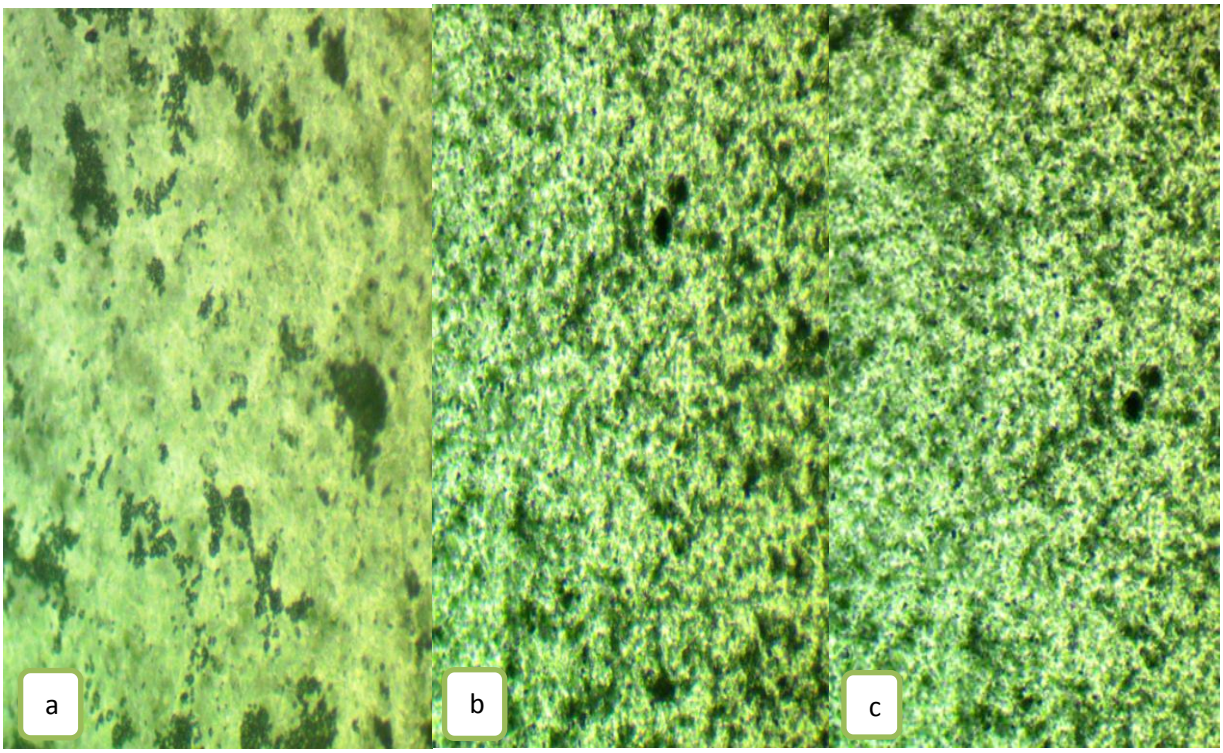

Fig. (4.2): Photomicrographs (100X) of nanocomposites a) PAAm-PEG :2wt.% Sb_2O_3 b) PAAm-PEG:4wt.% Sb_2O_3, and c) PAAm-PEG:6wt.% Sb_2O_3.

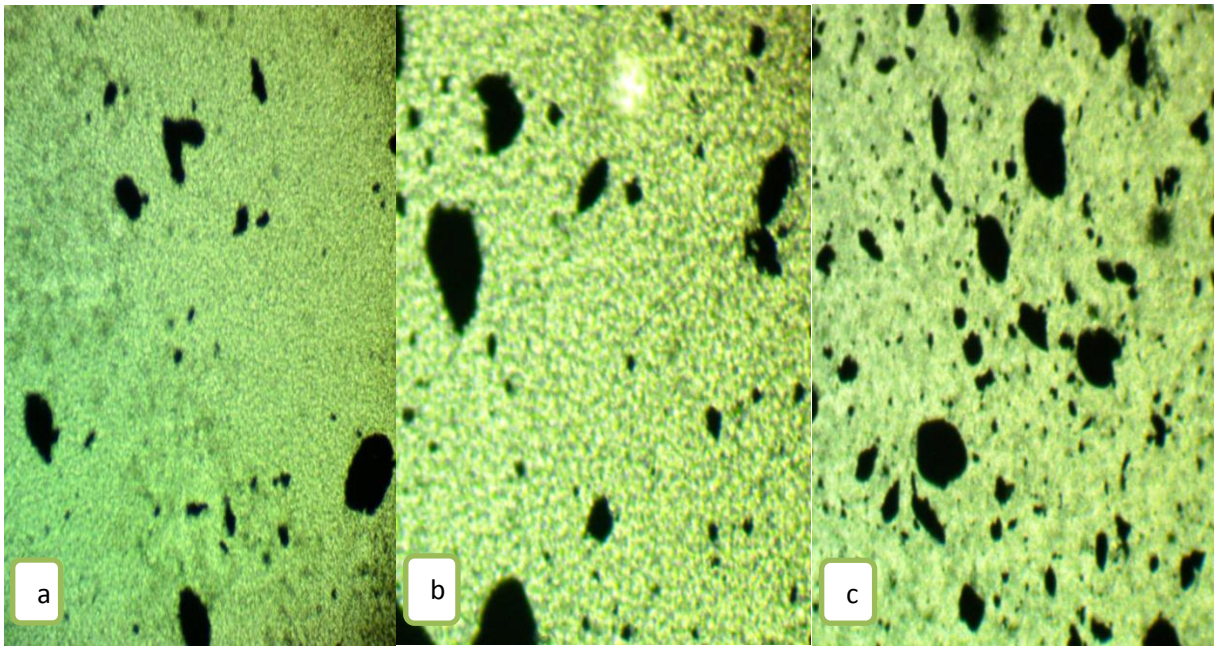

Fig. (4.3): Photomicrographs (100X) of nanocomposites a) PAAm-PEG :2wt.% Ag b) PAAm-PEG:4wt.%Ag, and c) PAAm-PEG:6wt.%Ag.

4.2.2 Scanning Electron Microscope Measurements (SEM)

SEM was used to fully investigate the effect of nanoparticles content and examine the dispersion of the particles in the polymer matrix and the interaction or agglomeration amony the nanoparticles. Figure (4.4) shows typical SEM images of PAAm-PEG films without nanomaterial concentrations where the polymers are softer, more homogeneous and cohesive.

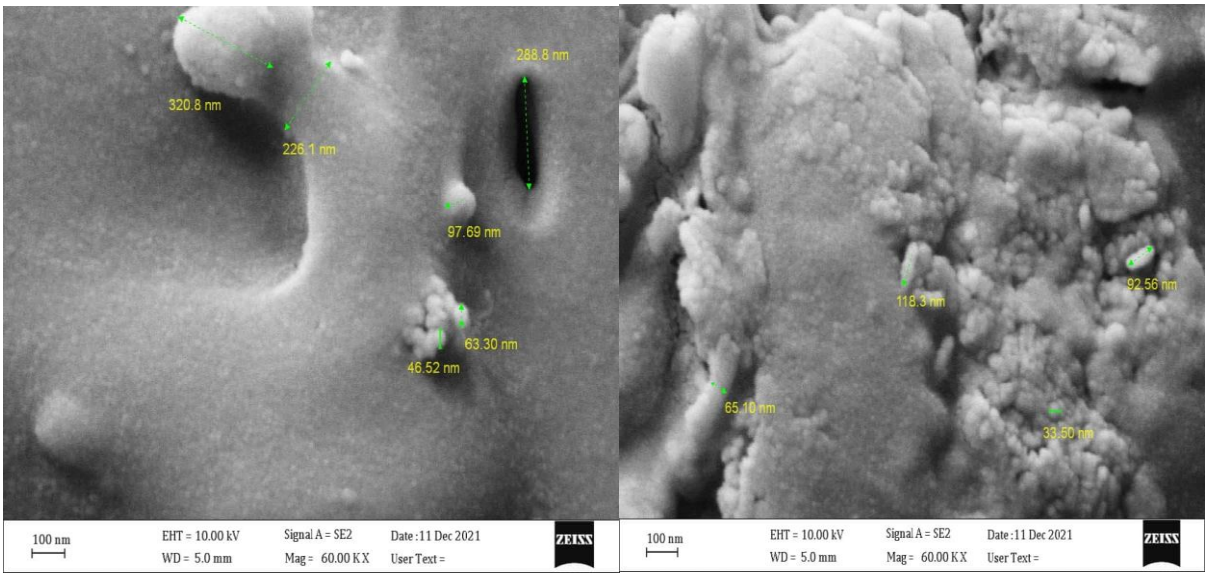

Fig. (4.4): SEM images of PAAm-PEG Blend.

Figures (4.5 and 4.6) show typical SEM images of films of (PAAm-PEG-Ag, Sb_2O_3) nanocomposites with different concentrations of (Ag, Sb_2O_3) Nps content. It is evident that the addition of nanoparticles in the nanocomposites (PAAm-PEG-Ag, Sb_2O_3) show changes in the surface morphology of this system. It can be seen from the images that the grains accumulate as the percentage of nanoparticles increases. The surface morphology of the nanocomposites (PAAm-PEG-Ag, Sb_2O_3) films shows many randomly distributed aggregates or pieces on the upper surface. The results show an increase in the number of white dots on the surface with increasing concentration of nanoparticles (Ag, Sb_2O_3). The films display a uniform density of grain distribution in the surface morphology. The results indicate that nanoparticles tend to form well-dispersed aggregates in PAAm-PEG composite films. From figures (4.5) and (4.6), it is understood that (Ag, Sb_2O_3) nanoparticles are randomly distributed in (PAAm-PEG) membranes and it is concluded that small agglomerates are formed in these membranes and make the films more fine [87]. These results are in agreement with [88].

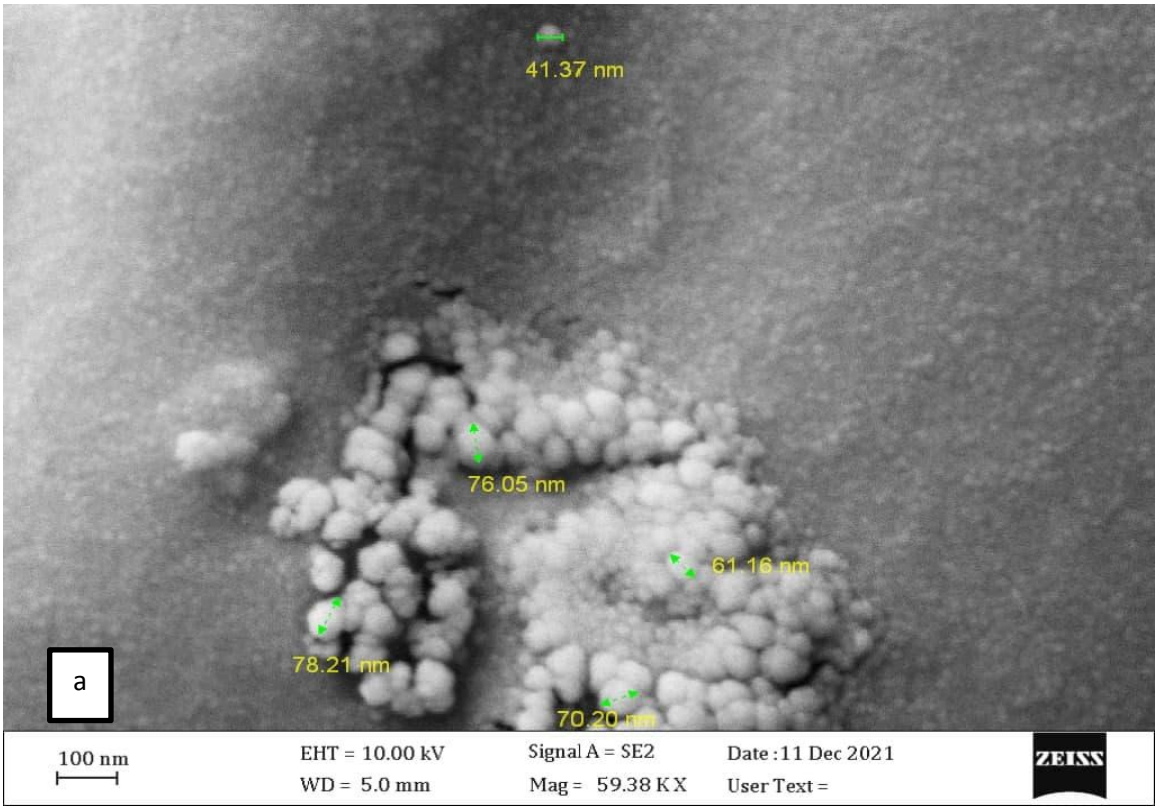
41.37 nm
76.05 nm
61.16 nm
78.21 nm
70.20 nm
a
100 nm
EHT = 10.00 kV
WD = 5.0 mm
Signal A = SE2
Mag = 59.38 K X
Date :11 Dec 2021
User Text =
ZEISS

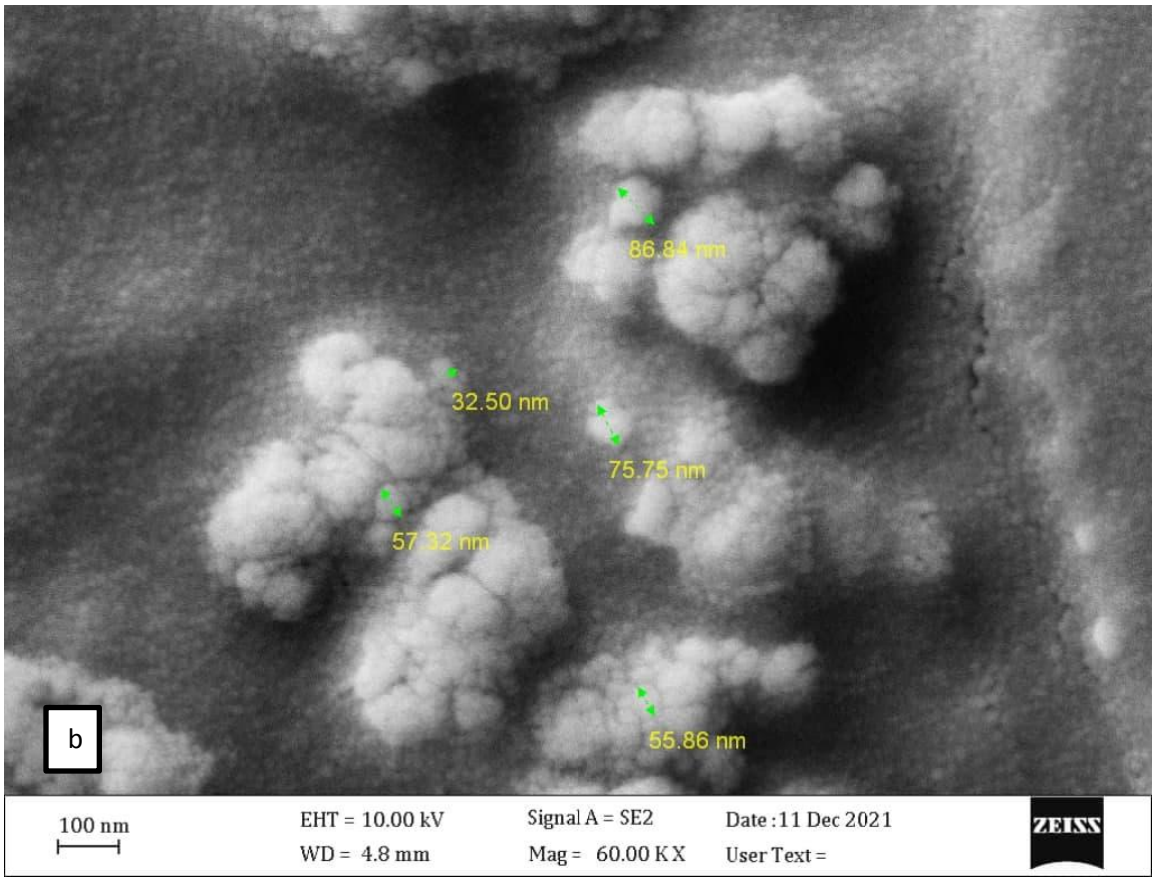
86.84 nm
32.50 nm
75.75 nm
57.32 nm
55.86 nm
b
100 nm
EHT = 10.00 kV
WD = 4.8 mm
Signal A = SE2
Mag = 60.00 K X
Date :11 Dec 2021
User Text =
ZEISS

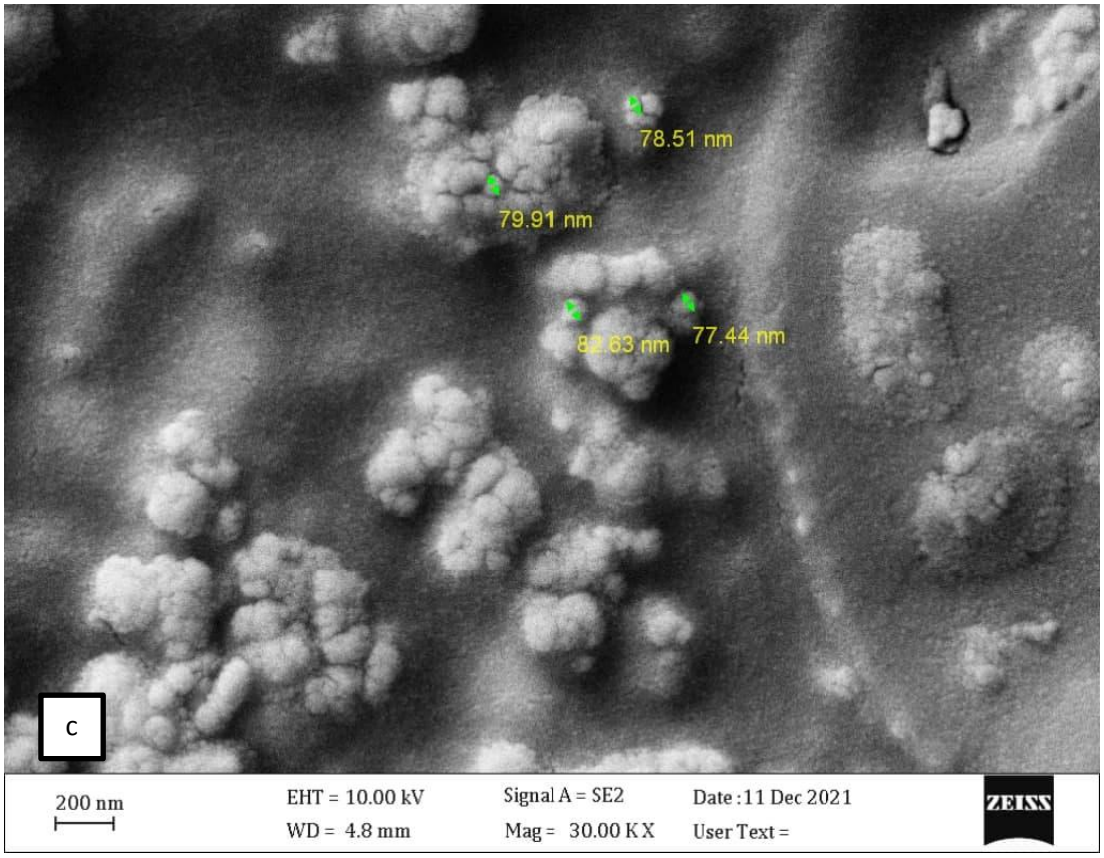
78.51 nm
79.91 nm
82.63 nm
77.44 nm
c
200 nm
EHT = 10.00 kV
WD = 4.8 mm
Signal A = SE2
Mag = 30.00 K X
Date :11 Dec 2021
User Text =
ZEISS

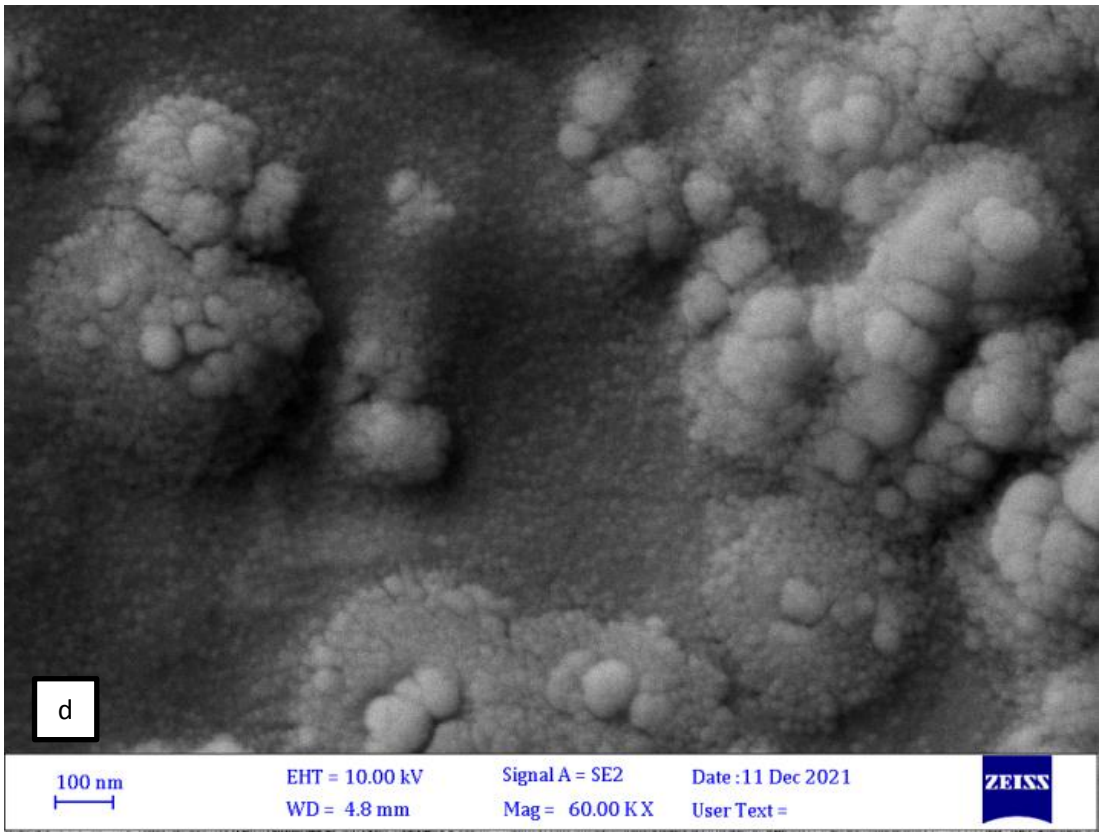
d
100 nm
EHT = 10.00 kV
WD = 4.8 mm
Signal A = SE2
Mag = 60.00 K X
Date :11 Dec 2021
User Text =
ZEISS

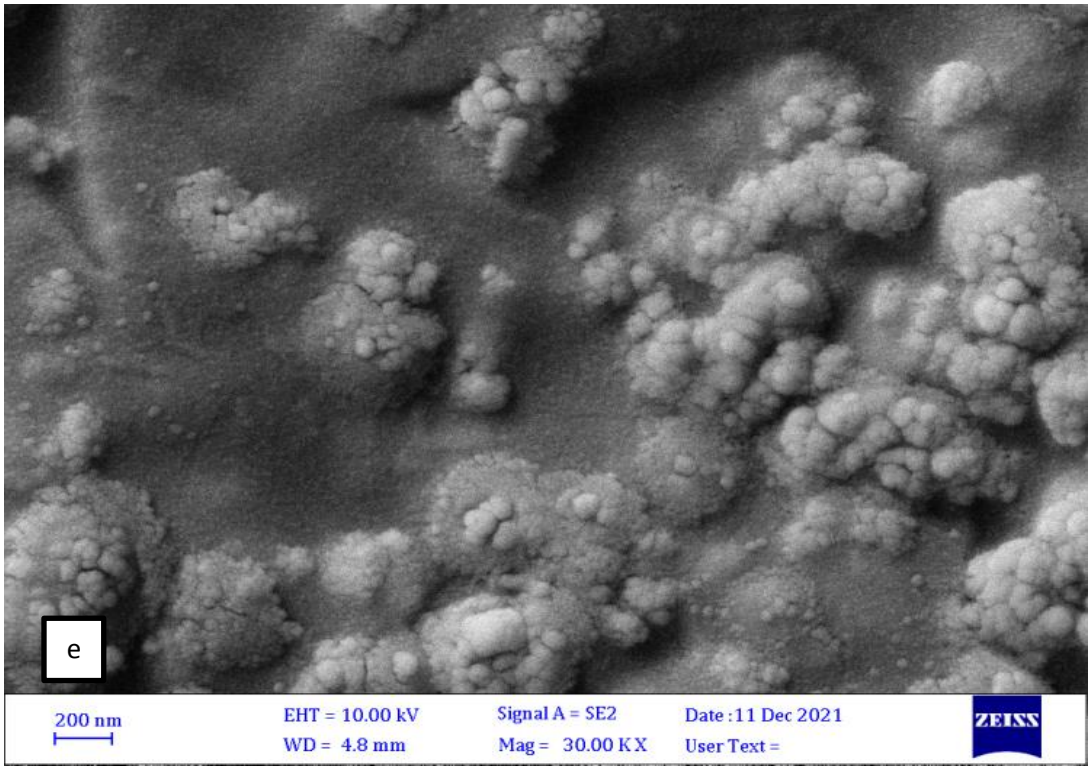

Fig. (4.5): SEM images of PAAm-PEG-Ag nanocompesite of (a): (2wt.%) Ag, (b) and (c): (4wt.%) Ag, (d) and (e): (6wt.%) Ag.

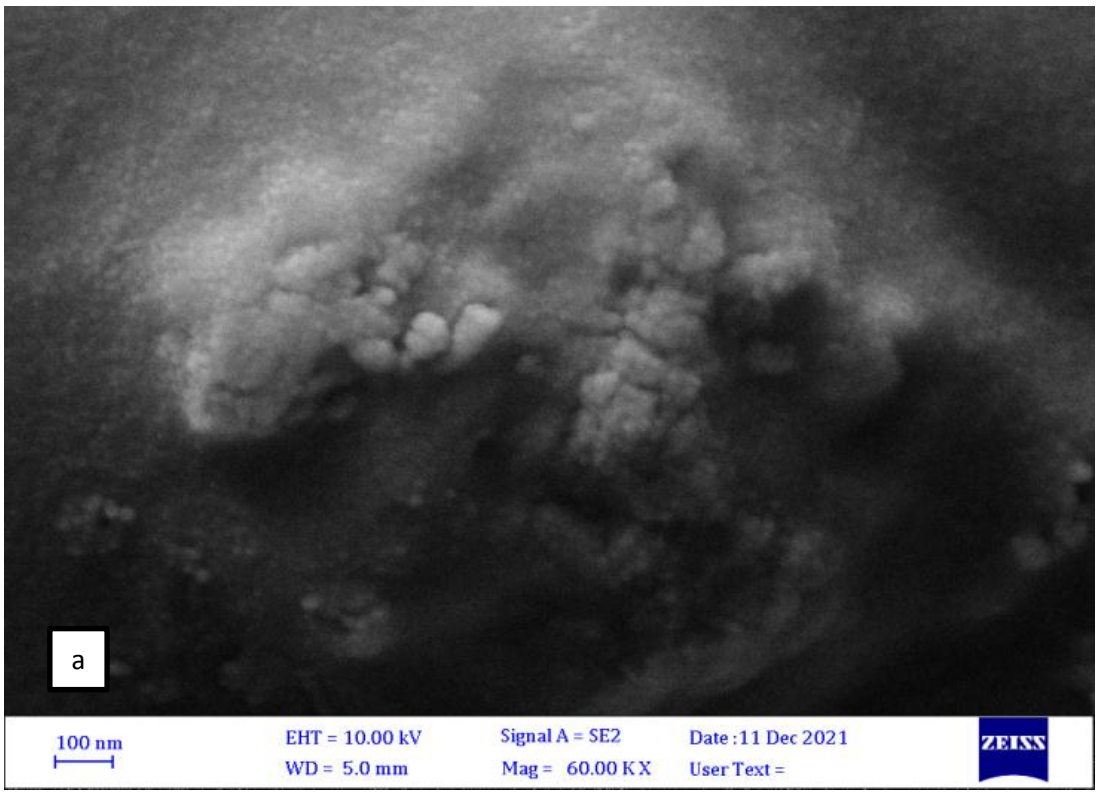

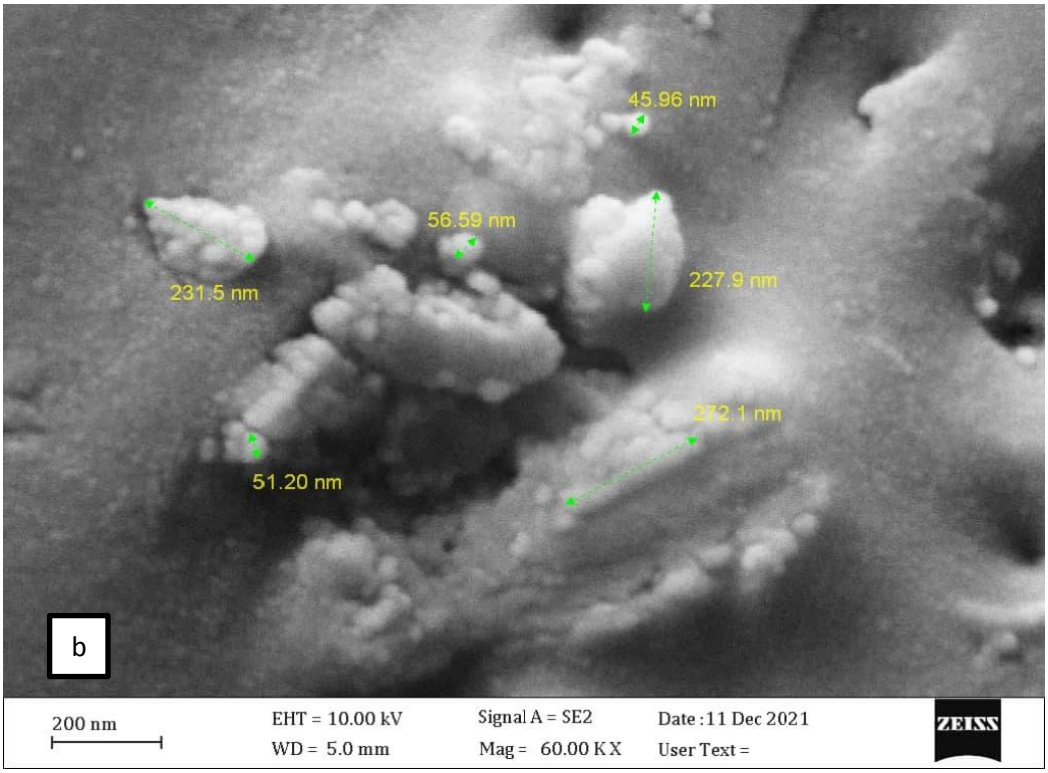

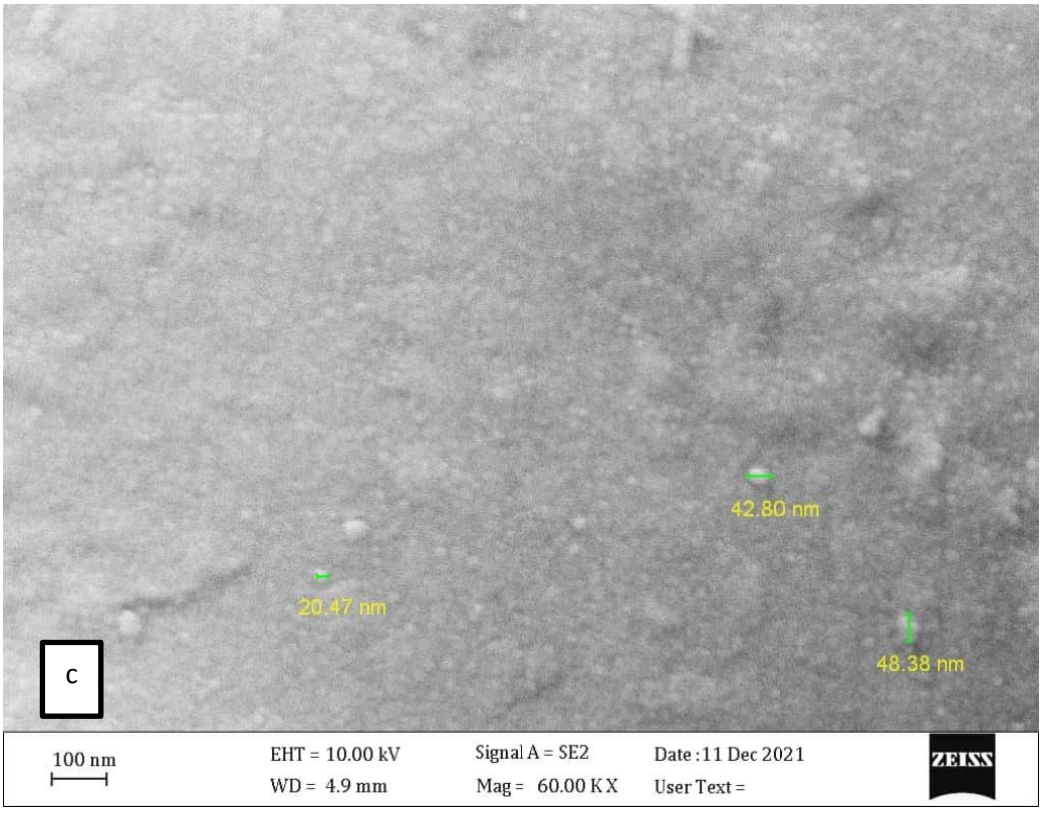

Fig. (4.6): SEM images of PAAm-PEG-Sb_2O_3 nanocompesite of (a): (2wt.%) Sb_2O_3, (b): (4wt.%) Sb_2O_3, (c): (6wt.%) Sb_2O_3.

4.2.3 Fourier Transform Infrared Rays (FT-IR)

FT-IR spectroscopy is an important technique for the investigation of polymer structure, as it provides information about the complication and interactions between the various constituents in the polymer complexes [89]. Reveals Fourier Transforms Infrared Spectroscopy analysis of (PAAm-PEG) blend at room temperature in the frequency region of (500–4000) cm^{-1}. The main function of using FT-IR is to evaluate the type of chemical bonding between different phases that are present, examine if there is a chemical reaction occurs or it is merely physical blending and qualitatively analyze the materials, which are in the bulk of films. All spectra exhibit the characteristic absorption bands of pure (PAAm-PEG) composite, which are (2886, 1648, 1455, 1341, 1108, 962 and 842) cm^{-1}. It can be noticed that these treatment cause some observable changes in the spectral features of the samples a part from new absorption bands and slight changes in the intensities of some absorption bands. The new bands may be correlated likewise to defects induced by the charge transfer reaction between the polymer chains. The vibrational peaks at (2886, 1648, 1455, 1341, 1108, 962 and 842) cm^{-1} are assigned to O-H stretching, C-H stretching, C= O stretching, C= C stretching, and C-O-C rocking of (PAAm-PEG) composite respectively as shown in Figure (4.7).

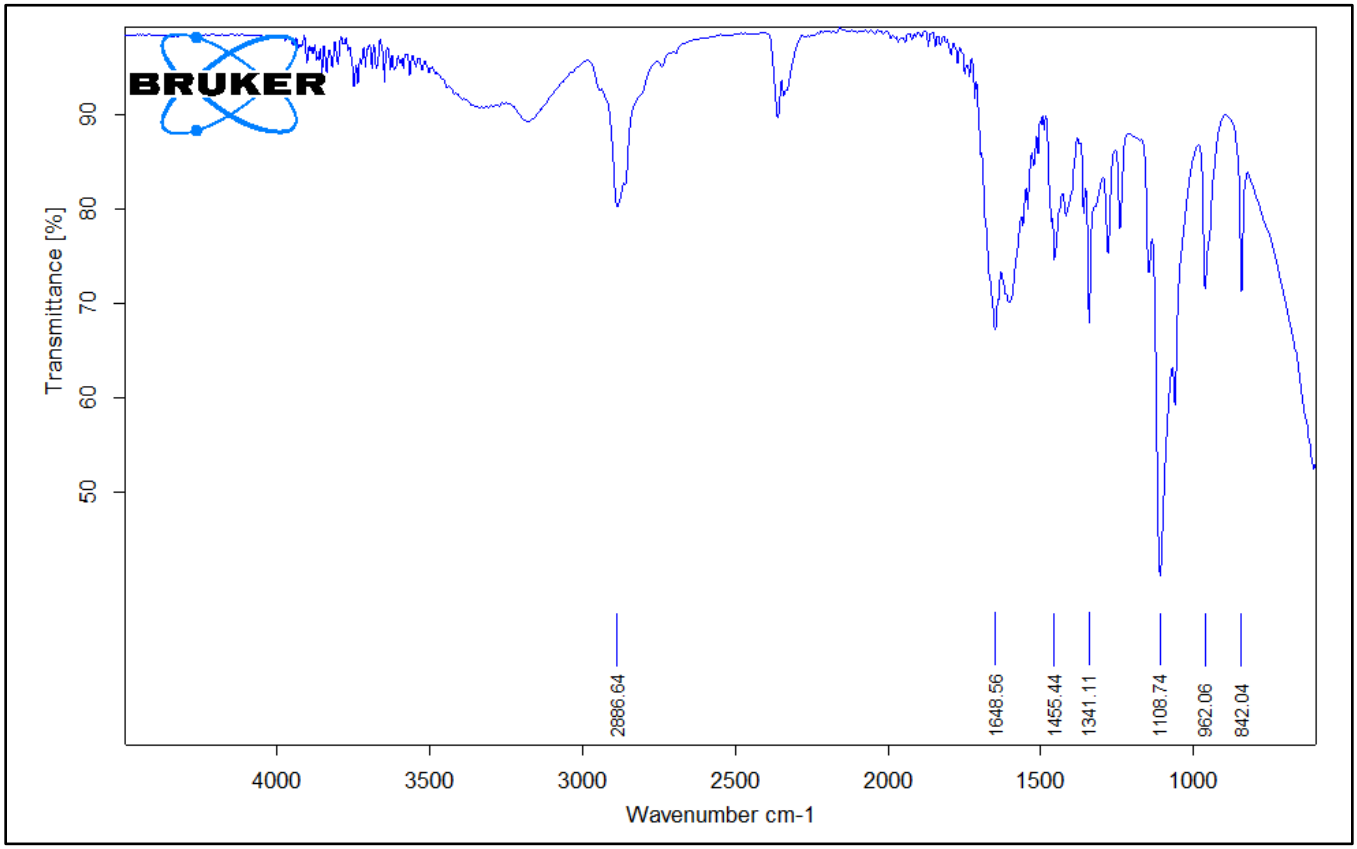

Fig. (4.7): FT-IR of (PAAm-PEG) blend.

The experimental data given in the Figures (4.8-4.10) after addition (Ag) nanoparticles with different percentages (0.02, 0.04, 0.06), some polymer chains have been broken and some other chains have been formed instead as shown in the table (4.1).

We notice through (FT-IR), if an (Ag) nanoparticle is present in films (PAAm-PEG-Ag) nanocomposites it leads to restriction of molecular vibrational motion, and special vibrational motion at three dimensions for (PAAm-PEG) composite and will most probably be affected by IR energy. This restricted of molecular polymers move reason occurrence apparent distortion for some the parts functional for polymers (functional groups); therefore, that films nanocomposites has characteristic nano approximately being restricted [90], as shown in figures (4.8-4.10). The Fourier transform infrared spectroscopy (FT-IR) spectra of pure (PAAm-PEG) and doped (Ag) nanoparticles films are in agreement with [91].

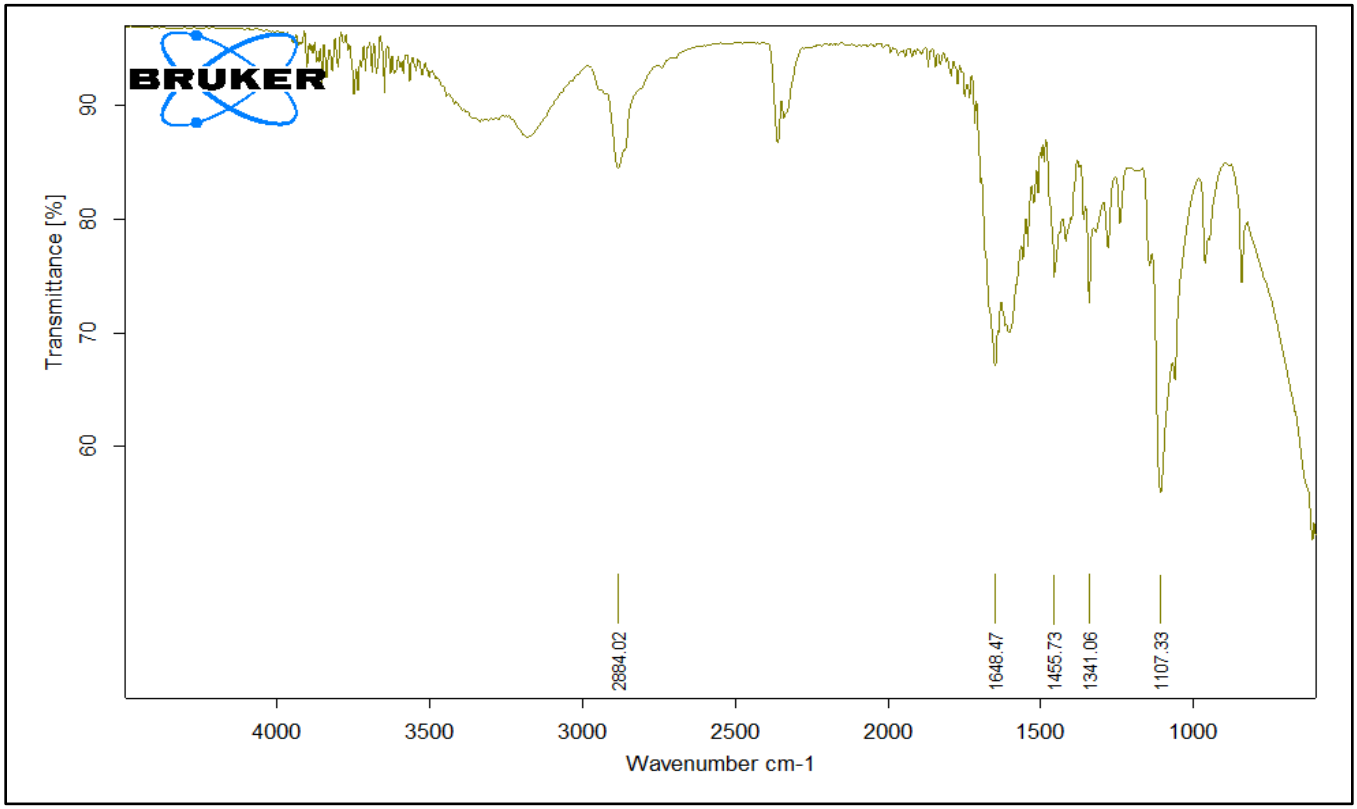

Fig. (4.8): FT-IR of (PAAm-PEG-Ag) nanocomposites for (2wt. %) Ag.

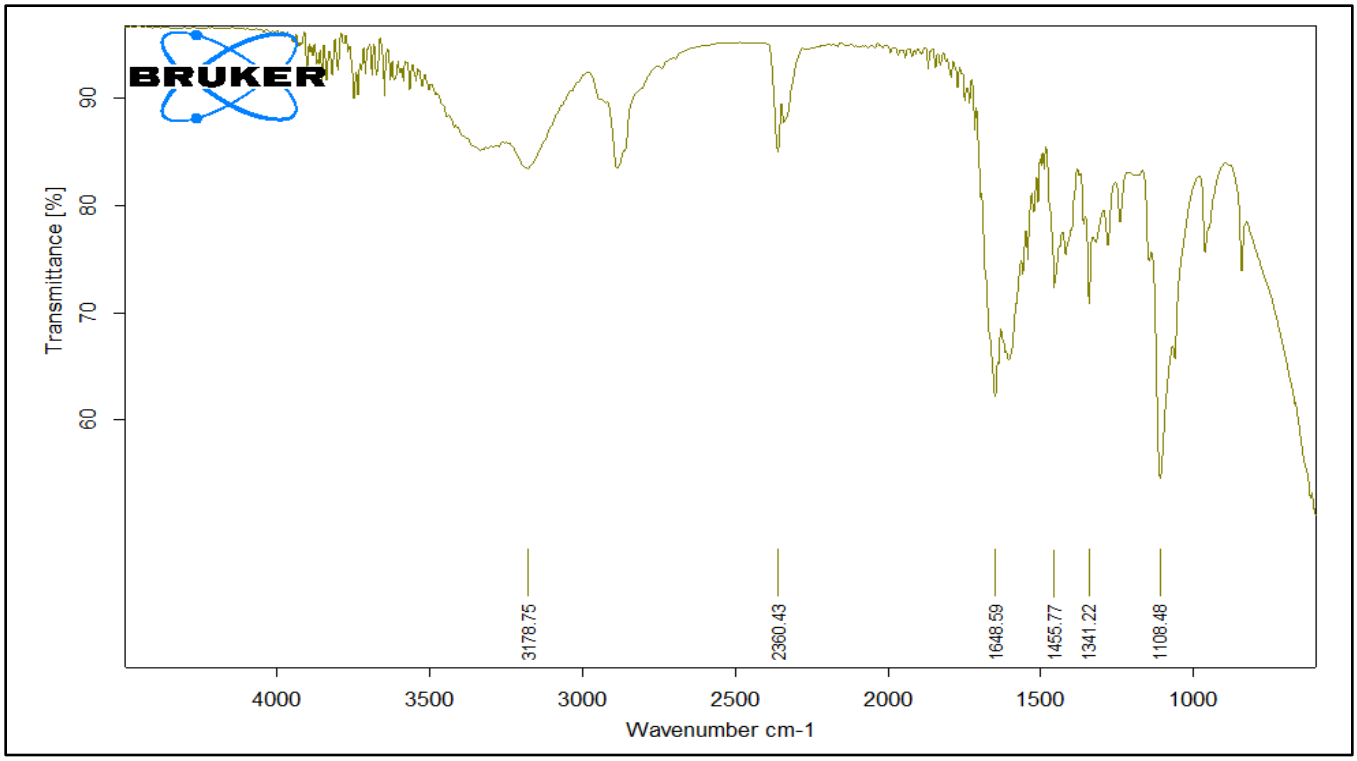

Fig. (4.9): FT-IR of (PAAm-PEG-Ag) nanocomposites for(4wt.%) Ag.

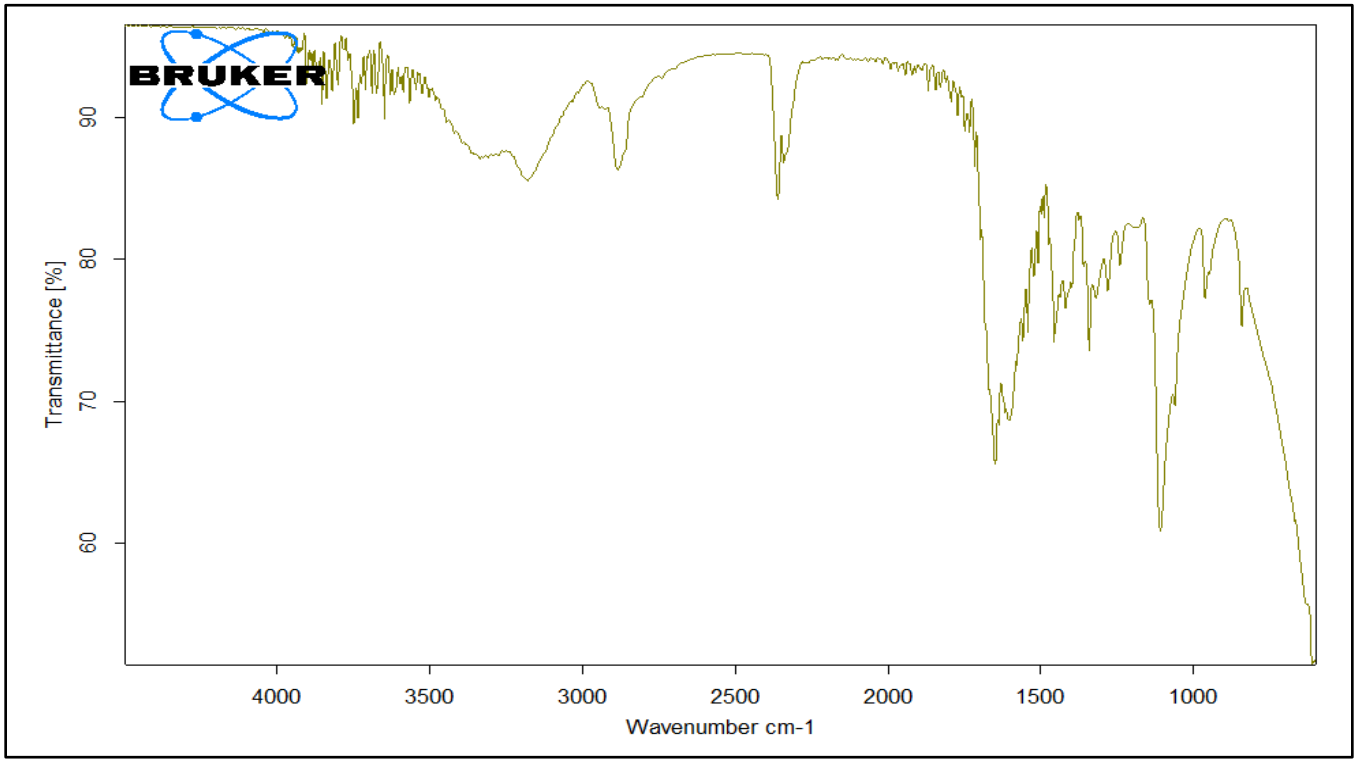

Fig. (4.10): FT-IR of (PAAm-PEG-Ag) nanocomposites for (6wt.%) Ag.

Table (4.1): FT-IR transmittance bands positions and their assignments for (PAAm-PEG-Ag) films with different ratio of Ag nanocomposites.

Ratio	2 wt. % Ag	4 wt. % Ag	6 wt. % Ag
Assignments	2884 (C-H)	3178 (O-H)	2886 (O-H)
	1648 (C=C)	2360 (C≡C)	1648 (C-H)
	1455 (C-N)	1648 (C=C)	1455 (C=O)
	1341 (C-N)	1455 (C-N)	1341 (C=C)
	1107 (C-O)	1341 (C-N)	1108(C-O)
		1108 (C-O)	

Adding (Sb_2O_3) with different weight (0.02, 0.04 and 0.06)g to basis material (PAAm-PEG) leads to increase in the number of bonds per unit area and hence density

increases as shown in the table (4.2), which led to increases the absorbance values, therefore decrease the value of transmittance as shown in Figure (4.11 - 4.13).

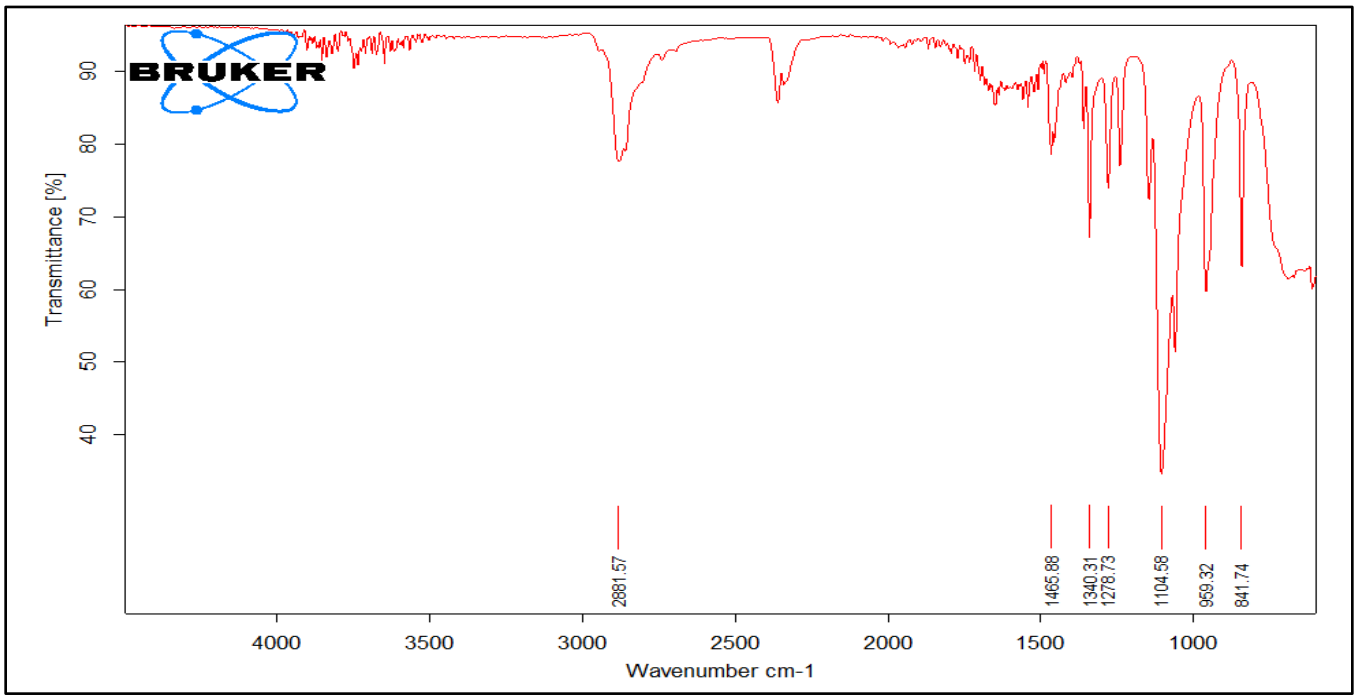

Fig. (4.11): FT-IR of (PAAm-PEG-Sb_2O_3) nanocomposites of (0.02wt.% Sb_2O_3).

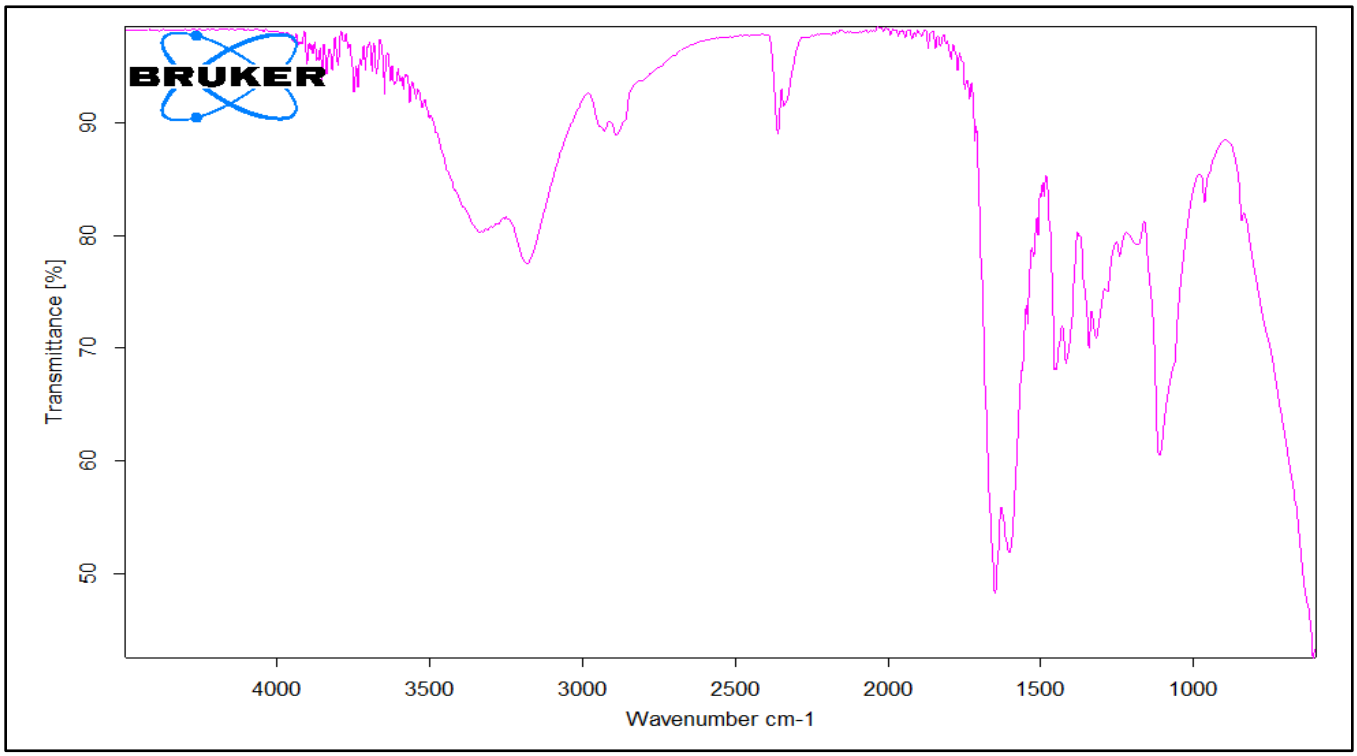

Fig. (4.12): FT-IR of (PAAm-PEG-Sb_2O_3) nanocomposites of (0.04wt.% Sb_2O_3)

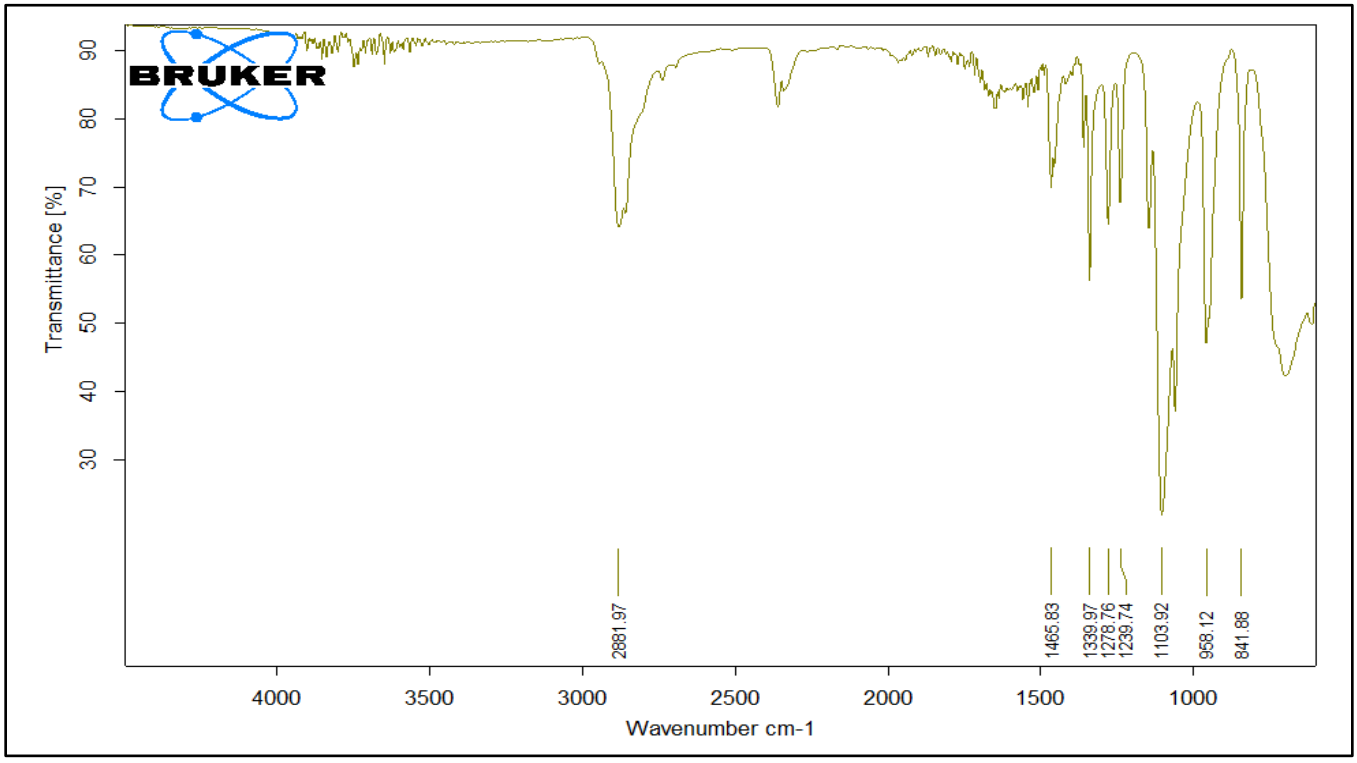

Fig. (4.13): FT-IR of (PAAm-PEG-Sb_2O_3) nanocomposites of (0.06wt.% Sb_2O_3)

Table (4.2): FT-IR transmittance bands positions and their assignments for (PAAm-PEG- Sb_2O_3) films with different ratio of Sb_2O_3 nanocomposites.

Ratio	2 wt.% Sb_2O_3	4 wt.% Sb_2O_3	6 wt.% Sb_2O_3
Assignments	2881 (C-H)	3300 (N-H)	2881 (O-H)
	1456 (C-N)	2390 (C≡N)	1456 (C-N)
	1340 (C-N)	1648 (C=C)	1339 (C-N)
	1278 (C-O)	1450 (C-N)	1278 (C-O)
	1104 (C-O)	1405 (C-N)	1239 (C-O)
	959 (C-C)	1255 (C-O)	1103 (C-O)
	841 (C-C)	1150 (C-O)	958 (C-C)

4.3 The Optical Properties

The main purpose of studying the optical properties of the (PAAm-PEG- Ag, Sb_2O_3) nanocomposites is to identify the effect of adding the (Ag, Sb_2O_3) nanoparticles on the optical properties.

The research covers the recording of the spectrum of absorbance for the (PAAm-PEG-Ag, Sb_2O_3) films at the room temperature and calculating the transmittance, absorption coefficient, extinction coefficient and other optical constants ,as well as identifying the types of electronic transitions and calculating the energy gaps.

4.3.1 Absorbance (A)

Figures (4.14 and 4.15) show the absorption spectrum of (PAAm-PEG-Ag, Sb_2O_3) nanocomposites as a function of the wavelength of the incident light. It can be noticed from the figure that the absorbance for all films have a high values at wavelength in the neighborhood of the fundamental absorption edge (250)nm, then the absorbance decreases with the increasing of wavelength. In general, the absorbance of the films has low values in the visible and near infrared region. This behavior can be explained as follows: at high wavelength the incident photons doesn't have enough energy to interact with atoms. Thus the photon will be transmitted, when the wavelength decreases, the interaction between incident photon and material will occur, and then the absorbance will increase [92].

In other words absorb the incident light by the free electrons. Consequently, by the increase of the weight percentages of nanoparticles, absorbance is increased. These results are similar to the results reached by the researchers [93, 94]. We notice an increase in the absorbance when adding Ag compared to adding Sb_2O_3.

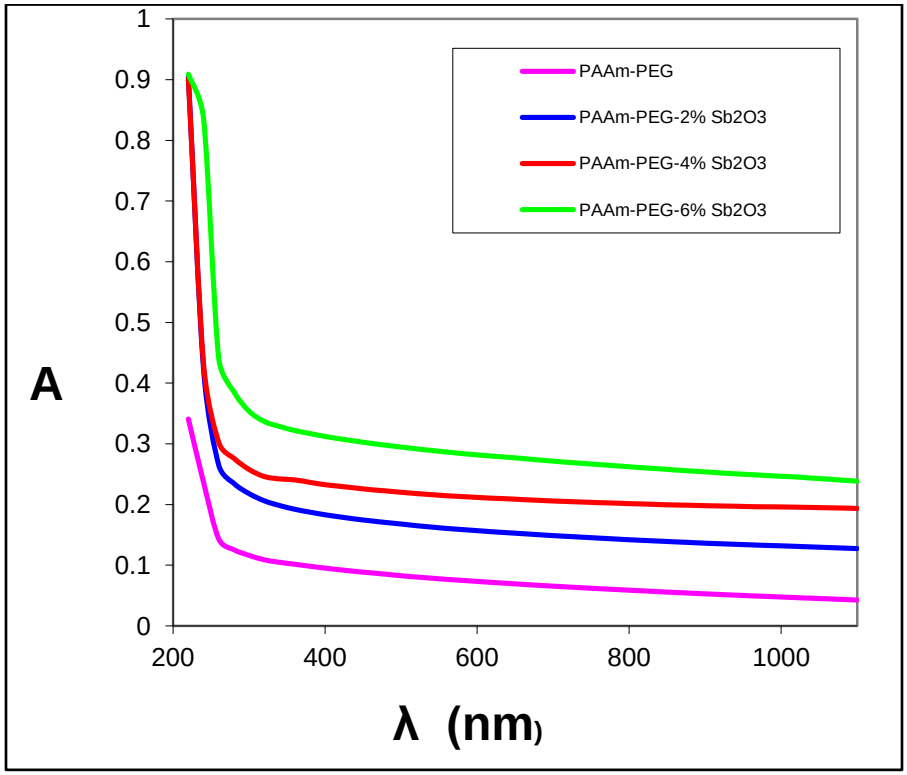

Fig. (4.14): Absorbance Behavior of (PAAm-PEG-Sb_2O_3)

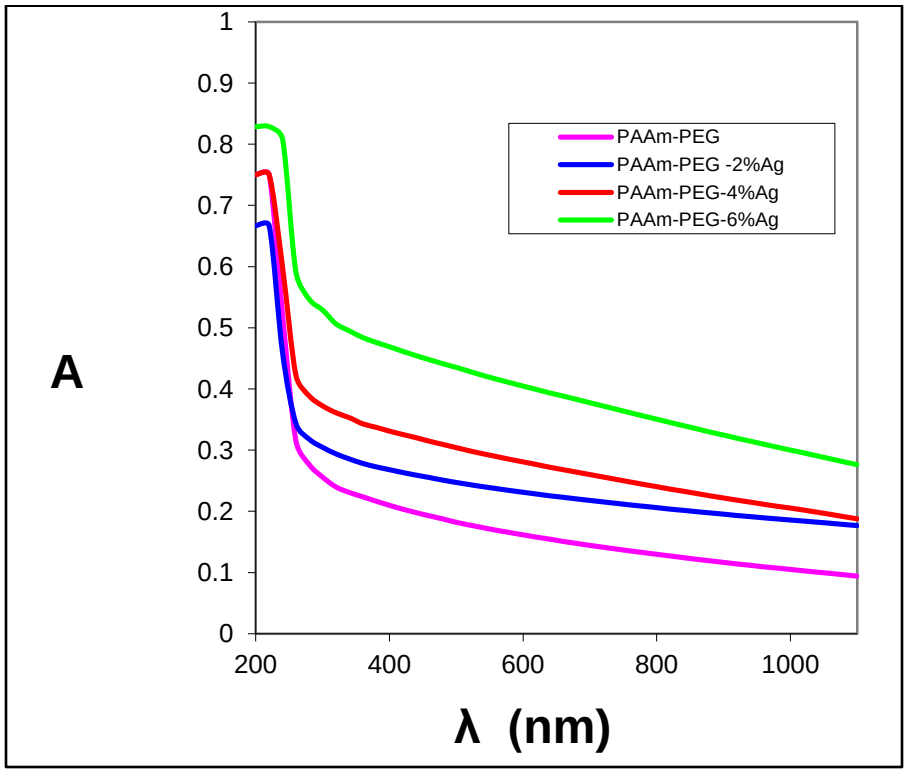

Fig. (4.15): Absorbance Behavior of (PAAm-PEG-Ag).

4.3.2 Transmittance (T)

Figures (4.16 and 4.17) show the optical transmittance spectra as a function of wavelength of incident light on (PAAm-PEG- Ag, Sb_2O_3) films with different rate of (Ag, Sb_2O_3) nanoparticles. The figures show that transmittance decrease with the increase concentration of nanoparticles, this is caused by the added (Ag, Sb_2O_3)nanoparticles contains electrons in it's outer orbits can be absorb the electromagnetic energy of the incident light and travel to higher energy levels, this process is not accompanied by emission of radiation because the traveled electron to higher levels have occupied vacant positions of energy bands, thus part of the incident light is absorbed by the substance and dose not penetrate through it, on the other hand, the pure poly (acrylamide- ethylene glycol) has high transmittance because there are no free electron(i.e. electrons are linked to atoms by covalent bonds), this is because the breaking of electron linkage and moving it to the conduction band need to photon with high energy [95]. We notice an increase in the permeability when adding Sb_2O_3 compared to adding Ag.

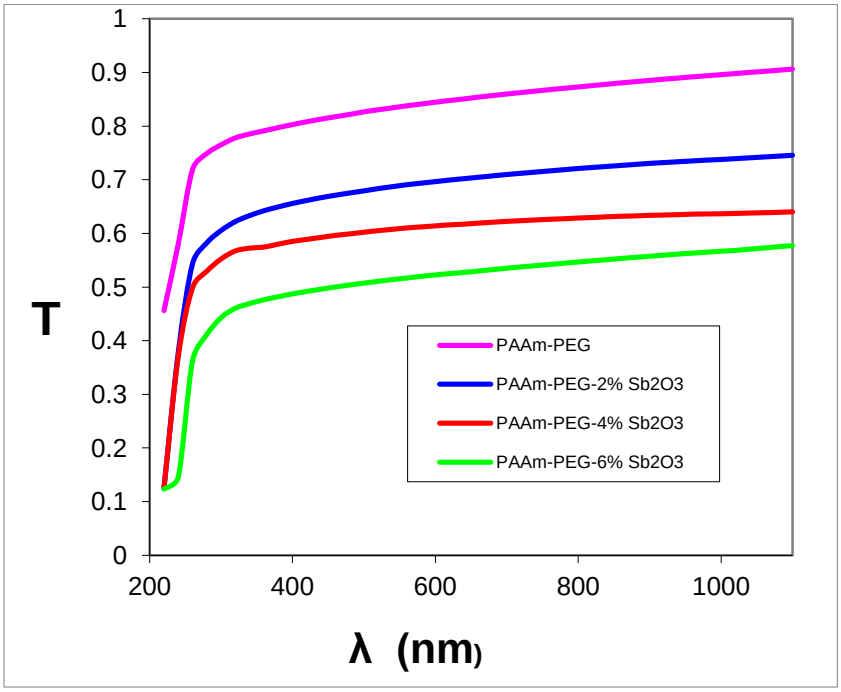

Fig. (4.16): Transmittance Behavior of (PAAm-PEG-Sb_2O_3)

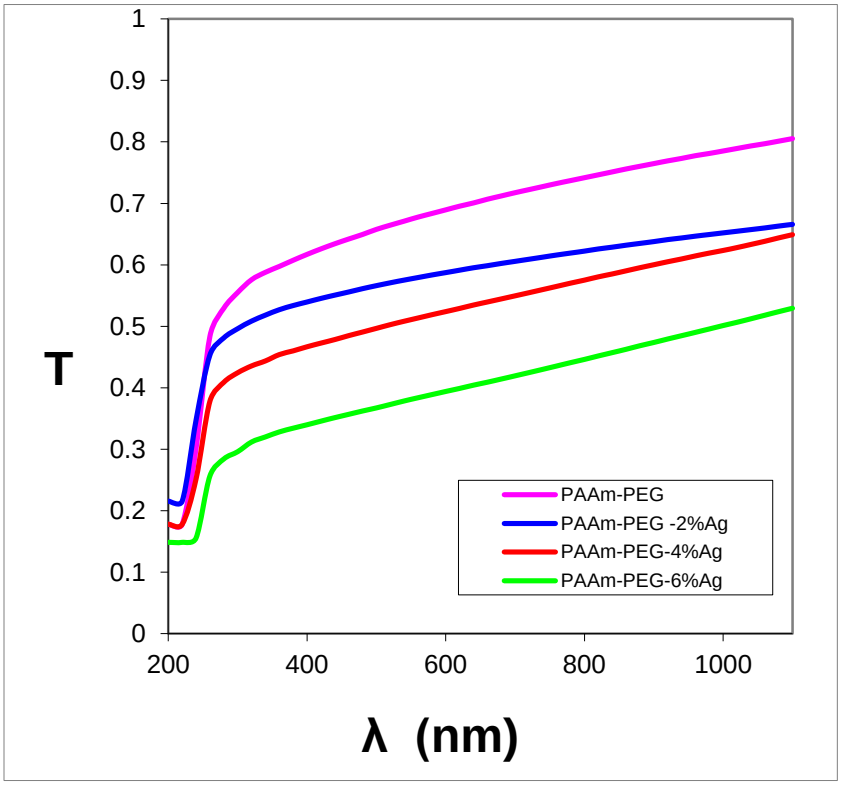

Fig. (4.17): Transmittance Behavior of (PAAm-PEG-Ag).

4.3.3 Absorption Coefficient (α)

Figures (4.18 and 4.19) show the absorption coefficient α $(cm)^{-1}$ as a function of wavelength for (PAAm-PEG-Ag, Sb_2O_3) nanocomposites. It can be seen that the absorption coefficient is the smallest at high wavelength and low energy; this means that the possibility of electron transition is little because the energy of the incident photon is not sufficient to move the electron from the valence band to the conduction band ($h\nu<E_g$).

At high energies, absorption is good, this means that a high possibility for electron transitions consequently, the energy of incident photon is enough to move the electron from the valence band to the conduction band, the energy of the incident photon is greater than the forbidden energy gap [94].

This shows that the absorption coefficient assists in figuring out the nature of electron transition, when the values of the absorption coefficient are high ($\alpha > 10^4$) cm^{-1} at

high energies it is expected that direct transition of electron occur, the energy and moment are maintained by the electrons and photons. While, when the values of the absorption coefficient is low ($\alpha < 10^4$) cm^{-1} at low energies, it is expected that indirect transition of electron occur, and the electronic momentum is maintained with the assistance of the phonon [95], among other results is that the absorption of coefficient for the (PAAm-PEG- Ag, Sb_2O_3) nancomposites is less than (10^4) cm^{-1}, this explains that the electron transitions is indirect. We notice an increase in the absorption coefficient when adding Ag compared to adding Sb_2O_3.

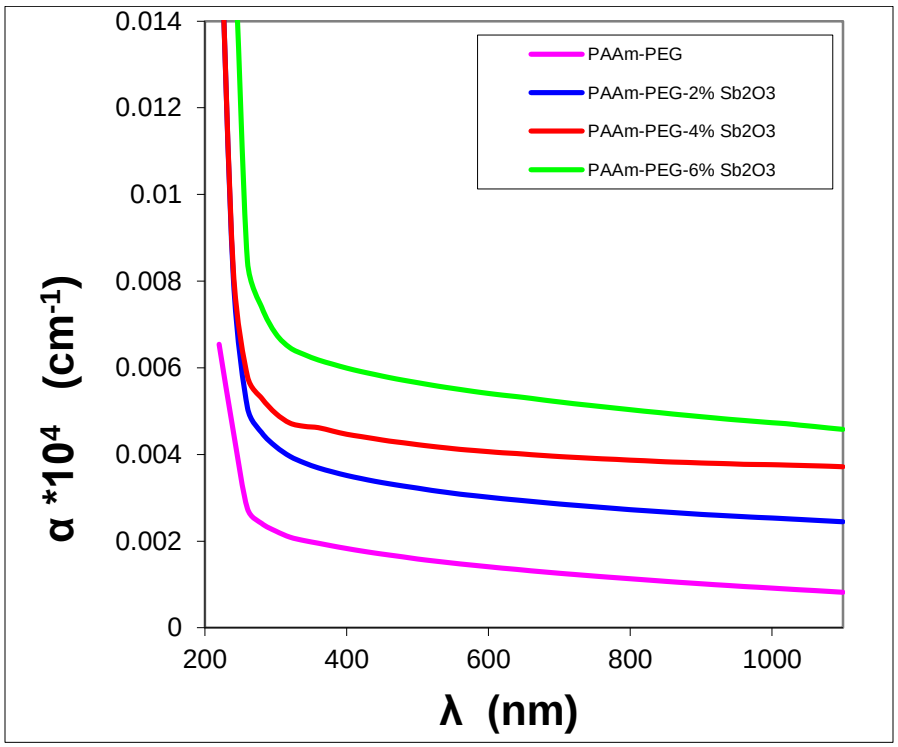

Fig. (4.18): Variation of Absorption Coefficient of (PAAm-PEG-Sb_2O_3).

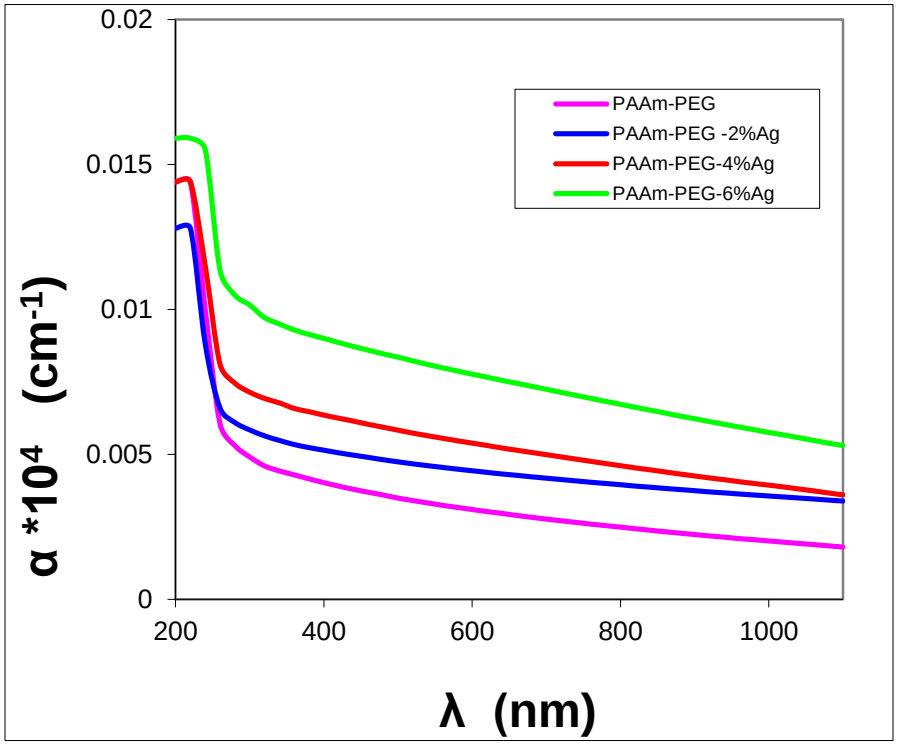

Fig. (4.19): Variation of Absorption Coefficient of (PAAm-PEG-Ag).

4.3.4 Refractive Index (n)

Figures (4.20 and 4.21) show the change of refraction index of (PAAm-PEG- Ag, Sb_2O_3) nanocomposites as a function of wavelength. It is obvious from the figures, the refractive index increase with increasing weight percentages of the (Ag, Sb_2O_3) nanoparticles to the poly (acrylamide- ethylene glycol) because of increasing in the density nanocomposites. In ultraviolet region we note that high values of the refractive index because of the little transmittance in this region, but in the visible region note that low values because of the high transmittance in this region. This behavior is consistent with Vlaeva et.al [84].

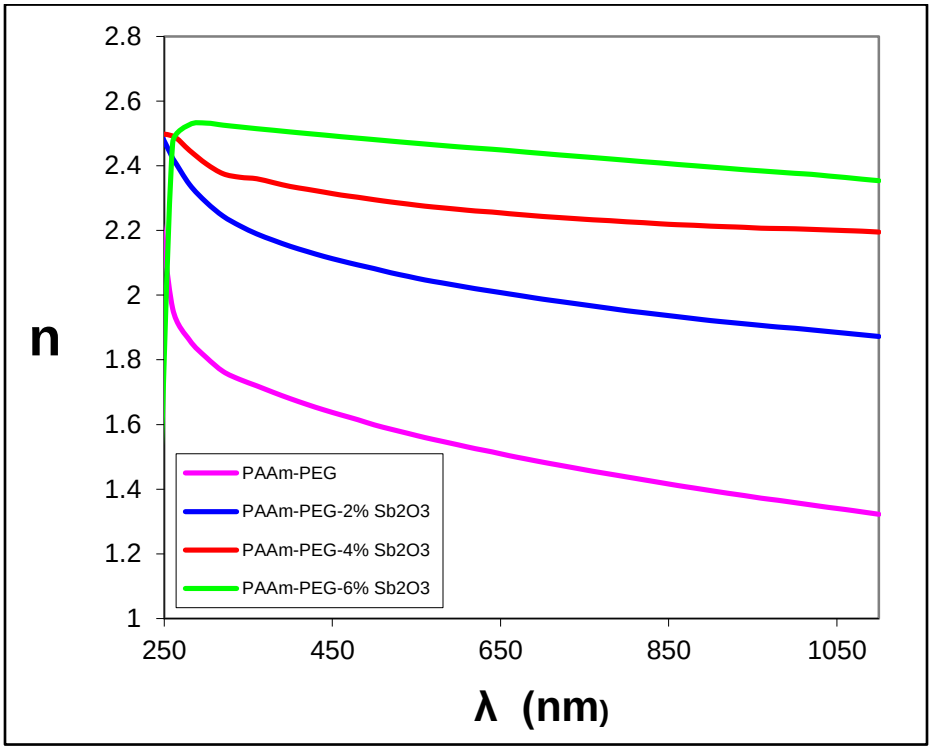

Fig. (4.20): Variation of Refractive Index with Wavelength of (PAAm-PEG-Sb_2O_3)

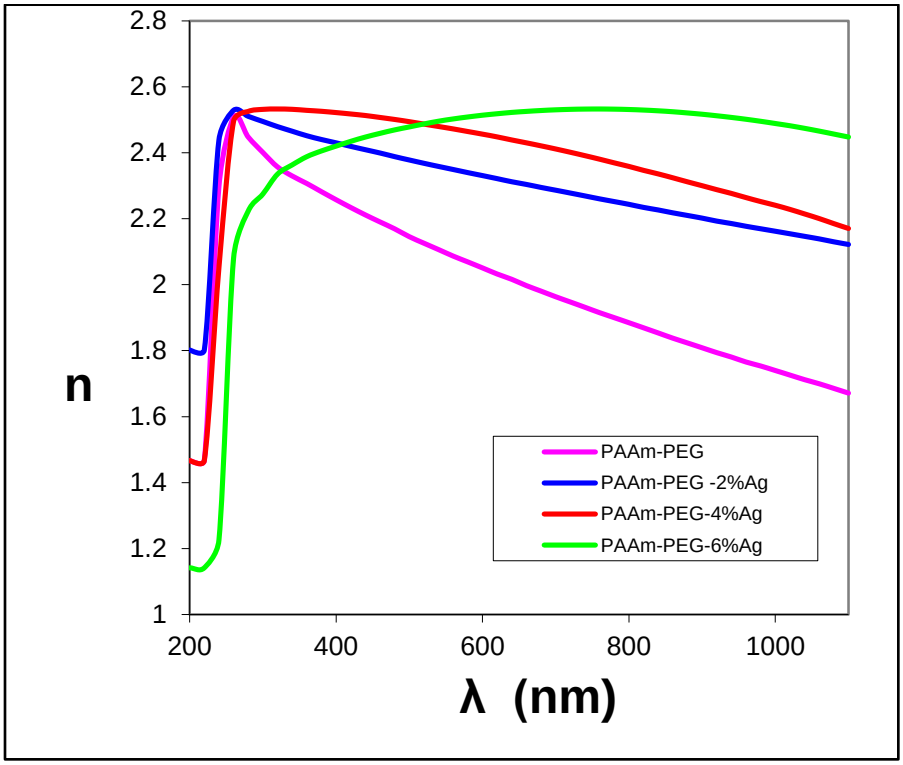

Fig. (4.21): Variation of Refractive Index with Wavelength of (PAAm-PEG-Ag)

4.3.5 Extinction Coefficient (k_o)

The variation of the extinction coefficient of (PAAm-PEG- Ag, Sb_2O_3) nanocomposites as a function of wavelength shown in the figures (4.22 and 4.23) respectively. It can be noted that (k_o) is lowering value at low concentration, but it increases with increasing of the concentration of (Ag, Sb_2O_3) nanoparticle. This is attributed to increased absorption coefficient with increased percentage of (Ag, Sb_2O_3) nanoparticles. This result indicates that the atoms of (Ag, Sb_2O_3) nanoparticles will modify the structure of the host polymer [91].

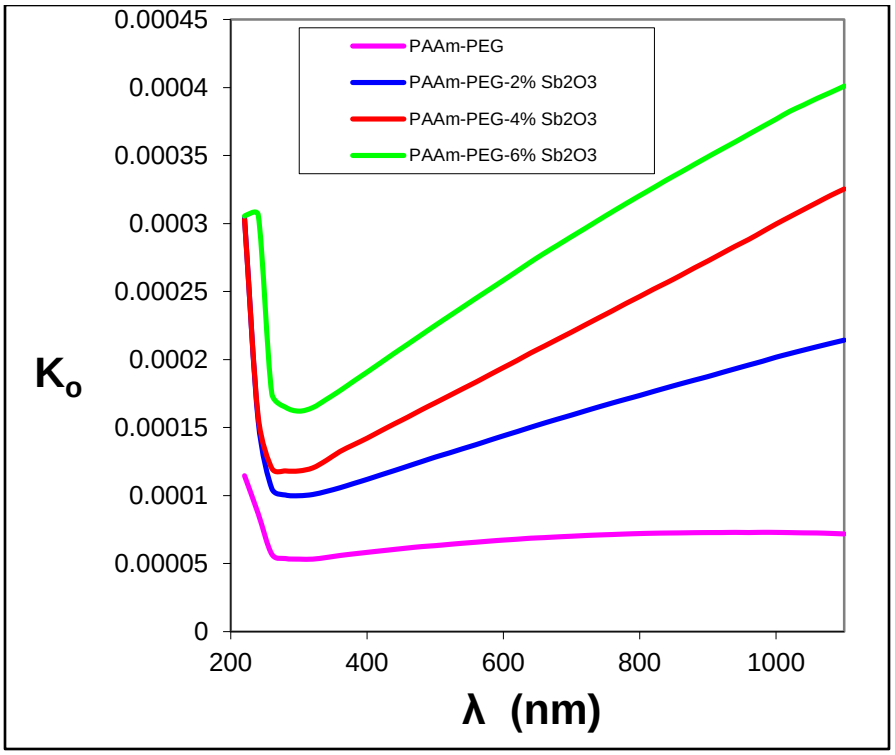

Fig. (4.22): Variation of Extinction Coefficient of (PAAm-PEG-Sb_2O_3).

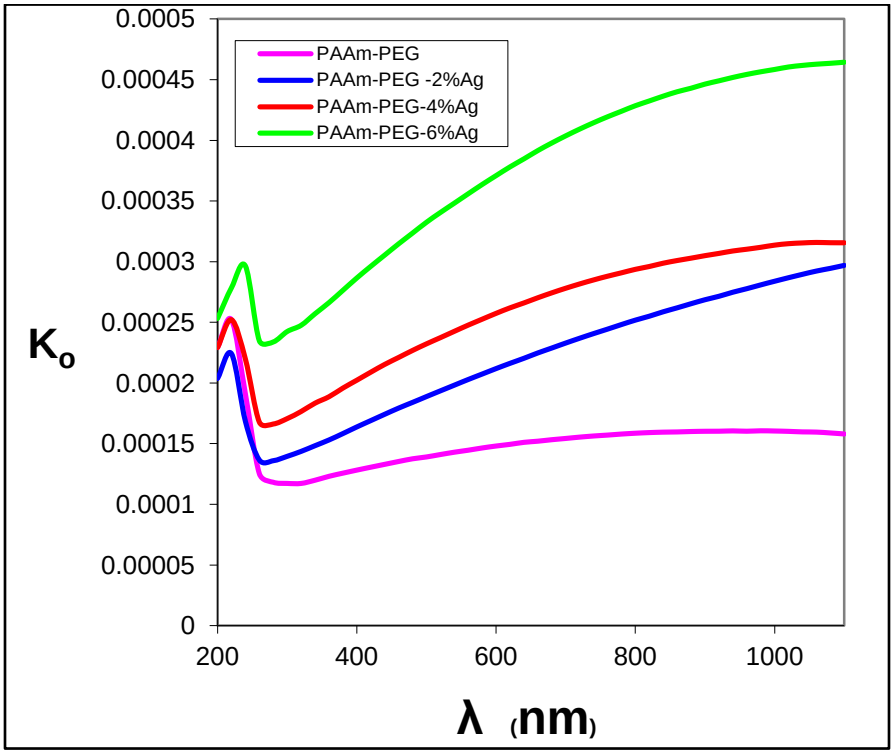

Fig. (4.23): Variation of Extinction Coefficient of (PAAm-PEG-Ag).

4.3.6 Real and Imaginary Part of Dielectric Constants (ε_1 and ε_2)

The figures (4.24 and 4.26) show the change of (ε1,) as a function of the wavelength. It can be seen that ε_1 considerably depends on (n^2) due to low value of (k_o^2) so, the real dielectric constant is increased with the increase of the concentrations of nanoparticles.

Figures (4.25 and 4.27) show the change of (ε_2) as a function of the wavelength, it can be seen that (ε_2) is dependent on (k_o) values that change with the change of the absorption coefficient due to the relation between (α) and (k_o). This behavior is consistent with [96].

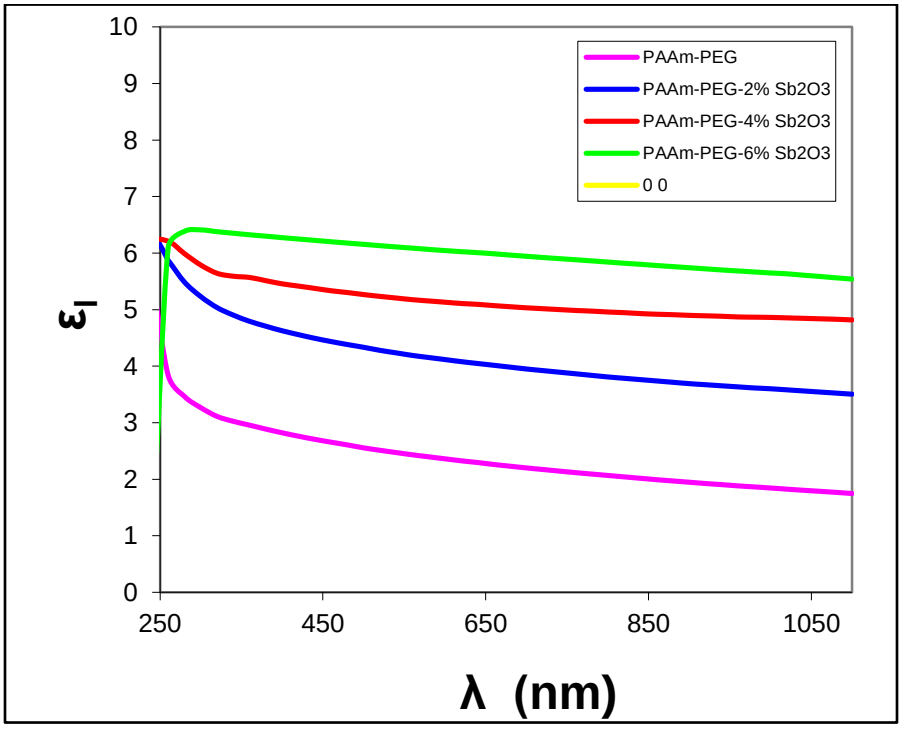

Fig. (4.24): The Real Part of (PAAm-PEG-Sb_2O_3).

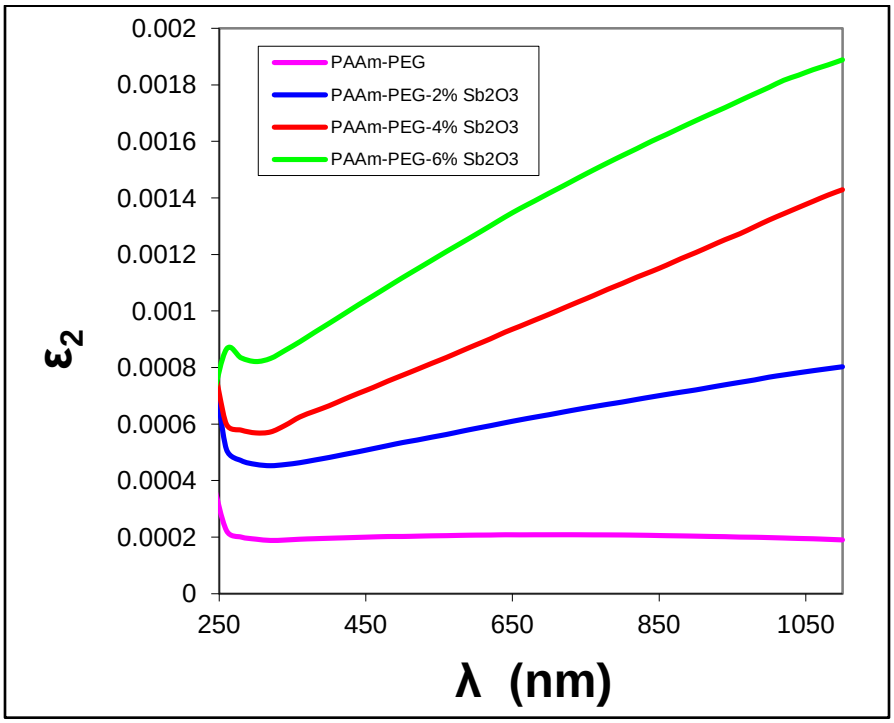

Fig. (4.25): The imaginary part of dielectric constant of (PAAm-PEG-Sb_2O_3).

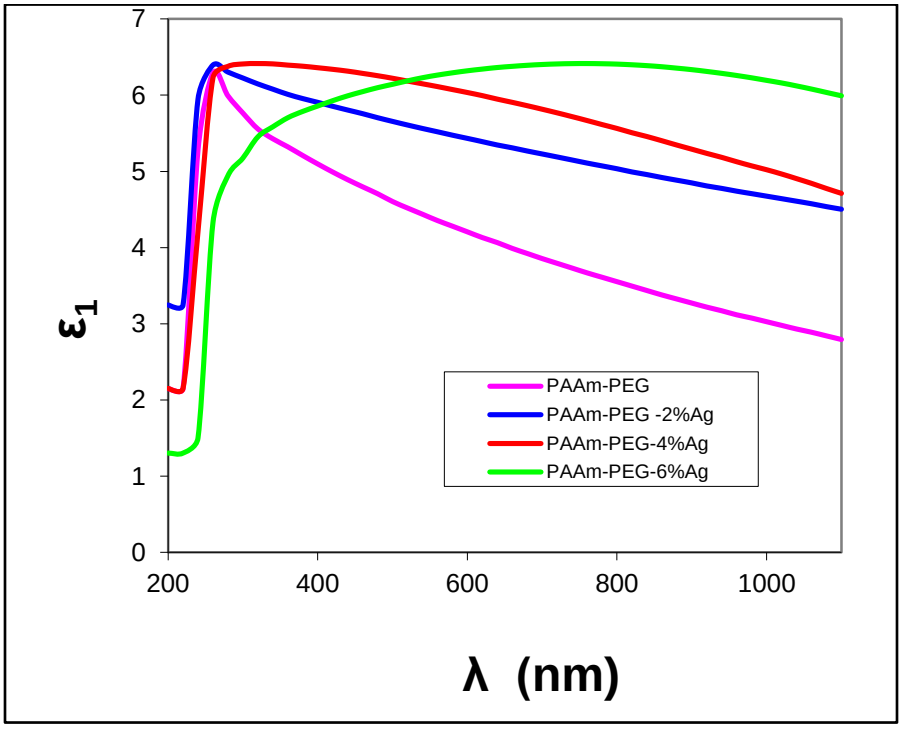

Fig. (4.26): The real part of dielectric constant of (PAAm-PEG-Ag).

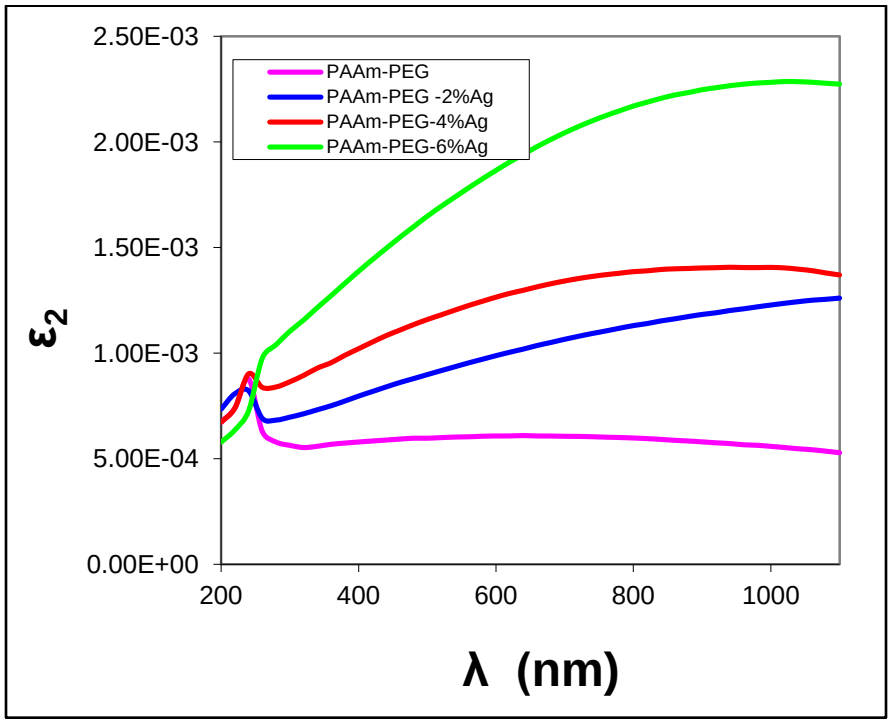

Fig. (4.27): The imaginary part of dielectric constant of (PAAm-PEG-Ag).

4.3.7 Optical energy gaps

Figures (4.28 and 4.29) show the relationship between edge absorption $(\alpha hv)^{1/2}$ of (PAAm-PEG-Ag, Sb_2O_3) nanocomposites as a function of photon energy, when drawing a straight line from the top of the curve towards the (x) axis at $(\alpha hv)^{1/2} = 0$ extrapolation, we get the energy gap of the permissible indirect transition. The obtained values are shown in Table (4.3). We can see that the energy gap values decrease with the increase in weight percentages of nanoparticles, and this is due to the creation of local levels in the forbidden energy gap [83], and the transition in this case takes place in two stages that includes the transition of the electron from the valence band to the local levels to the conduction band as a result of increasing the weight ratio of nanoparticles. The density of the spot state increased with the increase in the concentration of nanoparticles, which explains the decrease in the energy gap with the increase of nanoparticles as shown in figures (4.28 and 4.29) and these results are similar to the researchers [97].

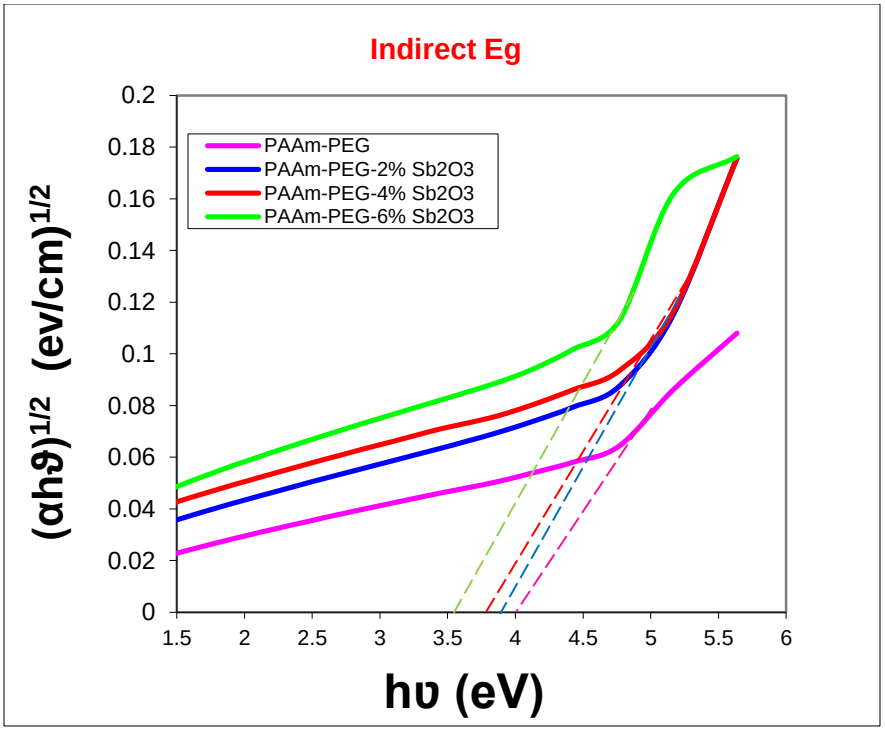

Fig. (4.28): Variation of $(\alpha hv)^{1/2}$ of (PAAm-PEG-Sb_2O_3).

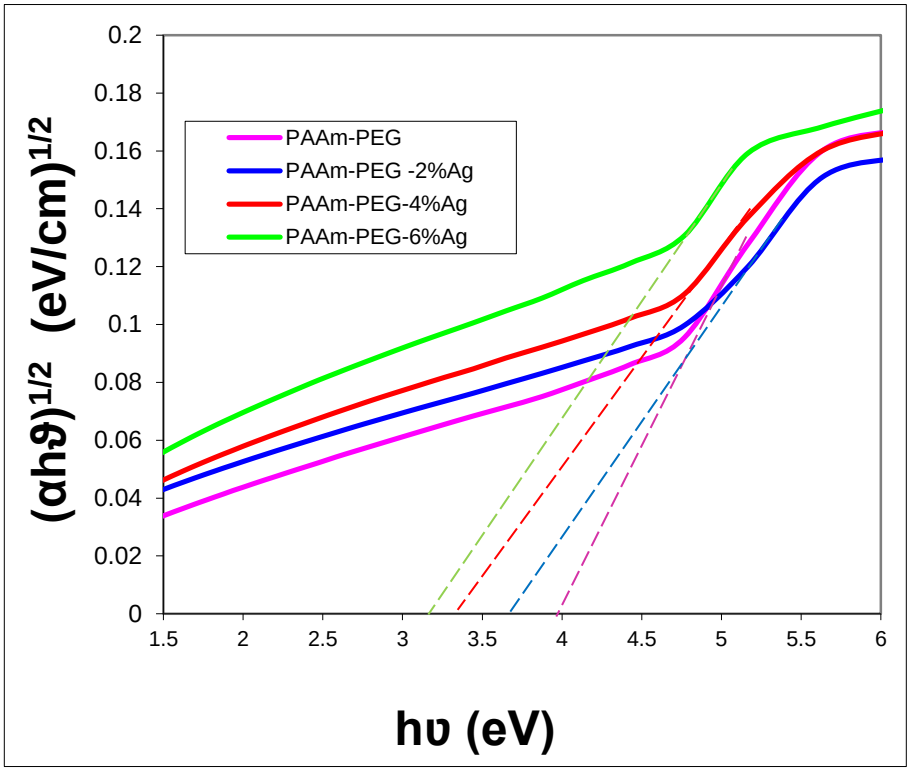

Fig. (4.29): Variation of $(\alpha h\upsilon)^{1/2}$of (PAAm-PEG-Ag)

Table (4.3): Eergy Gab Value of (PAAm-PEG-Sb_2O_3, Ag)

Sample	Eg(eV) of Sb_2O_3	Eg(eV) of Ag
PAAm-PEG	**4**	**4**
PAAm-PEG-0.02	**3.9**	**3.6**
PAAm-PEG-0.04	**3.7**	**3.45**
PAAm-PEG-0.06	**3.5**	**3.4**

4.4 Dispersion Paremeters

According to the figures (4.30-4.36), the values of E_d, E_o, were calculated and listed in the tables (4.3 and 4.4). From the table, the values of E_o /2 we get E_g. The very small values of E_g denote to the increase the nanoparticles **(**Sb_2O_3, Ag**)** to blend, with high reflectance because of the free electrons on the film surface. The index of refraction (n_∞) for the (PAAm-PEG-Sb_2O_3, Ag) nanocompesite was added by the interception of the

perpendicular axis in figures (4.31-4.33). These figures show the behavior of the dispersion parameter when different percentages of (Sb_2O_3) nanomaterial are added.

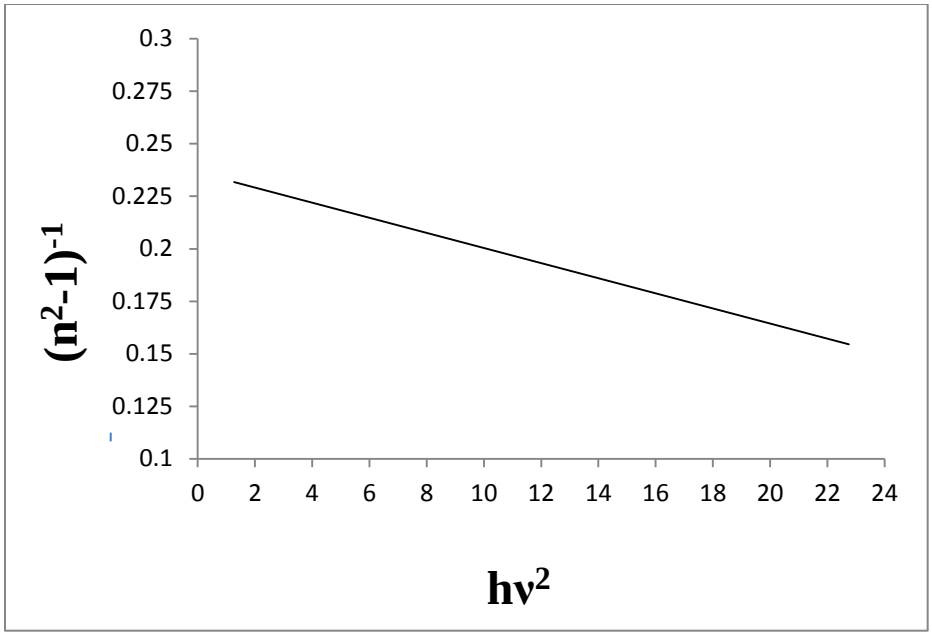

Fig. (4.30): $(n^2 -1)^{-1}$ versus $(h\upsilon^2)$ of the blend (PAAm-PEG).

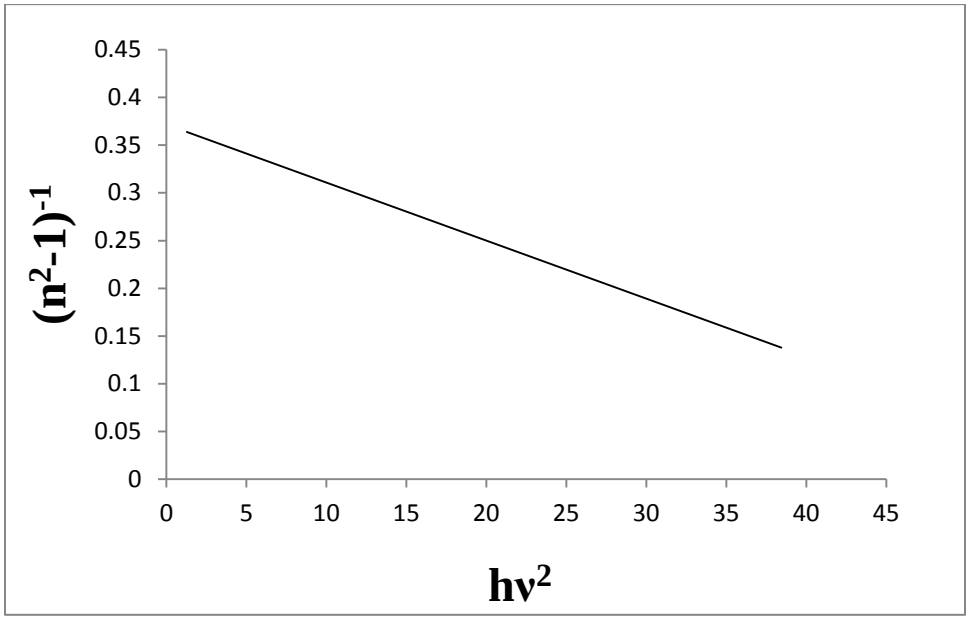

Fig. (4.31): $(n^2 -1)^{-1}$ versus $(h\upsilon^2)$ of the nanocomposite (PAAm-PEG-Sb_2O_3) with 2% of Sb_2O_3 NPs.

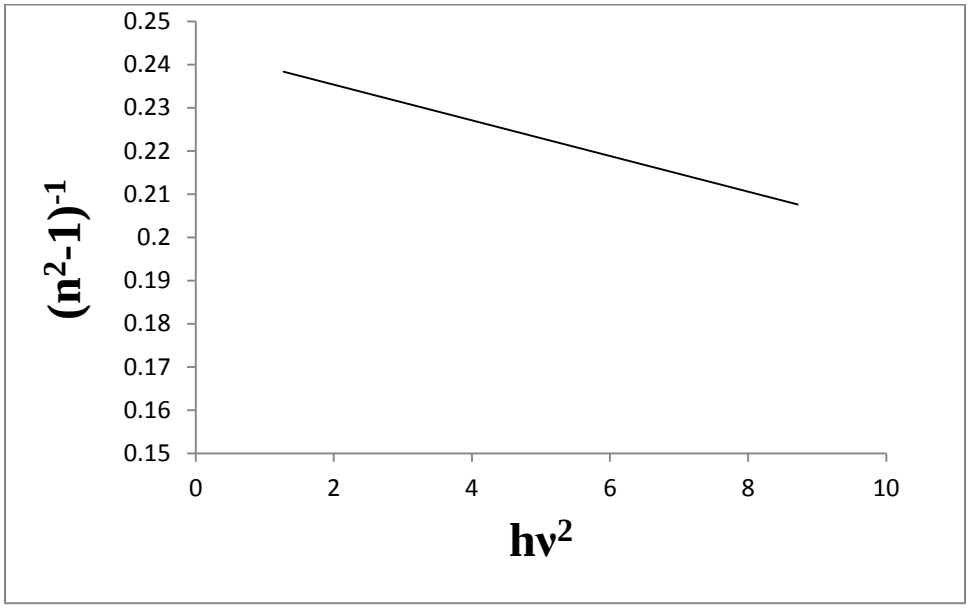

Fig. (4.32): $(n^2 -1)^{-1}$ versus $(h\upsilon^2)$ of the nanocomposite (PAAm-PEG-Sb_2O_3) with 4% of Sb_2O_3 NPs.

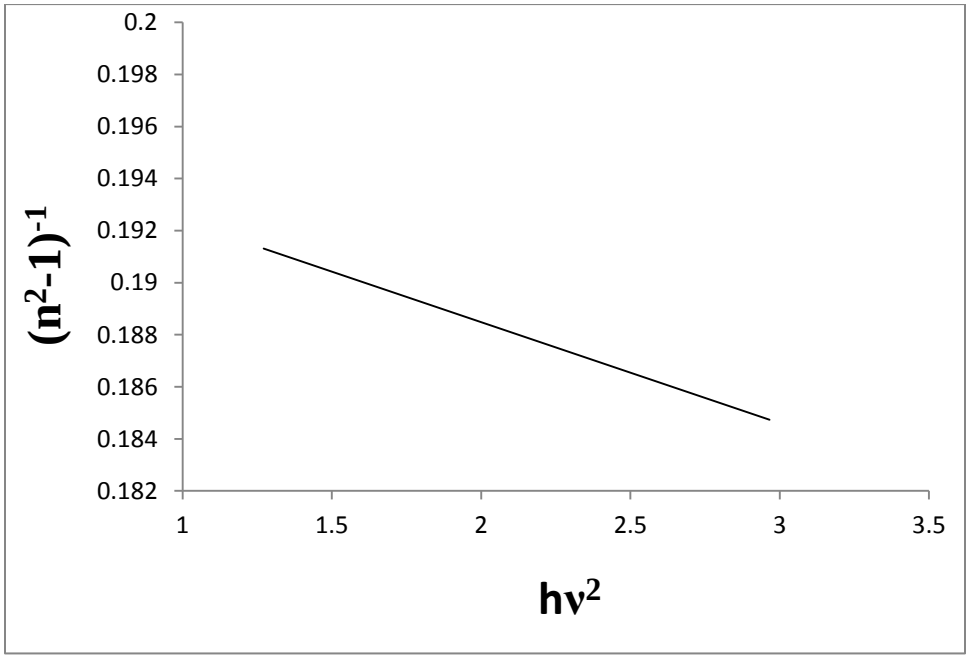

Fig. (4.33): $(n^2 -1)^{-1}$ versus $(h\upsilon^2)$ of the nanocomposite (PAAm-PEG-Sb_2O_3) with 6% of Sb_2O_3 NPs.

Table (4.4) shows the dispersion parameters of the nanocomposite (PAAm-PEG-Sb_2O_3). The M_{-1} and M_{-3} visual perception moments decrease with increasing

nanoparticle thickness. Using the Wemple-DiDomenico process, the dispersion parameters were determined. It is observed that with increasing nanoparticles, the scattering energy (E_d) and electronic transition energy of one oscillator (E_o) are reduced. Very small values of the energy gap indicate the films are conductive, which makes them suitable for optical devices.

Table (4.4): The dispersion parameters and energy gap resulted from Wemple-DiDomenico model of PAAm-PEG-Sb_2O_3.

Sample	Pure	2wt.%Sb_2O_3 additive	4wt.%Sb_2O_3 additive	6wt.%Sb_2O_3 additive
E_o	8.21	7.82	7.65	7.27
E_d	34.97	20.85	31.38	37.82
E_g	4.10	3.91	3.82	3.63
n(0)	2.29	1.91	2.25	2.49
E	5.25	3.66	5.09	6.20
M_{-1}	4.25	2.66	4.09	5.20
M_{-3}	0.06	0.04	0.06	0.09

Figures (4.34-4.36) shown the behavior of the dispersion parameter when different percentages of (Ag) nanomaterial are added.

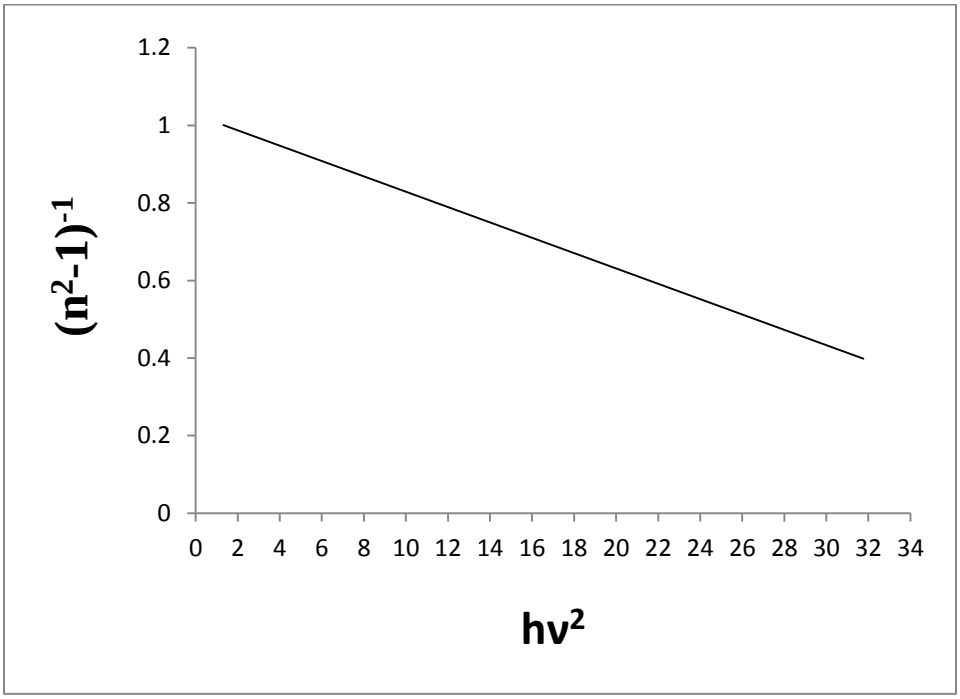

Fig. (4.34): $(n^2 -1)^{-1}$ versus $(h\upsilon^2)$ of the nanocomposite (PAAm-PEG-Ag) with 2% of Ag NPs.

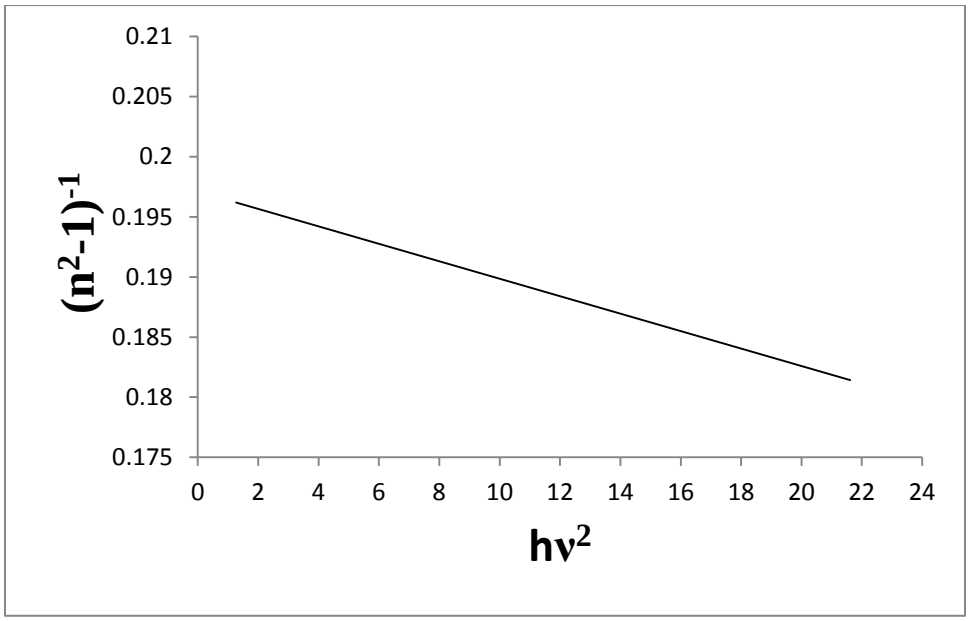

Fig. (4.35): $(n^2 -1)^{-1}$ versus $(h\upsilon^2)$ of the nanocomposite (PAAm-PEG-Ag) with 4% of Ag NPs.

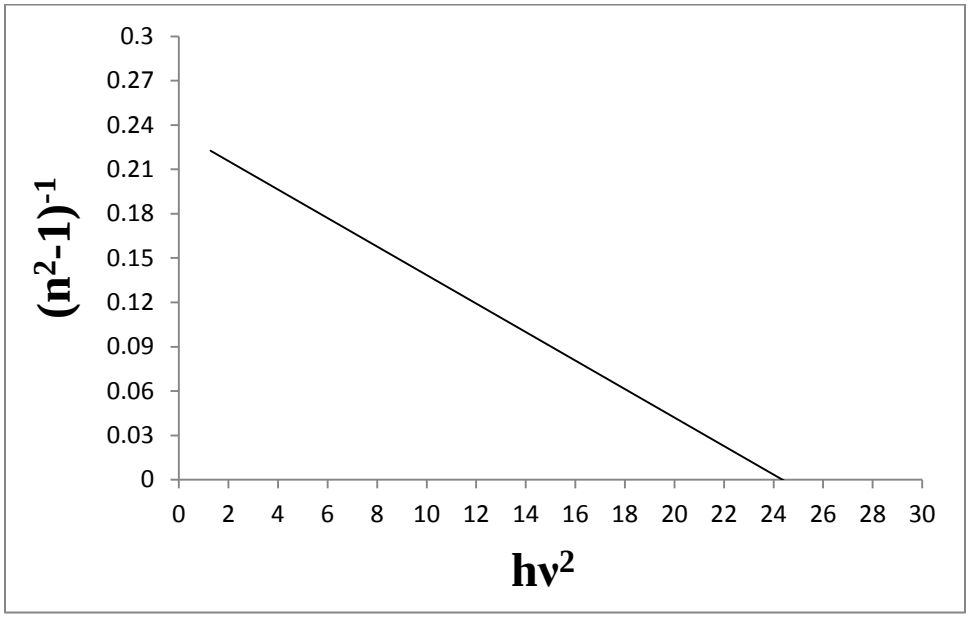

Fig. (4.36): $(n^2 -1)^{-1}$ versus $(h\upsilon^2)$ of the nanocomposite (PAAm-PEG-Ag) with 6% of Ag NPs.

Table (4.5) shows the optical parameters of the nanocomposite (PAAm-PEG-Ag). It is observed that with increasing nanoparticles, the scattering energy (E_d) and electronic transition energy of one oscillator (E_o) are reduced.

Table (4.5): The dispersion parameters and energy gap resulted from wemple-DiDomenico model of PAAm-PEG-Ag.

Sample	Pure	2wt.%Ag additive	4wt.%Ag additive	6wt.%Ag Additive
E_o	8.21	7.42	6.46	5.09
E_g	4.10	3.71	3.23	2.54
E_d	34.97	7.07	29.38	21.24
$n_2(0)$	2.29	1.95	5.54	5.16
$n_o(0)$	5.25	1.39	2.35	2.27
E		1.95	5.54	5.16
M_{-1}	4.25	0.95	4.54	4.16
M_{-3}	0.06	0.01	0.10	0.16

4.5 Conclusions

The following remarks are concluded during the present work:

1- These polymers show a continuous change in their physical properties as a result of adding (Ag, Sb_2O_3) to the PAAm-PEG polymer which improved these properties.

2- We conclude through the optical microscope that the nano-film is formed as a result of reactions between polymer mixtures, as well as between polymers and additives, and the distribution of nanomaterials well in the mixture because it is homogeneous and interactive with polymers.

3- Through the FT-IR examination, we noticed the emergence of a large number of bonds. This indicates the presence of an interaction between the polymers used, as well as between polymers and additives, and this indicates the emergence of a new material that differs from all the basic materials used. Evidence for this (individual bonds) gave new bonds.

4- SEM images showed that the addition of nanoparticles in the nanocomposites (PAAm-PEG-Ag, Sb_2O_3) shows changes in the surface morphology of this system. It is clear from the images that the grains accumulate with the increasing proportion of nanoparticles. The surface morphology of the nanocomposites (PAAm-PEG-Ag, Sb_2O_3) shows many randomly distributed aggregates or pieces on the upper surface. The results showed an increase in the number of white dots on the surface with increasing concentration of nanoparticles (Ag, Sb_2O_3).

5- Through the UV-Vis examination, we notice an increase in the absorption and absorption coefficient of compounds with an increase in the nanomaterial. The refractive index and extinction index were increased with increasing concentrations of Ag and Sb_2O_3. The energy gap of indirect transport (allowed, forbidden) decreases

with increasing particle concentrations. The photoconductivity increases with increasing proportions of Ag and Sb_2O_3 in a mixture (PAAm-PEG-Ag, Sb_2O_3).

6- Using the Wemple-DiDomenico model, the dispersion parameters were determined. Observed with increasing nanoparticles, the scattering energy (E_d) and electronic transition energy of one oscillator (E_o) were reduced. The very small values of the energy gap indicate both absorbent and conductive films, making them suitable for optical devices.

4.6 Future Works

From this study, other future works can be adopted as suggested below:-

1. Study the structural, optical and electrical properties of a (PAAm-PEG-Sb_2O_3, Ag) nano-film prepared by another method, such as the spin coating method.
2. Study the thermal and mechanical properties of (PAAm-PEG-Sb_2O_3, Ag) nanocomposites.
3. Effect of irradiation on the electrical and optical properties of (PAAm-PEG-Sb_2O_3, Ag) nanocomposites.
4. Effect of temperature on the A.C. electrical properties of (PAAm-PEG-Sb_2O_3, Ag) nanocomposites.

Scientific Activities

1- One research was published in an international journal (NeuroQuantology Journal).

2- One paper has been accepted for publication in scopus container.

3- The Patent is under Implementation in the Central Agency for Standardization and Quality Control.

4- A certificate of participation in the fifth international conference on chemical safety and security.

5- Participation in three seminars in the department of physics, the most important of which was how to raise the level of scientific research among graduate students, as well as about the importance of publishing in international journals.

6- Participation in the scientific symposium for postgraduate students held in the faculty of science, department of physics.

References

1-Diez-pascal A. M., Gomez-fatou M. A. and Ania F., "Progress in Materials Science Nanoindentation in Polymer Nanocomposites", Vol. 67, pp. 1-94, (2015).

2- Abdulridha A. R., Al-Bermany E., Hashim F. S. and Alkhayatt A. H. O., " Synthesis and Characterization and Pelletization Pressure Effect on the Properties of $Bi_{1.7}Pb_{0.3}Sr_2W_{0.2}Ca_2Cu_3O_{10+\delta}$ Superconductor System", Intermetallics, Vol. 127, p. 106967, (2020).

3-Layek R. K. and Nandi A. K., "A Review on Synthesis and Properties of Polymer Functionalized Graphene", Polymer, Vol. 54, No.19, pp. 5087-5103, (2014).

4-Jawad E., Khudhair S. H., and Ali H. N. A., "Thermodynamic Study of Adsorption of Some Days on Iraqi Bentoniet Modified Clay", European Journal of Scientific Research, Vol. 60, No.1, pp. 63-70, (2011).

5-Bai H., Xu Y., Zhao L., Li C. and Shi G., "Non-Covalent Functionalization of Graphene Sheets By Sulfonated Polyaniline", Chemical Communications, Vol. 13, pp. 1667-1669,(2009).

6-Al-Bermany E., Qais D. and Al-Rubaye S., "Graphene Effect on the Mechanical Properties of Poly (Ethylene Oxide)/Graphene Oxide Nanocomposites Using Ultrasound Technique", In Journal of Physics: Conference Series, Vol. 1234, No.1, p. 012011, IOP Publishing (2019).

7- Sui T., Song B., Zhang F. and Yang Q., "Effects of Functional Groups on the Tribological Properties of Hairy Silica Nanoparticles as an Additive to Polyalphaolefin", RSC advances, Vol. 6, No.1, pp. 393-402, (2016).

8-Feldman D., “Polymer History”, Designed monomers and polymers, Vol. 11, No.1, pp. 1- 15, (2008).

9-Dalgleish T., Williams J. M. G., Golden A. M. J., Perkins N., Barrett L. F., Barnard P. J. and Watkins E., “Reduced Specificity of Autobiographical Memory and Depression: the Role of Executive Control”, Journal of Experimental Psychology: General, Vol. 136, No.1, p. 23, (2007).

10-Pokropivny V., Lohmus R., Hussainova I., Pokropivny A. and Vlassov S., ” Introduction to Nanomaterials and Nanotechnology”, Tartu University Press, pp. 45-100, (2007).

11-Sahoo A., “Synthesis and Characterization of Bio-Composite”, Ph.D. Thesis, Physics Department, National Institute of Technology, India, (2011).

12-Bhatia T., “Novel Nanomaterials in Forensic Investigations: A Review”, Materials Today: Proceedings, (2021).

13-Schultz J. M., “Polymer Materials Science'Prentice-Hall”, New Jersey (1974).

14-Boenig H. V., “Polyolefins: Structure and Properties”, Elsevier Publishing Company, (1966).

15-Kolahalam L. A., Viswanath I. K., Diwakar B. S., Govindh B., Reddy V. and Murthy Y. L. N., “Review on Nanomaterials: Synthesis and Applications”, Materials Today: Proceedings, Vol. 18, pp. 2182-2190, (2019).

16- Zeynali M. E., Rabii A. and Baharvand H., “Synthesis of Partially Hydrolyzed Polyacrylamide and In vestigation of Solution Properties (viscosity behaviour)”, (2004).

17- Dweik H., Sultan W., Sowwan M. and Makharza S., “Analysis Characterization and Some Properties of Polyacrylamide copper complexes”, International Journal of Polymeric Materials, Vol. 57, No.3, pp. 228-244, (2008).

18- Lentz R. D., “Polyacrylamide and Biopolymer Effects on Flocculation, Aggregate Stability and Water Seepage in a Silt Loam”, Geoderma, Vol. 241, pp. 289-294, (2015).

19- Bailey F. E. and Koleske J. V., “Alkylene Oxides and Their Polymers”, CRC Press, (2020).

20- Bailey F. E. and Koleske J. V., “Polyoxyalkylenes”, Ullmann's Encyclopedia of Industrial Chemistry, Weinheim: Wiley-VCH, (2000).

21- Laurence P.B. “FDA Asks Philly Scientists to Study Miralax Side Effects in Kids”, (4 April 2017).

22- Chen J., Spear S. K., Huddleston J. G. and Rogers R. D., “Polyethylene Glycol and Solutions of Polyethylene Glycol as Green Reaction Media”, Green Chemistry, Vol. 7, No. 2, pp. 64-82, (2005).

23-Sweah Z.J., AL-Lami H.S. and Haddad A.M.,”Preparation and Swelling Behavior of L-Lactide Interpenetrating Networks” Open Journal of Organic Polymer Materials, Vol. 6, No. 4, (2016).

24-Nasirian D., Salahshoori I., Sadeghi M., Rashidi N. and Hassan zadeganroudsari M. Investigation of the gas permeability properties from polysulfone/polyethylene glycol composite membrane. Polymer Bulletin, Vol. 77, No. 10, pp. 5529-5552, (2020).

25-Greenwood N. N. and Earnshaw A., "Chemistry of the Elements", Elsevier, (2^{nd} E^{dn}.), (2012).

26-Voit E. I., Panasenko A. E. and Zemnukhova L. A., "Vibrational Spectroscopic and Quantum Chemical Study of Antimony (III) Oxide", Journal of Structural Chemistry, Vol. 50, No.1, pp. 60-66, (2009).

27- Cheong K.Y., "Review on Oxides of Antimony Nanoparticles: Synthesis, Properties, and Applications", Journal of Materials Science, Vol. 45, No. 22, (2010).

28- Kim Y. H., Lee D. K. and Kang Y. S., "Synthesis and Characterization of Ag and Ag–SiO_2 Nanoparticles", Colloids and Surfaces A: Physicochemical and Engineering Aspects, Vol. 257, pp. 273-276, (2005).

29- Lee J. J., Park J. C., Kim M. H., Chang T. S., Kim S. T., Koo S. M. and Lee S. J., "Silver Complex Inks for Ink-jet Printing: the Synthesis and Conversion to a Metallic Particulate Ink", Journal of Ceramic Processing Research, Vol. 8, No.3, p. 219, (2007).

30- Dankovich A. and Gray D. G., "Bactericidal Paper Impregnated with Silver Nano particles for Point-of-Use Water Treatment", Vol. 45, No.5, (2011).

31- Abou Ei-Nour K. M. M., Etihad A. and Al-Waltham A., "Synthesis and Application of Silver Nanoparticles", Journal of Chemistry, Vol. 3, pp. 135-140, (2010).

32- Smith D. R. and Fickett F. R., "Low-Temperature Properties of Silver", Journal of research of the National Institute of Standards and Technology, Vol. 100, No. 2, p. 119, (1995).

33- Herman F., "Encyclopedia of Polymer Science and Technology", John Wiley and Sons Inc., Vol. 14, New York, (1971).

34- Lee J. Y., Tanaka H., Takezoe H., Fukuda A., Kuze E. and Iwanaga H., "Novel Method of Preparing Ag–Hg Alloy on Polyacrylamide Films and Their Structure", Journal of applied polymer science, Vol.29, No.3, pp. 795-802, (1984).

35- Cakmak I., Hazer B. and Yagci Y., "Polymerization of Acrylamide By the Redox System Cerium (IV) With Poly (Ethylene Glycol) With Azo Groups", European polymer journal, Vol. 27, No.1, pp. 101-103, (1991).

36- Park Y. S., Won J. and Kang Y. S., "Facilitated Transport of Olefin Through Solid PAAm and PAAm-graft Composite Membranes With Silver Ions", Journal of Membrane Science, Vol. 183, No.2, pp. 163-170, (2001).

37- Ma X., Zhang Z., Li X., Du Y., Xu F. and Qian Y., "Micro-Sized Sb_2O_3 Octahedra Fabricated Via a PEG-1000 Polymer-Assisted Hydrothermal Route". Journal of Solid State Chemistry, Vol. 177, No.10, pp. 3824-3829, (2004).

38- Swamy T. M., “Studies on Miscibility of Polyacrylamide/Polyethylene Glycol Blends”. Journal of Applied Polymer Science, Vol. 104, No.3, pp. 2048-2053, (2007).

39- Guorong S. and Zhihai C., “A New Polymerization Method and Kinetics for Acrylamide: Aqueous Two-Phase Polymerization”. Journal of Applied Polymer Science, Vol. 111, No.3, pp. 1409-1416, (2009).

40- Banerjee S. L., Khamrai M., Sarkar K., Singha N. K. and Kundu P. P., “Modified Chitosan Encapsulated Core-Shell Ag NPs for Superior Antimicrobial and Anticancer Activity”. International journal of biological macromolecules,Vol. 85, pp. 157-167, (2016).

41- Hamood F. J., Mohammed M. K. and Abass K. H., “Study of AC Electrical Properties of (PVA-PEG-Sb_2O_3) Composites”, (2017).

42- Xu J., Yang W., Niu L., Dan X., Wang C. and Wen C., “Study on the Surface Modification of Sb_2O_3 Nanoparticles By Using Mechanochemical Method”. Inorganic and Nano-Metal Chemistry, Vol. 47, No.5, pp. 697-702, (2017).

43- Habubi N. F., Abass K. H., Sami C. S., Latif D. M., Nidhal J. N. and Al Baidhany A. I., “Dispersion Parameters of Polyvinyl Alcohol Films doped with Fe”, In Journal of Physics: Conference Series, Vol. 1003, No.1, p. 012094, IOP Publishing, (2018).

44- Fan X., Yahia L. H. and Sacher E. “Antimicrobial properties of the Ag, Cu nanoparticle system”. Biology, Vol. 10, No.2, p. 137, (2021).

45- Liu S., Tian X., Zhang X., Xu C., Wang L. and Xia Y., "A Green MXene-Based Organohydrogel with Tunable Mechanics and Freezing Tolerance for Wearable Strain Sensors". Chinese Chemical Letters, (2021).

46-Al-Shammari A. K. and Al-Bermany E., "Influence of Graphene Nanosheets on Thermal and Mechanical Properties of Water Soluble Polymers/ Graphene Oxide Nanocomposites", (2021).

47- Al-Shammari A. K. and Al-Bermany E. "New Fabricated (PAA-PVA/GO) and (PAAm-PVA/GO) Nanocomposites: Functional Groups and Graphene Nanosheets Effect on the Morphology and Mechanical Properties". In Journal of Physics: Conference Series, Vol. 1973, No.1, p. 012165, IOP Publishing, (2021).

48- Kadim A. M., Abdulkareem A. D. and Abass K. H., "Formation of PVA-PMMA-PAAm Blend with Various Content of Dextrin for Drug Delivery Application". Materials Today: Proceedings (2021) .

49- Samanta H. S. and Ray S. K., "Effect of Polyethylene Glycol and Nano clay on Swelling, Diffusion, Network Parameters and Drug Release Behavior of Interpenetrating Network Copolymer". Journal of Applied Polymer Science, Vol. 139, No.8, p. 51678, (2022).

50- Masti S. P. and Chougale R. B., "Influence of Poly (Vinylpyrrolidone) on Binary Blend Films Made from Poly (Vinyl Alcohol)/Chitosan". International Research Journal of Environment Sciences, Vol. 3, No.3, March (2014).

51- Sadiku-Agboola O., Sadiku R. E., Adegbola A.T. and Biotidara O. F., "Rheological Properties of Polymers: Structure and Morphology of Molten Polymer Blends". Materials Sciences and Applications, Vol. 2, pp. 30-41, (2011).

52- David I. B., "An Introduction to Polymer Physics". First Edition, Published by the Press Syndicate of the University of Cambridge, (2002).

53- Draaijer A., Sanders R., Gerritsen H. C. and Pawley J., "Handbook of Biological Confocal Microscopy", pp. 491-505, (1995).

54-PaddockS.W., "Confocal Laser Scanning Microscopy". Biotechniques, Vol. 27, No.5, pp. 992-1004, (1999).

55-Di Gianfrancesco A., "Technologies for Chemical Analyses, Microstructural and Inspection Investigations. Materials for Ultra-Supercritical and Advanced Ultra-Supercritical Power Plants", Elsevier Ltd, pp. 197–245, (2017).

56- Khursheed A., "Scanning Electron Microscope Optics and Spectrometers. Scanning Electron Microscope Optics and Spectrometers", World scientific, pp. 1– 403, (2010).

57- Lyman C. E., Newbury D. E., Goldstein J. I., Williams D. B., Romig A. D., Armstrong J. T., Echlin P., Fiori C. E., Joy D. C., Lifshin E. and Peters K., "Scanning Electron Microscopy, X-Ray Microanalysis and Analytical Electron Microscopy: A Laboratory Workbook, Plenum Press". New York, pp. 180-186, (1990).

58- Theophanides T., "Introduction to Infrared Spectroscopy", Infrared Spectroscopy-Materials Science, Engineering and Technology, pp. 1-10, (2012).

59- Hashim A., Rabee B. H., Habeeb M. A., Abd-alkadhim N. and Saad A., "Study of Electrical Properties of (PVA-CaO) Composites". American Journal of Scientific Research, Vol. 73, pp. 5-8, (2012).

60- Rabee B. and Kadhim A., "Study of the Dielectric Properties of (PVA-PVAC-Rice Shell) Composites". Journal of Industrial Engineering Research, Vol. 1, No. 4, pp. 9-12, (2015).

61- Abdulmitalib A. "Studying in Electric and Optical Properties of Polymers with Application on Non Crystal Films from Poly acrylic acid", M.Sc.Thesis, College of Sciences, University of Basrah, (1981).

62- Nalwa H. S., "Handbook of Surfaces and Interfaces of Materials", Elsevier (E^{d}.), Five-Volume set, (2001).

63- Rabee B. H., Razooqi F. Z. and Shinen M. H., "Investigation of Optical Properties for (PVA-PEG-Ag) Polymer Nanocomposites Films", Chem. Mater. Res., Vol. 7, No.4, pp. 103-109, (2015).

64- Pankove J. I., "Optical Processes on Semiconductors Dover Publication", Inc. New york, (1971).

65- Donald A. N., "Semiconductor Physics and Devices", IRWIN, Vol. 247, (1992).

66- Suryawanshi V. N., Varpe A. S. and Deshpande M. D., "Band Gap Engineering in PbO Nanostructured Thin Films By Mn Doping", Thin Solid Films, Vol. 645, pp. 87-92, (2018).

67- Nahida J. H., "Spectrophotometric Analysis for the UV-irradiated (PMMA)", International Journal of Basic and Applied Sciences, Vol.12, No.2, pp. 58-67, (2012).

68- Abass K. H. and Latif D. M., "The Urbach Energy and Dispersion Parameters Dependence of Substrate Temperature of CdO Thin Films Prepared By Chemical Spray Pyrolysis", International Journal of ChemTech Research, Vol. 9, No.9, pp. 332-338, (2016).

69- Obaid Z. S. "Physical Properties of PMMA/ZnO Composite Material". Diss. Ministry of Higher Education, (2017).

70- Chuang S. L., "Optical Processes in Semiconductors", Physics of Photonic Devices, 2nd ed.; Boreman, G., Ed, pp. 347-389, (2009).

71- Jenkins F. A. and White H. E., "Fundamentals of Optics", Indian Journal of Physics,Vol. 25, pp. 265-266, (1957).

72- Numai T., "Fundamentals of Semiconductor Lasers: Second Edition", Springer Ser. Opt. Sci, Vol. 93, No.28, pp.55147, (2015).

73- Pankove J. and Kiewit D., "Optical Processes in Semiconductors", J. Electrochem. Soc, Vol. 119, No. 5, pp.156, (1972).

74- Yakuphanoglu F. and Erten H., "Refractive Index Dispersion and Analysis of the Optical Constants of an Ionomer Thin Film", Optica applicata, Vol. 35, No. 4, pp. 969–976, (2005).

75- Morais W. A., Barros B. D., Cavalcanti I. M., Xavier F. H., Santos-Magalhães N. S. and Maciel M. A. M., "Coencapsulation of trans-Dehydrocrotonin and trans-Dehydrocrotonin: hydroxypropyl-β-cyclodextrin into Microparticles", Journal of the Brazilian Chemical Society, Vol. 28, pp.1494-1505, (2017).

76- Mwolfe C., Holouyak N., and Stillman G. B., "Physical Properties of Semiconductor", prentice Hall, New York, (1989).

77- Wemple S. H., "Refractive-Index Behavior of Amorphous Semiconductors and Glasses", Physical Review B, Vol. 7, No.8, p. 3767, (1973).

78- Hassanien A. S. and Akl A. A., "Influence of Composition on Optical and Dispersion Parameters of Thermally Evaporated Non-Crystalline $Cd_{50}S_{50-x}Se_x$ Thin Films", Journal of Alloys and Compounds, Vol. 648, pp. 280-290, (2015).

79- Wemple S. H. and DiDomenico Jr. M., "Behavior of the Electronic Dielectric Constant in Covalent and Ionic Materials", Physical Review B, Vol. 3, No.4, p. 1338, (1971).

80-Sze S. M. "Selected Solutions for Semiconductor Devices: Physics and Technology", Wiley, (1985).

81- Abdelamir A. I., Al-Bermany E. and Hashim F. S., "Important Factors Affecting the Microstructure and Mechanical Properties of PEG/GO-Based Nanographene Composites Fabricated Applying Assembly-Acoustic Method". In AIP Conference Proceedings, Vol. 2213, No. 1, p. 020110, AIP Publishing LLC, (2020).

82- AL-humairi M. H. R., "Study the Optical and Electrical Properties of (PVA-Ag) and (PVA-TiO_2) Nanocomposites". M.Sc. Thesis, College of Education for pure sciences, University of Babylon, (2013).

83- Gurland J., "Electrical Resistivity", J. Polym. Plast. Technol. Eng. Vol.19, No.1, pp. 21-51, (1982).

84- laeva V., Yovcheva T., Sainov S., Dragostinova1 V. and Stavrev S., "Optical Properties of PVA Films With Diamond and Titania Nanoparticles", J.of Phys. Conf. Ser. Vol. 253 , No.1, pp. 1-6, (2010).

85- Ragab H. M., "Spectroscopic Investigations and Electrical Properties of PVA/PVP Blend Filled With Different Concentrations of Nickel Chloride", J. Physica B, Vol. 406, No.20, pp. 3759–3767, (2011).

86- Rithin Kumar N. B., Crasta V., Bhajantri R. F. and Praveen B. M., "Microstructural and Mechanical Studies of PVA Doped With ZnO and WO_3 Composites Films", Journal of Polymers, (2014).

87- Cha H. R., Babu V. R., Rao K. S. V., Kim Y. H., Mei S., Joo W. H. and Lee Y. I., "Fabrication of Amino Acid Based Silver Nanocomposite Hydrogels From PVA-poly (acrylamide-co-acryloyl phenylalanine) and Their Antimicrobial Studies", Bulletin of the Korean Chemical Society, Vol. 33, No. 10, pp. 3191-3195, (2012).

88- John R., "Applications of Absorption Spectroscopy of Organic Compounds", Dyer, Prentice Hall of Pvt. Ltd., New Delhi, India, (1991).

89- Ghanipour M. and Dorranian D., "Effect of Ag-Nanoparticles Doped in Polyvinyl Alcohol on the Structural and Optical Properties of PVA Films", J. of nanomaterials, Vol. 4, No.5, pp. 1-10, (2013).

90- Eisa W. H., Abdel-Moneam Y. K., Shabaka A. A. M. and Abd ElHameed M. H., "In Situ Approach Induced Growth of Highly Monodispersed Ag Nanoparticles Within Free Standing PVA/PVP Films", Spectrochimica Acta Part A: Molecular and Biomolecular Spectroscopy, Vol.95, pp. 341-346, (2012).

91- Streetman B. G. and Banerjee S., "Solid State Electronic Devices". Vol. 10, Upper Saddle River, NJ: Pearson/Prentice Hall, (2006).

92- Feng Q., Dang Z., Li N. and Cao X., "Preparation and Dielectric Property of Ag–PVA Nano-Composite", Materials Science and Engineering: B, Vol. 99, No.1-3, pp. 325-328, (2003).

93-Jelinska N., Kalnins M., Tupureina V. and Dzene A., "Poly (Vinyl Alcohol)/Poly (Vinyl Acetate)", Rigas Tehniskas Universitates Zinatniskie Raksti, Vol. 21, p. 55, (2010).

94- Abdali K., "Structural, Morphological` and Gamma Ray Shielding (GRS) Characterization of HVCMC/PVP/PEG Polymer Blend Encapsulated with Silicon Dioxide Nanoparticles", Silicon, pp. 1-6, (2022).

95- Uddin M. J., Chaudhuri B., Pramanik K., Middya T. R. and Chaudhuri B., "Black Tea Leaf Extract Derived Ag Nanoparticle-PVA Composite Film: Structural and Dielectric Properties", Materials Science and Engineering: B, Vol. 177, No.20, pp. 1741-1747, (2012).

96- Dahshan M., "Introduction to Material Science and Engineering", *2nd*, McGraw Hill, New York, (2002).

97- Asogwa P. U., “Band Gap Shift and Optical Characterization of PVA-Capped PbO Thin Films: Effect of Thermal Annealing”, Chalcogenid Lett. Vol. 8, No.3, pp. 163-170, (2011).